SAHC

The Ultimate Load Capacity of the Road Historic Bridge

Sandryne Lefebvre

Czech Republic | 2019

ADVANCED MASTERS IN STRUCTURAL ANALYSIS
OF MONUMENTS AND HISTORICAL CONSTRUCTIONS

Master's Thesis

Sandryne Lefebvre

The Ultimate Load Capacity of the Road Historic Bridge

University of Minho

Czech Republic | 2019



ADVANCED MASTERS IN STRUCTURAL ANALYSYS
OF MONUMENTS AND HISTORICAL CONSTRUCTION

Master's Thesis

Sandryne Lefebvre

The Ultimate Load Capacity of the Road Historic Steel Bridge

Czech Republic | 2019

CZECH TECHNICAL UNIVERSITY IN PRAGUE
Faculty of Civil Engineering
Thákurova 7, 166 29 Prague 6, Czech Republic

MASTER'S THESIS PROPOSAL

study programme: Civil Engineering

study branch: Advanced Masters in Structural Analysis of Monuments and Historical Constructions

academic year: 2018/2019

Student's name and surname: Sandryne Lefebvre

Department: Department of Mechanics

Thesis supervisor: Pavel Ryjáček

Thesis title: The Ultimate Load Capacity of the Road Historic Steel Bridge

Thesis title in English see above

Framework content: The thesis contain the visual inspection of the bridge, preparation of the detailed drawings. based on that, the student will build detailed numerical model including the geometrical and material nonlinearities. The model will be validated using static load test results. The final goal is to find the ultimate load capacity till the bridge failure.

Assignment date: 1/04/2019 Submission date: 8/09/2019

If the student fails to submit the Master's thesis on time, they are obliged to justify this fact in advance in writing, if this request (submitted through the Student Registrar) is granted by the Dean, the Dean will assign the student a substitute date for holding the final graduation examination (2 attempts for FGE remain). If this fact is not appropriately excused or if the request is not granted by the Dean, the Dean will assign the student a date for retaking the final graduation examination, FGE can be retaken only once. (Study and Examination Code, Art 22, Par 3, 4.)

The student takes notice of the obligation of working out the Master's thesis on their own, without any outside help, except for consultation. The list of references, other sources and names of consultants must be included in the Master's thesis.

....
Master's thesis supervisor Head of department

Date of Master's thesis proposal take over: July 2019

.....
Student

This form must be completed in 3 copies – 1x department, 1x student, 1x Student Registrar (sent by department)

No later than by the end of the 2nd week of instruction in the semester, the department shall send one copy of BT Proposal to the Student Registrar and enter data into the faculty information system KOS. (Dean's Instruction for Implementation of Study Programmes and FGE at FCE CTU Art. 5, Par. 7)

MASTER'S THESIS ASSIGNMENT

I. Personal and study details

Student's name: **Lefebvre Sandryne** Personal ID number: **488987**

Faculty / Institute: **Faculty of Civil Engineering**

Department / Institute: **Department of Mechanics**

Study program: **Civil Engineering**

Branch of study: **Advanced Masters in Structural Analysis of Monuments and Historical Constructions**

II. Master's thesis details

Master's thesis title in English:

The Ultimate Load Capacity of the Road Historic Steel Bridge

Master's thesis title in Czech:

The Ultimate Load Capacity of the Road Historic Steel Bridge

Guidelines:

Bibliography / sources:

Name and workplace of master's thesis supervisor:

doc. Ing. Pavel Ryjáček, Ph.D., Department of Steel and Timber Structures, FCE

Name and workplace of second master's thesis supervisor or consultant:

Date of master's thesis assignment: **01.04.2019** Deadline for master's thesis submission: **08.07.2019**

Assignment valid until: _____

doc. Ing. Pavel Ryjáček, Ph.D. Supervisor's signature	Head of department's signature	prof. Ing. Jiří Máca, CSc. Dean's signature

III. Assignment receipt

The student acknowledges that the master's thesis is an individual work. The student must produce her thesis without the assistance of others, with the exception of provided consultations. Within the master's thesis, the author must state the names of consultants and include a list of references.

Date of assignment receipt	Student's signature

DECLARATION

Name: Sandryne Lefebvre

Email: sandryne.lefebvre@gmail.com

Title of the Msc Dissertation: The Ultimate Load Capacity of the Road Historic Steel Bridge

Supervisor(s): Doc. Ing. Pavel Ryjáček, Ph.D.

Year: 2019

I hereby declare that all information in this document has been obtained and presented in accordance with academic rules and ethical conduct. I also declare that, as required by these rules and conduct, I have fully cited and referenced all material and results that are not original to this work.

I hereby declare that the MSc Consortium responsible for the Advanced Masters in Structural Analysis of Monuments and Historical Constructions is allowed to store and make available electronically the present MSc Dissertation.

University: Czech Technical University in Prague

Date: July 8, 2019

Signature:

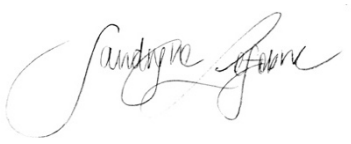

_____

This page is left blank on purpose.

ACKNOWLEDGEMENTS

A warm thank you to Professor Pavel Ryjáček, my thesis director for all of his guidance, advice and support during this thesis. I also want to thank Vojtech Stancik and Jakub Vujtech for their assistance. In addition, I want to thank the MSc Consortium responsible for the Advanced Masters in Structural Analysis of Monuments and Historical Constructions for giving me a scholarship for this academic journey. Finally, I want to thank my family and friends for their continuous support throughout this year outside of Canada.

Un remerciement chaleureux à professeur Pavel Ryjáček, mon directeur de thèse pour son aide, ses conseils et son support durant cette maitrise à l'étranger. Je tiens aussi à remercier Vojtech Stancik and Jakub Vujtech pour leur conseils. De plus, je souhaite remercier MSc Consortium qui est responsable de la « Advanced Masters in Structural Analysis of Monuments and Historical Constructions » pour m'avoir offert une bourse pour mes études. Finalement, je tiens à remercier ma famille et mes ami(e)s pour leur appui continue durant cette année à l'extérieur du Canada.

This page is left blank on purpose.

ABSTRACT

Much infrastructure around the world is ageing and has reached its service life or is soon expected to reach it. This is wide spread for steel road and railway bridges, which were often built at the beginning of the 20th century or near the end of the 19th century in the country of the Czech Republic. A lot of these structures even with their age are still in areas being used today: highways, routes and railways. Without the proper understanding of their behavior, of the construction techniques used at the time of their erection and of the signs of existing damages or deterioration, the use of traditional techniques, such as visual inspections to assess these ageing structures may lead to very conservative decisions about the state of conservation of such bridges. These decisions are often limited to mainly qualitative information obtained via these visual inspections and via a limited number of tests that do not permit the complete assessment of such structure in which case a higher residual capacity than expected could also be discovered since the original know how is often lost through time due to the use of more modern techniques. There is therefore a need for further assessment using adequate and quantitative measurements in order to obtain more information on historical bridges' load-bearing capacity, serviceability and dynamic properties. By obtaining such measurements, knowing that budgets are often limited for such structures for any type of repair, strengthening or replacement, costs can only be limited to what is truly necessary for the bridge assessed, therefore preserving the structure in place instead of opting for a full replacement.

A solution to more qualitative visual inspections is the use of static and dynamic testing of historical bridges. Both tests are performed as non-destructive tests providing valuable information on the behaviour of structures, their load carrying properties as well as their dynamic properties in terms of traffic induced vibrations, wind and earthquakes. Such valuable information helps to provide an appropriate maintenance plan or interventions for the existing bridge. However, in some instances where bridges have been decided to be replaced, the destructive testing of these bridges can be used in addition to non-destructive testing, which can then permit to have a complete understanding of the ultimate capacity of a typical typology of historical bridges and avoid the unnecessary demolition and replacement of historical bridges.

KEYWORDS

Steel truss bridge, Rivetted connections, Structural health monitoring, Operational modal analysis, Static load test, Strengthening, SMA, Model calibration, Ultimate capacity.

This page is left blank on purpose.

ABSTRAKTNÍ

Mezní únosnost silničního historického mostu

Velká část existující infrastruktury stárne a postupně dosahuje konce své životnosti nebo v blízké době tohoto konce dosáhne. To platí v ČR obzvláště pro ocelové silniční a železniční mosty, které byly často budovány na přelomu devatenáctého a dvacátého století. Tyto konstrukce jsou však stále používány, i přes jejich věk.

Bez dostatečné znalosti o jejich skutečném působení, o jejich výstavbě a výrobě a o reálném stavu, poškození či korozi, běžné metody diagnostiky jako vizuální hodnocení mohou vést k velmi konzervativnímu rozhodnutí o osudu uvedených konstrukcí.

Tato rozhodnutí jsou často založena na kvalitativních informacích z vizuálního hodnocení a z omezeného množství, které těžko popisují komplexní stav konstrukce. To generuje potřebu zjištění podrobnějších informací a stavu, chování a výstavbě historických ocelových mostů pro zlepšení pochopení jejich mezní únosnosti, použitelnosti a dynamických vlastnostech. Na základě takto upřesněných informací lze lépe využít omezené rozpočty na opravy a zesílení, které jsou skutečně nezbytná pro most, zachovat tak konstrukci i dále namísto její výměny.

Řešením pro zlepšení vizuálního hodnocení je využití statických a dynamických zkoušek historických konstrukcí. Oba typy jsou nedestruktivní a lze jimi získat cenné informace o jejich chování, dynamických vlastnostech a do určité míry i o únosnosti. Nicméně, v některých případech, jako je i most v této práci, kde je rozhodnuto o demolici mostu, může zkouška do porušení přinést pochopení mezní únosnosti daného typu mostu a tak prodloužit i životnost dalších mostů .

KLÍČOVÁ SLOVA

Zatěžovací zkouška, Nýt, Monitoring, Modální analýza, Zatěžovací zkouška, Zesílení, SMA, Validace, Mezní únosnost

This page is left blank on purpose.

RÉSUMÉ

La charge ultime d'un pont de route en acier

Une grande partie des infrastructures à travers le monde sont vieillissantes et ont atteint leur durée de vie utile ou devraient l'atteindre sous peu. Le cas présent est largement répandu en ce qui a trait aux ponts en acier ayant souvent été construits au début du 20ème siècle ou près de la fin du 19ème siècle dans le pays de la République Tchèque. Malgré leur âge, un large nombre de ces structures sont encore utilisés aujourd'hui: autoroutes, routes et voies ferroviaires. Sans une bonne compréhension de leur comportement au niveau structural, des techniques de construction utilisées au moment de leur construction et des signes de dommages ou de détériorations existantes, le recours à des techniques d'inspections traditionnelles, telles que des inspections visuelles pour évaluer ces structures vieillissantes peut conduire à des décisions très conservatrices sur l'état de conservation de ces ponts. Ces décisions se limitent souvent à des données principalement qualitatives obtenues par le biais de ces inspections visuelles et par un nombre limité d'essai non-destructifs ne permettant pas une évaluation complète et précise de cette structure. Dans un tel cas, une capacité résiduelle plus élevée qu'estimé pourrait être découverte en raison de la perte du savoir-faire initial aux techniques plus modernes. Il est donc nécessaire de poursuivre l'évaluation de telles structures à l'aide de mesures quantitatives afin d'obtenir davantage des données sur la capacité limite ultime, la capacité limite de service et les propriétés dynamiques des ponts historiques. En obtenant de tels résultats, sachant que les budgets de ces structures sont souvent très limités pour tout type de réparation, de renforcement ou de remplacement, les coûts peuvent maintenant être limités qu'à ce qui est réellement nécessaire pour le pont évalué, préservant ainsi la structure en place au lieu de la remplacer.

L'utilisation d'essais statiques et dynamiques sur les ponts historiques présente une solution afin d'approfondir les inspections visuelles plus qualitatives. Ces deux tests sont réalisés en tant qu'essais non-destructifs et fournissent des données précieuses sur le comportement des structures, leur charge portante ainsi que leurs propriétés dynamiques en termes de vibrations causées par le vent, par les tremblements et par le trafic. Ces données peuvent par la suite aider à mettre en place un plan d'entretien approprié ou de planifier des interventions pour le pont historique. Cependant, dans le cas où un pont a été décidé d'être remplacé, des essais destructifs en plus d'essais non destructifs sur ce pont peuvent être utilisés. Ceci peut ensuite permettre de mieux comprendre les conditions de charge de rupture pour une typologie typique de ponts historiques et donc, d'éviter la démolition et le remplacement inutiles de ponts historiques.

MOT-CLÉS

Pont à treillis en acier, connexions rivetées, surveillance de l'état des structures, analyse modale opérationnelle, essai de charge statique, renforcement, SMA, calibration de modèle, capacité ultime.

This page is left blank on purpose.

TABLE OF CONTENTS

List of Tables

List of Figures

APPENDICES

1. INTRODUCTION

As for many historical structures found around the world, the loss of knowledge of traditional techniques leads to the misunderstanding of the behaviour of many existing structures since historical structures tended not to be designed according to any codes, but often to a workmanship and craftmanship that was transmitted from the master worker to the apprentice worker. Unfortunately, with the arrival of more modern techniques that are more effective for nowadays economy and time of construction, a lot of these traditional techniques were lost without any true record of them. This is the case for many historical steel bridges and railway bridges, which have no record of construction left with them other than their physical presence or if lucky, a few limited records.

It is well known that the anticipated structural demand for these bridges as part of the original design intention was lower than nowadays traffic loads. The knowledge of the original design loads might be obscured as well as the capacity of bridges leading to a lack of understanding of their structural behaviour. The complexity of riveted steel bridges with their elaborated built-up sections and connections including plates, angles, rivets, makes it even harder to assess and to predict their behaviour in terms of rotational stiffness. Originally, at the time of construction, simplifying assumptions, such as a fixed or a pinned connection, would be used due to the lack of better technology to fully comprehend the connections' semi-rigidity. In the light of the new technologies and tools that are now accessible to designers, it is possible with more innovative techniques to obtain a proper understanding of the structural behaviour of such complex structures via the use of static and dynamic testing combined with the numerical modelling of the structures. This enables the assessment of the load capacity of bridges, their serviceability as well as their dynamic response without performing any damage to the structure, which is desired for a continuous and prolonged use. Such advantage is even more important in the case of heritage structures, which cannot be damaged and are required to be protected. This assessment of properties can then lead to more appropriate a maintenance plan, repair, strengthening, and rehabilitation without the original structure suffering a full replacement. However, if a replacement cannot be refuted, the opportunity of testing to their ultimate capacity these historical structures should be taken in order to provide the complete assessment of their properties passed the elastic state, which can be covered by non-destructive testing. This information can then be used for bridges built with similar construction techniques and during similar time periods, and avoid any unnecessary interventions.

The purpose of this case study of the Bridge No. 11-097 Petrov nad Desnou located is to use the demolition of a historic bridge for research purpose by assessing its ultimate loading. This study entails to prove that such bridges can still be used safely even with their age and depending on their level of deterioration and that full replacement is not always the best solution. The main goals

associated with this project include the monitoring of the bridge using strain gauges, accelerometers and temperature sensors; the performance of a load test on the existing bridge; the performance of an operational modal analysis; the strengthening of the bridge using the shape memory alloy (SMA) technology; a load test after the strengthening phase; a dynamic test; the detection of global and local damages via modal analysis and visual inspection; and, the final load test to reach the failure of the bridge based on existing load and resistance models.

2. STATE OF THE ART

The state of the art of this thesis presents a review of the typologies of steel bridges based on their construction materials, type of traffic, main structural system with a focus on trusses, and on the carriageway position. In addition, it reviews previous load tests and modal analysis conducted on existing bridges as well as testing conducted on bridges up until failure.

2.1 Steel Bridges

Steel bridges have been seen as advantageous constructions which have helped with their spread in numerous European countries, including the Czech Republic. This is due to many advantages such as their load-carrying capacity with a minimal self-weight, speed of erection, seismic resistance, and serviceability. (Institute for Steel Development & Growth, 1998a)

2.1.1 Construction Materials

Steel is characterized by its strength, ductility and brittleness, weldability, weather resistance and additional characteristics. These characteristics are dependent on the steel's carbon content, presence of alloys, cooling rates, and mechanical deformation. (Institute for Steel Development & Growth, 1998a) Prior to modern steel bridges, examples of wrought iron, cast iron and early steel bridge could be found. Wrought iron structures present more desirable advantages due their ductility and their strength in both tension and compression as cast-iron structures which are good in compression, but have a brittle failure and a low tensile strength leading to potentially catastrophic failures. (Sparks, 2008) In between, one can find the early steel, or mild steel, examples with a wide range of ductility and properties depending on their time period. As wrought iron, they have a good compressive and tensile strength and have a good ductility. (Larsson & Lagerqvist, 2019) Nowadays, three main optimized categories of steel are used for the construction of steel bridges: carbon steel, high-strength steel and heat-treated carbon steel. Carbon steels are usually the material used when the stiffness of the structure is of greater importance than its strength. High strength steels are characterized due to their higher strength and additional properties due to the presence of alloy. In addition, these steels can also have better resistance to atmospheric corrosion and are characterized as weathering steels. Heat-treated carbon steels are another category which includes the steels with the highest strength. Their increased properties are given following a heat-based treatment, rolling, quenching or tempering. (Institute for Steel Development & Growth, 1998a)

2.1.2 Bridges Based on Type of Traffic

Three main types of bridges can be seen in terms of type of traffic: highway or road bridges, railway bridges and a composition of both. (Institute for Steel Development & Growth, 1998a)

2.1.3 Bridges Based on Type of Main Structural Systems

Various structural systems exist for steel bridges and they often depend on the span length, the width size and the type of traffic. They include girder bridges, rigid frame bridges, arch bridges, cable-stayed bridges and suspension bridges. Girder bridges are characterized by the bending of vertical supports as the main structural action using solid web girders, truss girder or box girder. Truss bridges are classified as part of the girder bridges. Rigid frame bridges use longitudinal girders which are continuous with either vertical or diagonal member via moment resisting joints. Arch bridges use arches being the main structural element for which the compression of the arch is the main action. Cable stayed bridges are characterized by nearly vertical or vertical cables supporting the main longitudinal girders and suspension bridges can be identified when the deck is suspended using cables that are stretched over the whole span, passing over towers and anchored at both ends. In this case study, truss bridges are of greater importance. (Institute for Steel Development & Growth, 1998a)

2.1.3.1 Truss Bridges

Three main arrangements of trusses exist, either simple, planar or space frame where multiple types of trusses can be used. Various types of trusses exist for the construction of bridges (Figure 1). The Pratt truss is designed where its diagonal support slopes down towards the centre and variations of this truss, like the Baltimore truss, lead to the design of additional bracing in lower sections. The Howe truss is a truss system in which its diagonals are sloping towards the centre and variations, such as the Allan truss, exist where multiple Howe trusses are designed for a longer span. The Fink truss is another type where the truss is placed under the deck of a bridge. Similarly, the Bowstring truss, the Parker truss and the Camelback truss are trusses with an either smooth or rigged arch shape connecting the edges of the diagonal and vertical members. The Waddell truss uses a tall triangular shape reinforced by inward facing triangle and the Pennsylvania truss has its lower section reinforced with additional members. The K truss uses members that provide a “k” shape from the centre to the support with its vertical and diagonal members and the Warren truss consists of two parallel chords with diagonal equally separating where a few variations exist. Another example is the Lattice truss, which has a large quantity of small closely spaced diagonals. (Historic American Engineering Record, 1976) (Waddell, 1916) Trusses, in general, are characterized by their main structural action being resist mainly axial forces, however, within the truss, the members characterized as chord members resist bending moments and the web members resist shear forces. (Institute for Steel Development & Growth, 1998b)

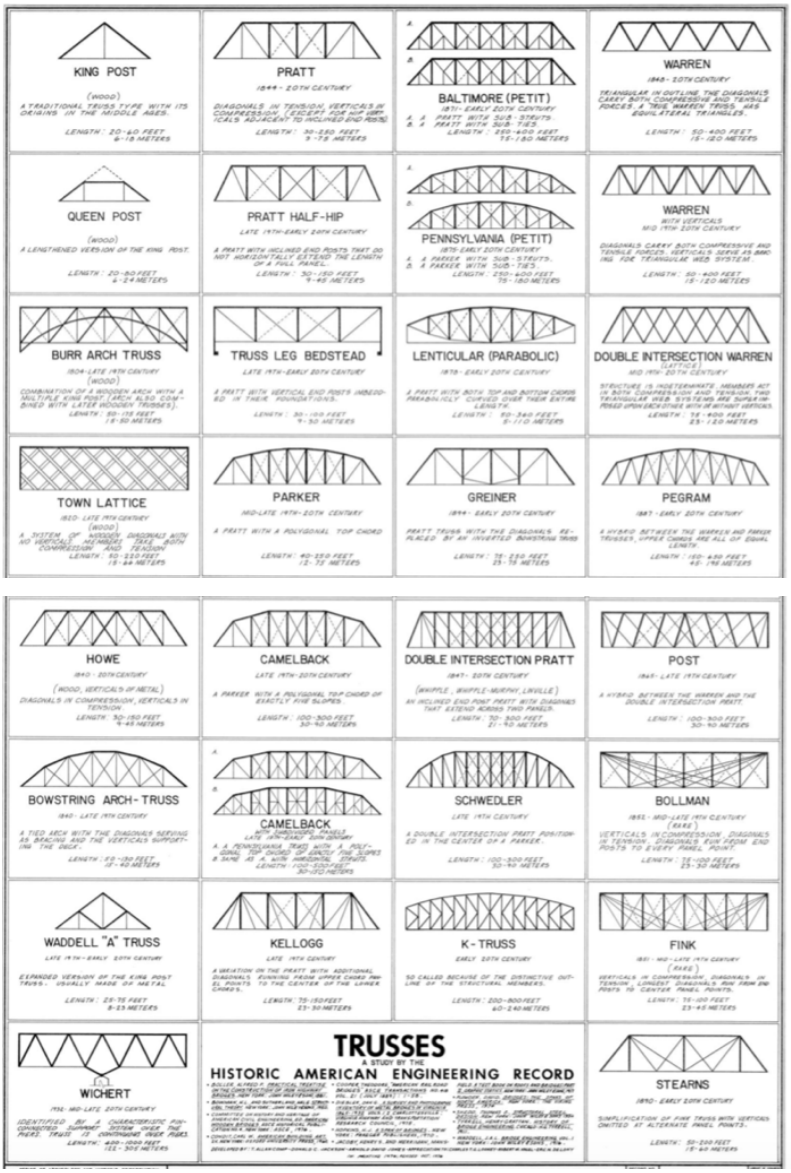

Figure 1. Truss Types (Historic American Engineering Record, 1976)

In order to transfer forces, three typical connecting systems are used: rivets, bolts and welds. Riveting is a technique that was historically used, but that is no longer currently used due to the need for a specific type of workmanship and to the work force demand. It was seen as advantageous for railways where fatigue is a problematic. Bolting is more commonly used today and new techniques such as high-strength friction grip bolting exist replacing historical ones. Welding is still being used and can be useful today for prefabrication of shorter span trusses. Using these techniques, some additional members may be required. Additionally, for tie members that are using either T sections or angle diagonals, they can be connected directly to the web of the T-section using riveting, welding or bolting, however, if members cannot be directly connected, gusset plates are used to accommodate all the

members. The shape and size of the gusset plates are dependent on member size and they normally range between 8 mm to 12 mm in thickness. (Institute for Steel Development & Growth, 1998c)

2.1.4 Bridges Based on the Carriageway Position

Bridges have three main carriageway positions: the deck type bridge, the through type bridge and the semi-through type bridge. The deck type bridge is characterized by its carriageway resting on top of the main structural system. In contrast, the through type bridge has its carriageway located at the bottom layer of the main structural elements. Finally, the semi through type bridge which combines the first two types, where the deck is positioned between the top and the bottom of the main load carrying structural members. (Institute for Steel Development & Growth, 1998a) (Wright, 2015)

2.2 Previous Studies on Load Test on Bridges

The use of non-destructive testing for the assessment of historical bridges including static testing provides valuable information on the behaviour of the structure including its load carrying based on deflections and stresses of members. Such testing is typically associated with a typical methodology as per following case studies show. They first generally consist of the creation of a simplified numerical model of the bridge often using 3D beam elements with simplifying assumptions for the connections. The model can then be associated with a parametric study of the bridge if some material properties are unknown and can then later be updated once material testing is conducted, for example, the properties of the metal used to build a certain bridge. This simplified model is useful for determining the positioning of the sensors for static tests and potentially later modal analysis, and these sensors often include strain gauges, displacement sensors, accelerometers and/or temperature sensors. Temperature sensors can permit to avoid assessing temperature dependent responses of an element. Once the data from the material testing as well as static testing is conducted, the initial model can be calibrated and updated to be the closest to the actual response of the bridge under study. With the calibration, a refinement of the connections in place can be performed by looking at the interaction, in the case of riveted bridge, of the members, gusset plates and the rivets and at the general behaviour of the connection as pinned, semi-rigid or rigid. From this assessment, the load-bearing capacity of the bridge can be obtained which can greatly affect the decisions regarding the maintenance, repairs, strengthening, rehabilitation or in some instances replacement possibility of the bridge. This permits to provide a minimal intervention, which is very important, when working with a heritage bridge that might be protected from various invasive interventions.

Many studies have been conducted using static tests for existing steel bridges and railway bridges. They often tend to have been be associated with the dynamic testing of the same structure. This is the case for a steel railway bridge across the Orlík dam near Červená in Czech Republic dating from 1889, which study aimed to prove that even if steel structures in Czech Republic are aging and with a

certain degree of deterioration, they can still be operational. This was done via the development of an initial numerical model and then, with the use of static and dynamic testing which allowed to verify operability of the railways, the compliance of the results with initial finite element model (FEM) and the calibration of a model based on the testing. The load test was conducted two types of trains: an HV engine with a weight of 75 tons and a braking force of 190 kN and a normally passing passenger train of series 814-914 with a weight of 55 tons. As a result, recommendations proposed the continuous use of the bridge, but with a reduction of the load-bearing capacity of the bridge. (Plachý, Polák, & Ryjáček, 2017) The Politi railway bridge and Karakoy railway bridge in Turkey were also assessed using non-destructive testing, both static and dynamic. With the static testing, the capacity of the bridge was assessed for a minimum factor safety index of “3” for a train set with an axle load reaching up to 225 kN. The load test was then applied to a 3D beam for members and 1D rigid bar elements for gusset plates model. For the modelling of the connections, a semi-rigid behaviour was adopted instead of fixed by using rotational spring elements and at the supports, spring elements were also used to provide adequate stiffness. The comparison between the experimental and the calibrated initial numerical model permitted to adequately assess reliability of the two bridges. (Caglayan, Ozakgul, & Tezer, 2012) A study on multiple bridges was conducted in 2002, where both static and dynamic testing were performed on a few bridges in order to assess the applicability of maintenance, repairs, rehabilitation and strengthening. The static testing that was conducted was performed with the monitoring system in place in order to help determining the load capacity of the bridge and was then compared with the models of the bridges only considering the undamaged structure. (Cunha, Caetano, & Calçada, 2002) The presented case studies are a few of many still being conducted on contemporary and historical bridges.

2.3 Previous Studies on Modal Analysis of Bridges

The use of non-destructive testing for the assessment of historical bridges including a dynamic testing provides valuable information on the behaviour of the structure in terms of its dynamic properties induced by vibrations from traffic, wind and earthquakes. Such testing is typically associated with a certain methodology as per following case studies show. They first consist of the creation of a simplified numerical model of the bridge often using 3D beam elements with simplified connections. This model is normally associated with a parametric study of the bridge and can then later be updated. This simplified model helps for determining the positioning of the sensors for static and dynamic tests. In addition, material testing can also be conducted if material properties are unknown. Once the data from the material testing and dynamic testing is conducted, the initial model can be calibrated and updated to be the closest to the actual response of the bridge under study. With the calibration, a refinement of the connections can be conducted by looking at the interaction, in the case of riveted bridge, of the members, gusset plates and the rivets and at the general behaviour of the connection as pinned, semi-rigid or rigid. From this assessment, the dynamic behaviour of the bridge can be

obtained and can provide additional information on any zones of damages and disconnections or on any changes in stiffness after interventions being conducted on a bridge.

Examples of dynamic testing conducted on road and railway bridges include the assessment of a steel railway bridge across the Orlík dam near Červená in Czech Republic. An initial numerical model and then with the use of static and dynamic testing which allowed to verify operability of the railways, the compliance of the results with initial finite element model (FEM) and the calibration of a model based on the testing. The dynamic testing was conducted using a HV751 engine at speeds ranging from 10 km/h to 60 km/h where the bending vibration was the main focus, where the 60 km/h was not performed. As a result of this study, it was determined that from this specific bridge, horizontal vibrations were too high for the comfort of the train which showcased a lack of horizontal bracing. In this case, recommendations resulted in the continuous use of the bridge, but with a reduction of the load-bearing capacity of the bridge and the speed of trains. (Plachý et al., 2017) The Luiz I Bridge in Portugal was also tested using similar techniques, but in this case it was done prior to a strengthening intervention and after the strengthening. Such strengthening was necessary in order to provide continuous use of the bridge by increasing original capacity to welcome additional traffic loads. The tests in conjunction with the numerical models permitted to assess the changes in stiffness of the structure which were of interest for this study via the dynamic testing of the bridge. The models were completed using 3D frame elements and shell elements for slab and plate action. The newest model is intended to be conserved in order to compare in the future as the bridge ages. (Costa, Magalhães, Cunha, & Figueiras, 2014)

An additional example includes the Politi railway bridge and Karakoy railway bridge in Turkey. The vibrations of the trains or its ambient vibrations and their acceleration were recorded from which the modal parameters were then obtained. Pre-processing of the recorded data was first conducted and followed by the modal identification of the bridge using the Fast Fourier Transform technique. The measured and modelled mode shapes were then compared to each other based on the COMAC techniques. The model was completed with 3D beams for members and 1D rigid bar elements for gusset plates. For the modelling of the connections, a semi-rigid behaviour was adopted instead of fixed by using rotational spring elements and at the supports, spring elements were also used to provide adequate stiffness. The comparison between the experimental and the calibrated initial numerical model permitted to adequately assess reliability of the two bridges. (Caglayan et al., 2012) As previously mentioned, a study on multiple bridges was conducted in 2002, using static and dynamic testing on a few bridges in order to assess the applicability of any intervention. Short-term and long-term monitoring were performed to assess the dynamic response of the bridge as well as for to detect any global structural problems. The dynamic testing was conducted to determine modal parameters for validation of numerical models. The modelling was, however, only performed for the undamaged structure and the response was observed to be affected, for example, by the pavement

level of deterioration. (Cunha et al., 2002) This study showcases the importance of incorporating the existing damages in a model in order to obtain the most realistic results. In addition to the presented case studies, many other studies by various authors were also conducted for steel bridges.

2.4 Previous Studies on Bridges Tested to Failure

In a few instances, non-destructive testing and destructive testing (or the failure of a structure) can be conducted for a study purpose in order to fully assess the ultimate capacity of a bridge. This therefore provides a complete assessment of the properties of the bridge and the results can then be used to compare with other similar structures, therefore creating a baseline for structures for which such information cannot be obtained in this fashion. In the same fashion as the two previous chapters, a series of load tests are first conducted on the bridge to assess the deflections and stresses of its members with an operational modal analysis to obtain mode shapes. From this, the model is calibrated and the ultimate capacity can be estimated.

An assessment of the Aby River bridge in Sweden, a historical steel truss bridge of over 50 years in age was tested up to its ultimate limit state. This study had for objective to prove that even after bridges have passed their theoretical service life that they do not always need to be replaced even with increasing loads and traffic and that this can be shown with the technology that is now available. In this specific case, the Aby River bridge was already to be replaced therefore the testing was conducted on it to provide intel on a similar bridge, the Rautasjokk River bridge, that would not suffer replacement. Both non-destructive static and dynamic testing were conducted on the Aby River bridge. Train loads were monitored for a period of time and the bridge was also monitored using digital image correlation (DIG) measurements at the joints to evaluate degree of constraint. The bridge was simulated with a finite element model (FEM) using shell elements with constraint at the joints and therefore, providing fully rigid connections. The tests were conducted with predefined load series which were then compared with the experimental results. The model and experimental results for the full-scale testing resulted in similar results for the global deformation within linear elastic range, but with different results for yielding with the numerical model being more conservative in terms of stress redistribution. In sum, this study therefore concluded that historical bridges might be able to carry higher load in terms of ULS, however, fatigue may be another issue to be addressed. (Blanksvärd, Häggström, & Collin, 2016)

3. DESCRIPTION OF THE BRIDGE

The Bridge No. 11-097 Petrov nad Desnou was built in 1906 in the city of Petrov nad Desnou on route 11 in the Czech Republic in order to allow for crossing the Desná river. This bridge is part of a collection of bridges in the area that crosses this river network in the region of the county of Šumperk (Figures 2 and 3). The available information and recorded data about the Bridge No. 11-097 Petrov nad Desnou is very limited in addition to although historical it was never attributed any heritage designation.

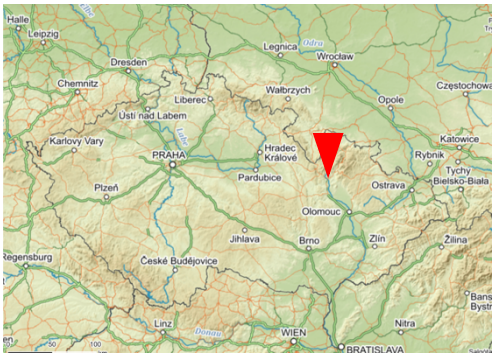

Figures 2 and 3. Map of the Czech Republic (left); Location of the Site (right). (Seznam.cz, 2019)

In total, only four historical pictures of the construction of the bridge still remain showing different stages of work and levels of completion. No original drawings were found or still exist. Figure 4 depicts the construction of the upper chord of the truss. Figures 5 to 7 showcase various views of the bridge will rivets appear to be put in place. It is interesting to note that these picture permit to provide a general idea of the construction techniques used at the beginning of the 20th century.

Figures 4 and 5. Historical Pictures During Construction Facing North (left); Facing East (right). (Courtesy of the Czech Republic Highway Administration)


Figures 6 and 7. Historical Pictures During Construction Facing West (left); Facing North (right). (Courtesy of the Czech Republic Highway Administration)

3.1 Geometry

The bridge is a skewed semi-through truss bridge of approximately 20 m long by 8 m wide by 3 m tall. It was built using a mild steel Warren truss with verticals spaced about every 5 m with its structural elements, including angles, built-up girders and I sections, connected using rivets and gusset plates. The bridge is symmetrical and supported by six bearings installed over concrete retaining walls and its railing is prolonged into masonry walls on both sides of the bridge. Figures 8 and 9 provide a general overview of the bridge.


Figures 8 and 9. Overall Views from the Bridge: Side View (left); Front View (right).

The structure can be summarized as the following:

- Shape: One level 52° oblique bridge skewing to the left;
- Dimensions: 21.4 m long 7.8 m wide by 3.2 m tall;
- Bearing: Soil and concrete abutment;
- Supports: 2 hinged connections above the western abutment from two external support, 2 rollers above the eastern abutment from two external supports allowing longitudinal support, and the 2 secondary supports allowing omnidirectional sliding;
- Cross beams: Built-up sections riveted together consisting of a plate of P15x620 or P15x698 with 2 angles of L90x90x9 at the top and the bottom with up to 3 additional plates of P10x230 on the top and bottom flange and with riveted shear plates P10x400 on the web near the supports;
- Stringers: I350 and I300 sections;
- Braces: “L“ profile 70x70x9 connected with a pin connecting the two crossing braces;
- Deck: About 300 mm thick with a ”ZORES“ section decking and a roadbed consisting of gravel layers of approximately 130 mm thick covered by an asphalt layer of approximately 80 mm thick;
- Truss vertical members: symmetric riveted built-up section of with 3 pairs of “L“ profile 80x80x10 separated by a P10x320 plate;
- Truss diagonal members: Outside trusses with the first diagonal consisting of 2 pairs of riveted back-to-back L“ profile L120x120x14 and the second diagonal of 2 pairs of riveted back-to-back L“ profile L120x75x14 – Inside trusses with the first diagonal consisting of 2 pairs of riveted back-to-back L“ profile L90x90x10 and the second diagonal of 2 L90x90x10 profiles, corner to corner;
- Truss upper chord: Built-up section riveted together consisting of a plate P15x260 with 2 angles of L145x95x12 at the top with up to 3 additional plates of P10x340 on the top flange; and,
- Truss lower chord: Built-up section riveted together consisting of a plate P15x250 with 2 angles of L90x90x10 at the bottom with up to 3 additional plates of P15x250 on the bottom flange.

Various riveted connections are used across the bridge to connect directly, or member to member, and indirectly members, using gusset plates, the different structural members. They are presented in Table 1 below.

Table 1. Typical Connections.

Central connections at the top chord	Side connections at the top chord
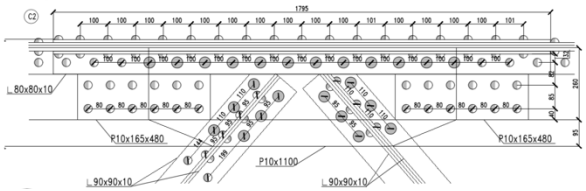	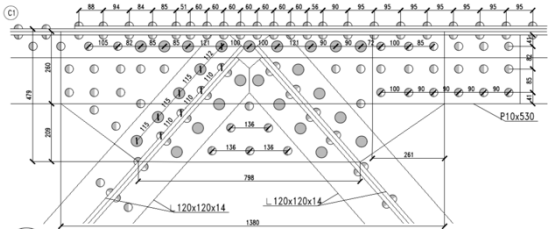
Central connection at the bottom chord	Side connections at the bottom chord
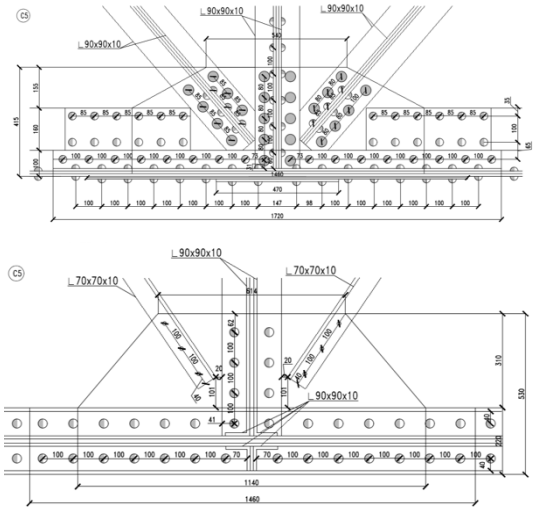	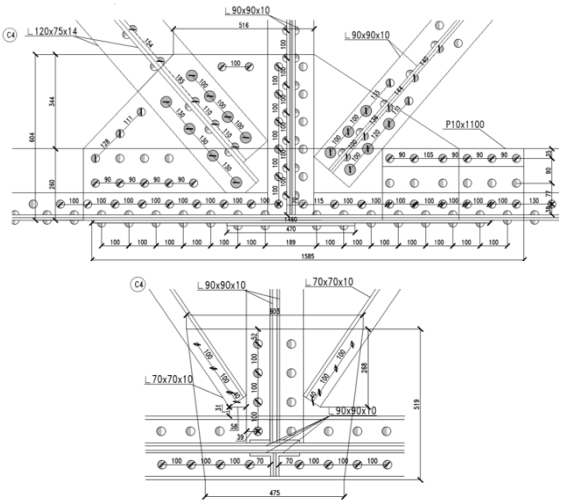
Cross beam connection at hinged support	Cross beam connection at roller support
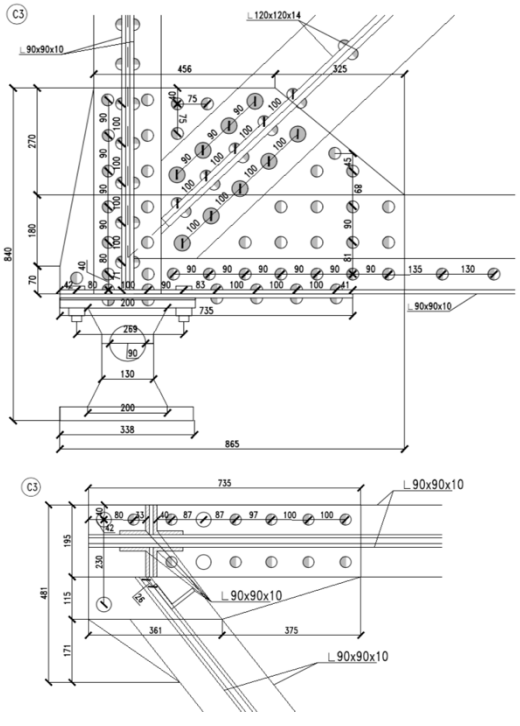	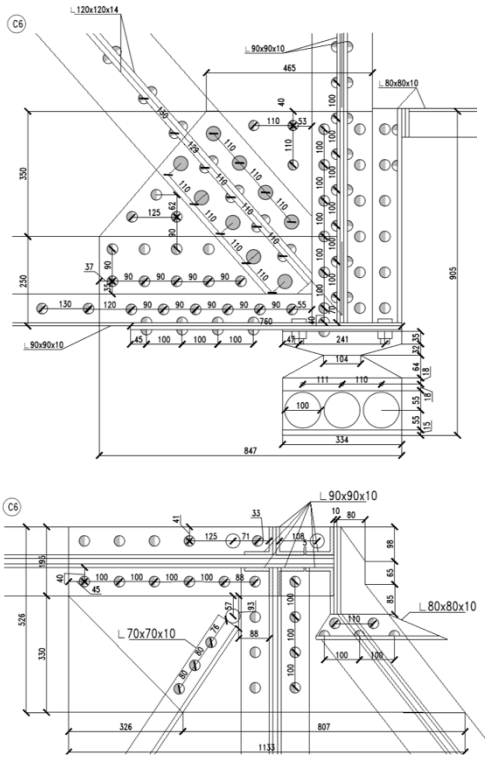

Secondary support connection

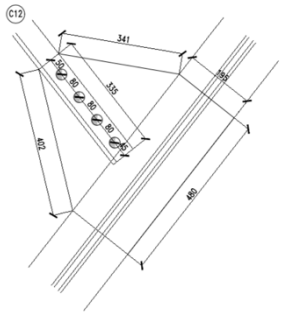

Diagonal girder and stringer connection

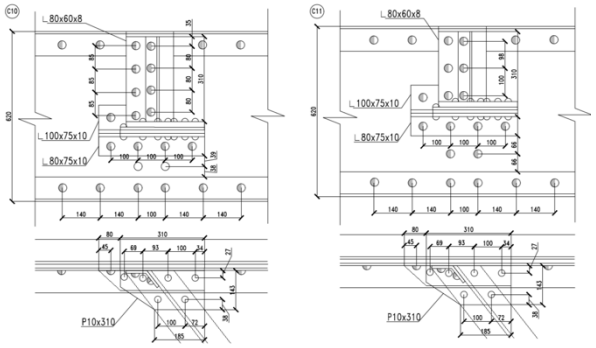

Cross beam and stringer connection

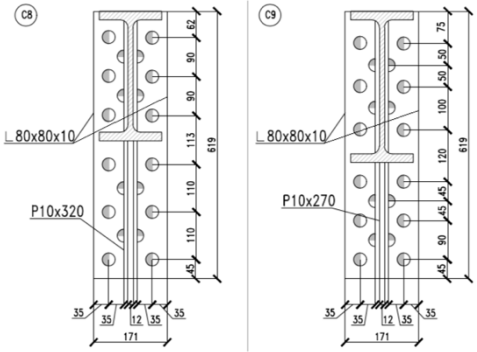

3.2 State of Conservation

The bridge showcases signs of deterioration at various locations, mainly on the underside of the bridge. In general, an accumulation of dirt and corroded fragments on most of the horizontal members, i.e. gusset plates, bracing, and bottom flange of built-up sections can be observed across the bridge (Figure 10). No cleaning campaign appears to have ever occurred. Such a quantity of debris might increase the amount of dead weight on the structure since accumulations up to 10 cm in thickness could be observed along some of the members. In addition, some vandalism was observed where a cloth appeared to be set on fire and thrown on one of the bridge trusses. Furthermore, a reduction in the cross-section was also observed along some of the structural members. This appears to be caused by corrosion of the members. The deterioration is more advanced on horizontal surfaces at connections and near the supports. Such presence on horizontal members showcases the presence of an accumulation of water or of snow on the members leading to the expansion of the steel corroding, which was observed during the winter months by the team on the project. One of the typical corroded members includes the gusset plates, which have lost part of their thickness and are flaking. In some areas, the plates have lost almost half of their original shape. In addition, some segments of plates and angles of the bottom chord built-up sections are also corroded as well as part of the bracing angles. Few of the bracing angles have lost part of their cross-section mainly at connecting gusset plates and have also suffered an expansion in thickness due to their corrosion (Figure 11).


Figures 10 and 11. Bridge Condition: Accumulation of Debris (left); Gusset Plate Corrosion (right).

The bottom flange of the cross-beams in some areas also shows signs of expansion due to corrosion by-products. Signs of corrosion can be observed on the upper flange of the I sections in addition to the semi-circular steel members “ZORES” forming the deck of the bridge (Figure 12). Based on this observation, it can be assumed that there might be a loss of integrity of the structure dues to corrosion weakening. Furthermore, near the supports, in the cross-beams, corrosion has weakened the beams to an extent to which the web has a started to have an opening in it with the surrounding material being almost inexistent, i.e. thin sheets of corroded steel. This can be a critical location when assessing the ultimate capacity of the bridge due to the close proximity of the weakening to the support and due to the loads the member carries. In addition, light corrosion can be observed on the vertical and diagonal members above the deck where ferric staining can be seen emerging from below the paint and some flaking of the paint can be observed (Figure 13). For the top chord of the truss, a surface corrosion can be seen on top of the plates and angles with the presence of some biological growth. This really showcase the effects of the exposure to the elements that the bridge undergoes through where biological growth only grows with adequate growing conditions. It is to be noted that the bridge is located on an open field along a river and therefore, has no protection. The exposure to the elements might also be another accelerating factor for the corrosion of the members.


Figures 12 and 13. Bridge Condition: Corrosion of the Bottom of the Deck (left); Light Corrosion on the Section Over the Deck (right).

3.3 Previous Repairs

Between its erection and our current day and time, the bridge appears to have undergone through a few repair campaigns, however, all structural elements appear to be original. Such work could include repainting of the bridge upper part, i.e. the parts visible to its users which could have been associated with an anti-corrosion treatment, the repair of the asphalt route going over it (Figure 14) as well as the installation of temporary wooden supports along the diagonal cross-beams at the support (Figure 15). Such supports appear to prevent the bearing soil to further deteriorate. No documentation is available on any of these interventions, but they were possible to record through a visual inspection of the bridge. Further assessment could be conducted by, for example, doing a paint analysis of the various paint layers on the bridge or additionally by inspecting investigating the use of temporary supports.

Figures 14 and 15. Previous Repairs: Asphalt Layer (left); Temporary Wooden Supports (right).

4. MODELLING OF THE BRIDGE

A numerical model was created for the assessment of the load-carrying capacity and of the dynamic properties of the Bridge No. 11-097 Petrov nad Desnou. The modelling consisted of establishing the material properties of the bridge, its acting loads as well as a preliminary parametric survey of the bridge in order to obtain a more refined model.

4.1 Material Properties

Destructive testing was conducted on the bridge in order to determine the type of material used and its properties. In total, three specimens were taken in total from the bridge; two from an angle (U1, U2) and one from a plate (P1). In order to obtain further information on the type of steel used for the construction of the bridge, three test were conducted: the testing of the metallography of the steel, its chemical composition as well as the testing of its yield and ultimate strength.

In terms of the metallography of the specimens, all specimens contain very similar microstructure and metallic components. For the plate sample, P1, it has a ferric structure with cementite particles and small inclusion of sulfides or phosphides (Figures 16 and 17). For the two angle samples, U1 and U2, they also have a ferric structure, but with a small quantity of perlite and some inclusions of sulfides or phosphides for U1 (Figures 18 and 19) and with a small quantity of perlite and cementite and other intermetallic phases some inclusions of sulfides or phosphides for U2 (Figures 20 and 21). (ČVUT v Praze, 2019)

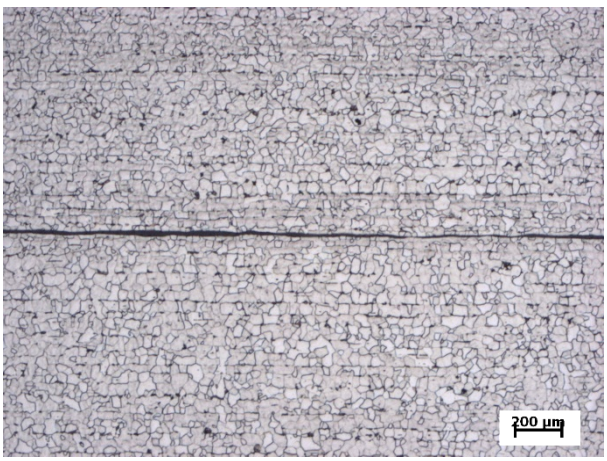

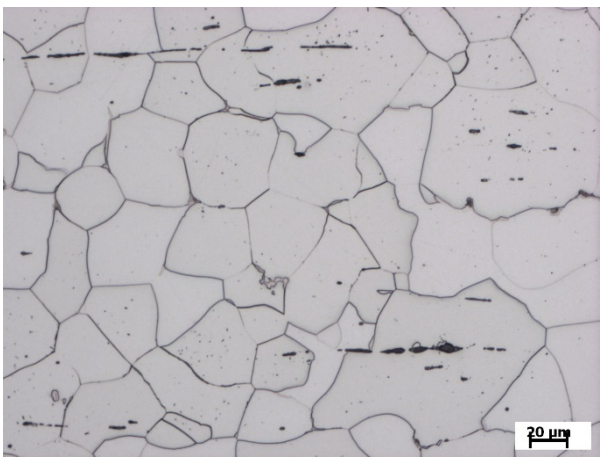

Figures 16 and 17. Metallography of P1: 25x (left); 200x (right). (ČVUT v Praze, 2019)

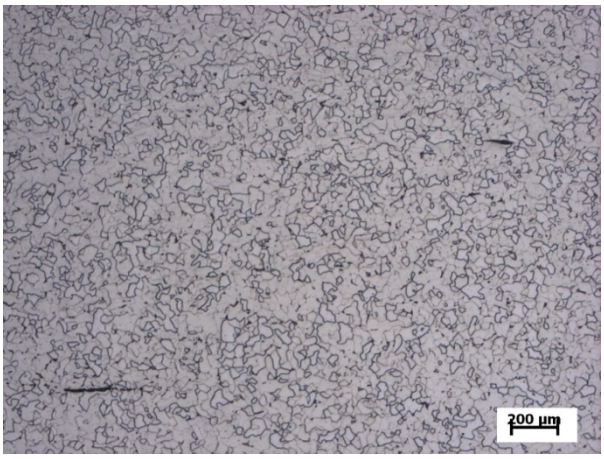

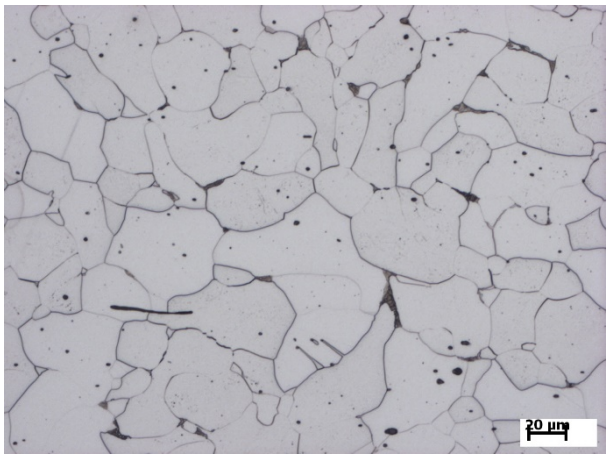

Figures 18 and 19. Metallography of U1: 25x (left); 200x (right). (ČVUT v Praze, 2019)

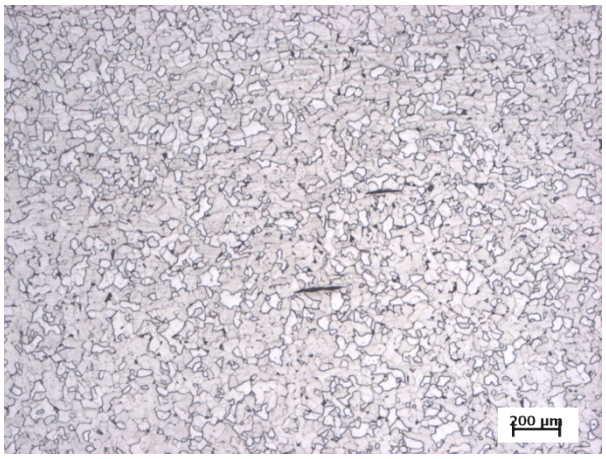

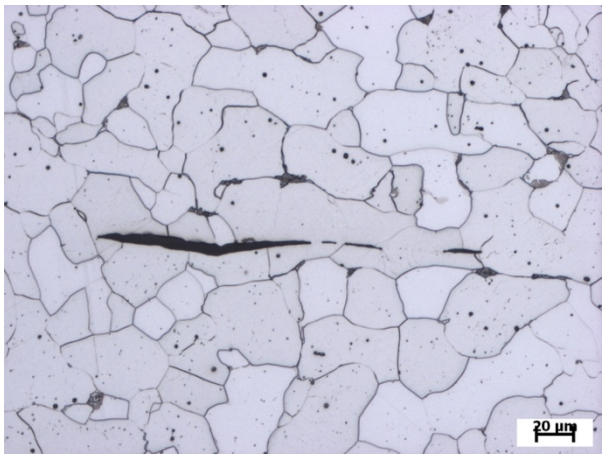

Figures 20 and 21. Metallography of U1: 25x (left); 200x (right). (ČVUT v Praze, 2019)

In terms of the chemical composition of the specimens, the test results indicated that for the plate, P1, and the two angles specimen, U1 and U2, the steel is composed of mainly of iron with some manganese and copper traces. Table 2 showcases the part of the chemical composition of each specimen with some of the critical minerals.

Table 2. Chemical Composition of the Specimens.

	C [%]	Si [%]	Mn [%]	P [%]	Ni [%]	Cu [%]	As [%]	N [%]	Sb [%]	Fe [%]
Plate, P1	0.06	0.012	0.293	0.005	0.02	0.159	0.042	0.021	0.022	99.09
Angle, U1	0.067	0.016	0.3834	0.011	0.013	0.133	0.046	0.028	0.024	99.01
Angle, U2	0.06	0.017	0.404	0.015	0.016	0.172	0.042	0.028	0.028	98.95

The last test conducted aimed to determine the yield strength and the ultimate strength of the material. The three specimens (P1, U1, U2) were then separated in three samples each and tested. Table 3 presents the results for each sample tested.

Table 3. Tested Material Properties of Steel Members.

Section	Sample	Yielding Strength	Ultimate Strength
Plate	P1-1	235 MPa	348 MPa
	P1-2	245 MPa	356 MPa
	P1-3	236 MPa	351 MPa
Angle	U1-1	301 MPa	397 MPa
	U1-2	300 MPa	398 MPa
	U1-3	288 MPa	380 MPa
	U2-1	280 MPa	412 MPa
	U2-2	283 MPa	395 MPa
	U2-3	283 MPa	390 MPa

Based on these results (Table 3), the yield strength and ultimate strength were then averaged separately based on the specimen type (Table 4). In addition, to obtain the stress-strain curve for the non-linear behaviour of each type of section, points along each curve were selected and then averages form a percentage elongation of 0, 0.2, 2, 5, 10, 15 and 20%. The averaged results are presented in Figures 22 and 23. From the all of the testing, the bridge was determined to be made of mild steel. It is to be noted that the angle properties were also used for the other rolled sections including the stringers and the ZORES sections. Furthermore, since the cross-sections for beam elements can only be assigned one material property, built-up section properties were based ratio of angle's and plate's properties where the area of the two materials is considered as well as the direction of the resisting moments.

Table 4. Updated and Averaged Material Properties of Steel Members.

Section	Yielding Strength	Ultimate Strength
Plate	238.7 MPa	351.7 MPa
Angle	289.2 MPa	395.3 MPa

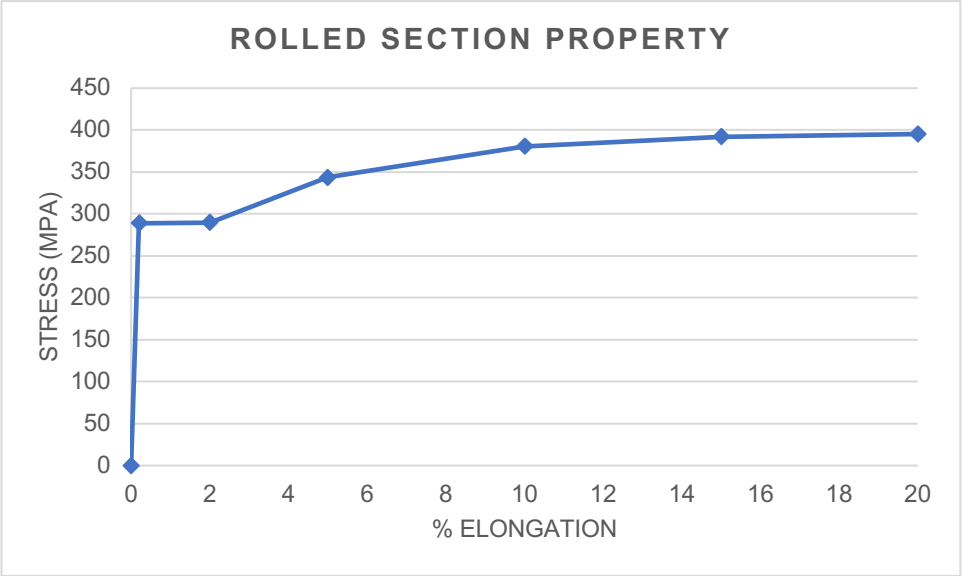

Figure 22. Material Properties of Rolled Sections.

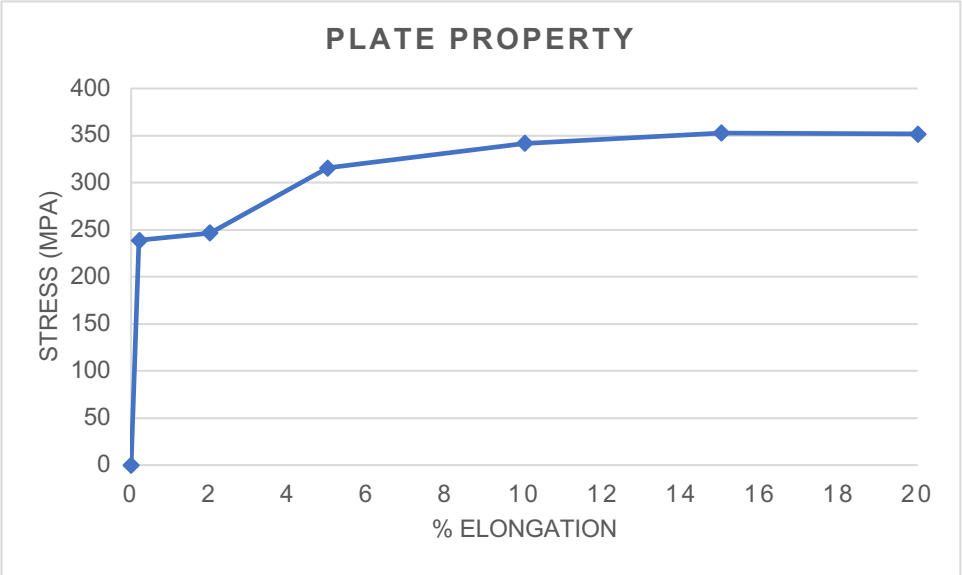

Figure 23. Material Properties of Plates.

Prior to the material testing, the material property of the steel in place were assumed to be S235 steel, which is a good estimate of the plate properties. However, once the results of the tested specimen were obtained they were used to update the preliminary numerical models. Table 5 presents the material properties range used for the preliminary model.

Table 5. Preliminary Model Steel Section Properties (Stančík, 2019).

Material Properties	Determining minimal load-bearing capacity (5% quantile)	Determining maximal load-bearing capacity (95% quantile)
Yield strength	$f_{y0,05}$ = 235 MPa	$f_{y0,95}$ = 296 MPa
Ultimate strength	$f_{u0,05}$ = 360 MPa	$f_{u0,95}$ = 419 MPa
Material model	linear elastic	real stress/strain curve
Failure limit	elasticity -> M /($f_{y0,05}$* W_{el}) < 1.0	full plasticity -> M /($f_{u0,95}$ * W_{pl}) < 1.0
Assumed material safety factor	$\gamma_{M,0}$ = 1.0	$\gamma_{M,0}$ = 1.0

In addition, the rivet properties were also updated from the preliminary models. No testing was conducted on the rivets in this study. The updated properties were based on the previous testing of single rivets of various dimensions and grip size. (Kulak, Fisher, & Struik, 2001)(Munse & Cox, 2007) Based on the resulting force versus deformation diagram obtained during the shear test of a 7/8 inch rivet with a 4 1/2-inch grip, a simplified model of the testing was created using beam elements as the rivets and shell elements as the shear plates with solid contact elements in between the plates as per the modelling of the connections in the main model. A rigid friction coefficient of 0.35 with a failure in tension was used. In addition, a prestressing load due to a temperature of -400 degrees Celsius was used to portray the installation of the rivets between the plates. The simplified model was observed to provide similar results to the experimental data when within the linear range of the rivets. Based on the previous study, the material properties of the rivets were then proposed to be an average of the testing results for the plates and angles therefore resulting in the properties presented in Table 6.

Table 6. Updated Rivet Properties.

Material Properties	Values
Yield strength	f_y = 264 MPa
Ultimate strength	f_u = 374 MPa

Prior to the modelling of rivet properties with a simple model based on experimental data, the rivet properties of the preliminary models were based on valid codes and are shown in Table 7 below. It can be observed that the previous given properties were much weaker than the new updated properties.

Table 7. Preliminary Model Rivet Properties (Stančík, 2019).

Material Properties	Values
Yield strength	$f_{y0,05}$ = 230 MPa
Ultimate strength	$f_{u0,05}$ = 360 MPa

Since a road overpasses on top of the bridge, the properties of the asphalt layer and of the gravel ought to also be considered for the modelling of the bridge. As a simplifying assumption, the two layers were joined together and modelled based on the properties presented to Table 8 below according to micro-modelling studies of asphalt behaviour. (Kim & Buttlar, 2009)(Dreher & Batterson, 1962)

Table 8. Asphalt Properties.

Material Properties	Values
Modulus of Elasticity	E = 10,000 MPa
Poisson's Ratio	v = 0.25
Coefficient of Thermal Expansion	$\alpha = 4*10^{-5}$ 1/K

In addition, the bridge was strengthened with SMA (shape memory alloys) from the German manufacturer Weimar. The properties of this material are presented in the table below (Table 9). The layout of the SMA's for strengthening purpose is discussed later in this thesis.

Table 9. SMA's Properties.

Material Properties	Values
Modulus of Elasticity	E = 173,000 MPa
Poisson's Ratio	v = 0.406
Coefficient of Thermal Expansion	$\alpha = 9.03*10^{-6}$ 1/K

4.2 Acting Loads

For the steel structure, a generalized density of 7700 kg/m^3 was assumed for the rolled sections. As for the built-up sections, the same density was assumed, but then multiplied by a factor from 1.1 to 1.35 in order to take into account the plates that were not included in the model for simplification purpose via the use of 3D beam elements. The information on the self-weight of the structure is presented in the table below (Table 10).

Table 10. Self-weight of the Steel Structure.

Properties	Density of steel	Gravitational acceleration	Load factor
Mild Steel	ρ_s = 7700 kg/m^3	g = 9.81 m/s^2	γ_m = 1.3

Additional acting dead loads included the road bed and the railing. For the road bed, the acting loads were based on the preliminary visit where an average thickness of $t_{g,avg}$ = 130 mm for the gravel layer and asphalt layers with a total thickness t_a = 80 mm were recorded. The properties changed from the preliminary model to the updated model due to the merging of the asphalt and gravel layers into a

shell in the updated model instead of only a dead weight in the preliminary model. Table 11 presents the additional loads self-weight for the update model and Table 12 for the preliminary models.

Table 11. Self-weight of Additional Loads.

	Combined Gravel and Asphalt	Load factor
Self-weight	γ_g = 20 kN/m^3	γ_{Goth} = 1.0

Table 12. Preliminary Self-weight of Additional Loads.

	Gravel	Asphalt	Railing	Load factor
Self-weight	γ_g = 15-20 kN/m^3	γ_a = 18-22 kN/m^3	g_r = 1.0kN/m	γ_{Goth} = 1.0

4.3 Preliminary Numerical Models and Parametric Study

Preliminary numerical models aimed to first determine the global behaviour of the bridge using more simplified models of the structure. This included a parametric study of the bridge leading to the creation of multiple models with a variation of some of the key parameters including the load effects, the model itself and resistance uncertainties (Table 13). The uncertainties due to loading were seen as a variance in self-weight, the uncertainties due to the model itself were described as rigidity of connections, geometric imperfections, rivet holes, and corrosion weakening, and the uncertainties due to resistance and material properties were present as the variance in the material behaviour. The material properties were assumed in some of these cases based on available literature, but the models were then later updated once further testing of the steel was conducted. As a general baseline, all models were produced using Dlubal RFEM 5.13 where 3D models of the created using 1D Euleur-Bernoulli type beams with six supports. (Stančík, 2019)

Table 13. Parametric Analysis (Stančík, 2019).

Uncertainties	Proposed Configuration	Final Configuration
L – Loading Uncertainties	L1 – Variance in material self-weight	L1 – Inferior values of material self-weight is used.
M – Model Uncertainties	M1 – Rigidity of vertical and diagonal members connection to main truss chords	M1 – Connections of vertical and diagonal members to main truss chords are considered rigid
	M2 – Rigidity of stringer to crossbeam connection	M2 – Stringer to crossbeam connection allows vertical rotations.
	M3 – Geometric imperfections	M3 – Geometric imperfections are neglected.
	M4 – Holes for rivets in basic material	M4 – Holes for rivets are neglected.
	M5 – Assuming corrosion weakening	M5 – Corrosion weakening is neglected.
R – Resistance and Material Uncertainties	R1 – Variance in material yielding and ultimate strength	R1 – The 95% quantile value of a before tested similar material yield and ultimate strength is used.
	R2 – Assumed material model (linear elastic or real stress/strain diagram determined by testing)	R2 – A real stress/strain material diagram is used.

As a result of the parametric study, the chosen model was determined to be the one with the highest load-bearing capacity to in order to assess the probability of collapse (Figure 24). These results were then used to determine the critical locations of the bridge and therefore to decide upon the best locations for monitoring and future testing in terms of strain gauges and accelerometers. This thesis is based on this preliminary model, which was then updated with more accurate material properties, a detailed connection and with experimental results from both static and dynamic testing.

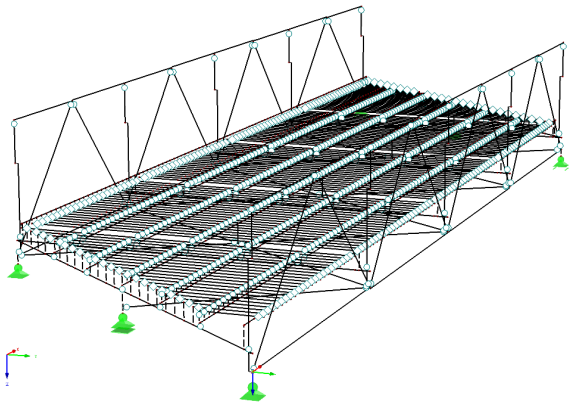

Figure 24. Preliminary Model (Stančík, 2019).

4.4 Updated Model with Connections

The primary objective of this thesis was to recreate a model with what was most critical connection in terms of failure, i.e. the centre lower chord connection and to create a calibrated model. In order to make an update model, the original preliminary beam elements model was updated by adding the centre lower chord connection as a mix of beam, shell, solid elements to represent the built-up sections, the gusset plates as well as the rivets.

First, the original model was modelled as beam elements and the cross-section of each member with the exception of the bracing was created with the software SHAPE-THIN from Dlubal. The material properties of each member were defined as per the tested material properties. In this regard, as a simplification, the rolled sections, including the bracing, the stringers and the “ZORES” sections, as well as a few built-up sections including the verticals, the cross-beams and the side beams were modelled with linear material properties. For the reminder, the truss elements including the diagonals, the upper chord and the lower chord were modelled with non-linear material properties.

As a base, the supports were modelled with a simplification using hinged connections for the Rýmařov side on either side of the bridge and rolled connections for the Šumperk side (Figures 25 and 26). In addition, the secondary supports were modelled as pinned connections. In order to connect the supports to the rest of the bridge structure, rigid links were used between the connection of the structural elements and the supports.

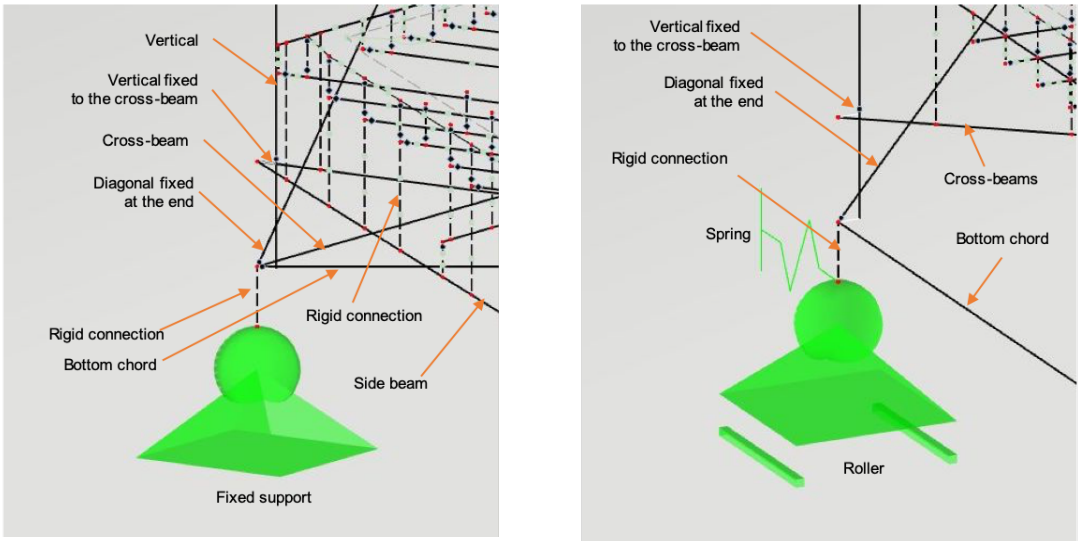

Figures 25 and 26. Connection: at a Hinged Support (left); at a Roller (right).

In regards to the connections between members, all connections at the top chord and bottom chord level were modelled as rigid with the exception of the one of the centre lower chord connection

modelled with shell elements and therefore exhibiting a semi-rigid behaviour. Therefore, the two ends of the diagonals and of the verticals were drawn as fixed. For the verticals, its end is fixed to the cross-beam (Figures 27 and 28). It is to be noted that throughout the model, member eccentricities were used in order to obtain the perfect match of the members at the connections.

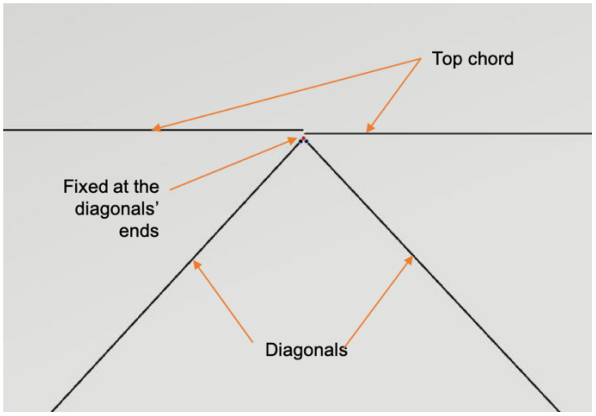

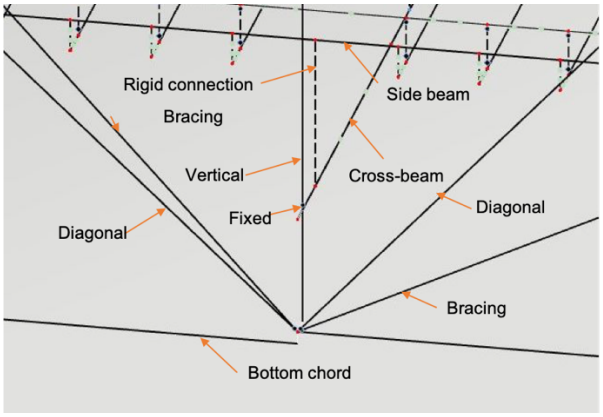

Figures 27 and 28. Rigid Connection: at the Top Chord (left); at the Bottom Chord (right).

The connection between the cross-beams and the stringers was done with a rigid element and the stringer ends were only allowed to rotate around the y-axis. For the deck composed of ZORES sections, these sections are connected to the side beams via rigid links with a hinge at the end of the ZORES beam elements and to the stringers via a rigid element allowing for rotation in z (Figure 29). For the bracing, the ends of the beam element are pinned to the main connections and where the two braces meet, one of the members is pinned at the junction and the other continuous due to the link between them found on site. Such link was then attached via a rigid connecting member to its respective cross-beam (Figure 30).

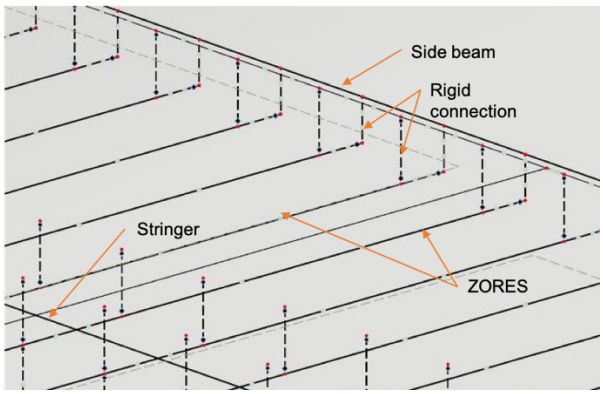

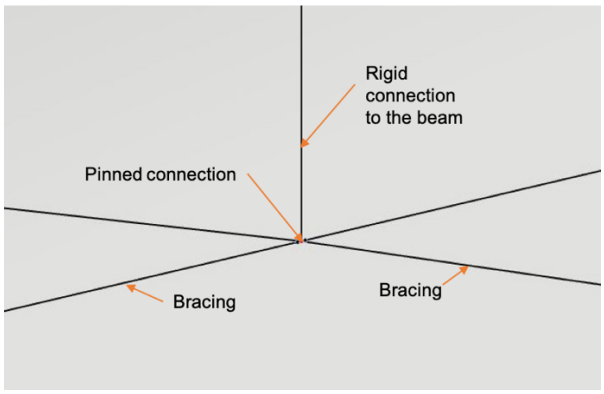

Figures 29 and 30. Connections: Deck (left); Cross-bracing (right).

For updating the original model, the centre lower chord connection was modelled as a mix of beam, shell, solid elements to represent the built-up sections, the gusset plates as well as the rivets (Figure

31). For the creation of this detailed connection, the gusset plates and built up sections composed of angles and plates were modelled as shell elements instead of beam elements as per the rest of the model. The material properties of each shell elements were modelled as non-linear as per the material properties presented in the previous chapter. In order to recreate the friction between the angles and plates, solid contact elements were used. The solid elements were given a rigid friction coefficient of 0.35 and an assumed failure under tension. In order to connect the detailed connection to the rest of the original model, rigid surfaces at the end of the cross-beam, the vertical and the two sides of the lower chord were modelled. The node linking the beam element to the shell was then connected to the new surface.

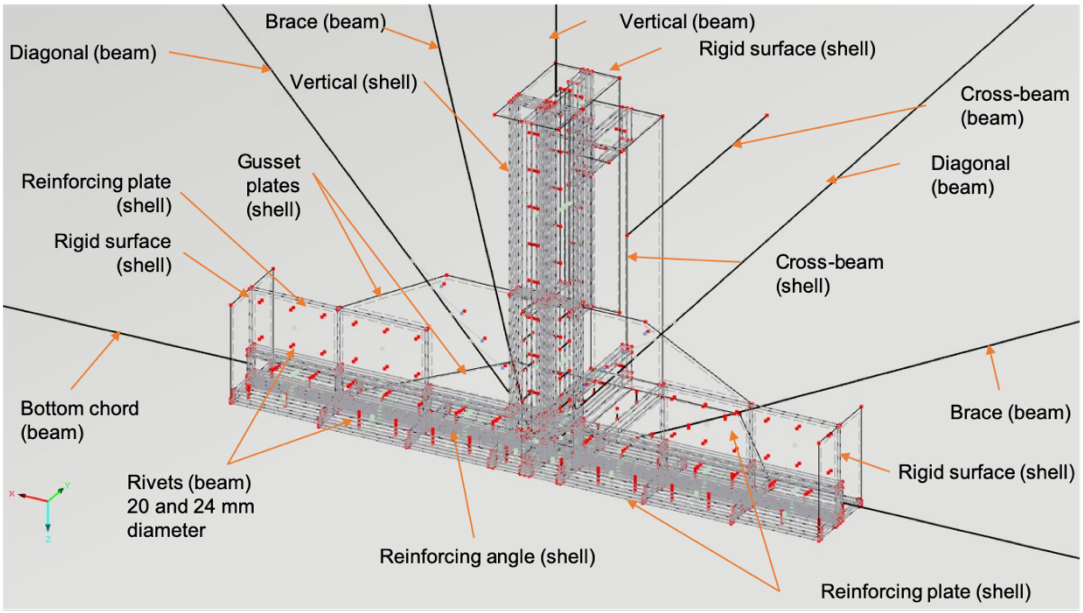

Figure 31. Modelled Connection with Gusset Plates.

In order to activate the friction between the shell elements, the same layout as found on-site for the rivets were used. Rivets size included 20 mm and 24 mm diameters. For the rivets to be modelled, beam elements were used with a non-linear behaviour at the member hinge based on the properties of rivet samples tested in previous studies (Figure 32). (Kulak et al., 2001; Munse & Cox, 2007) Such properties were modified with a 5% loading slope to simplify the modelling of the rivet behaviour and to reduce chances of creating instabilities in the model. In addition, a ratio between the ultimate strength of the rivets and of the rivets from the study was a completed furthering modify the curve. The ultimate strength of the rivet was then calculated using the $0.6*A_0*f_u/\gamma_m$ where γ_m was made equivalent to 1 and where A_0 is the area of the rivet. It was therefore calculated that the maximum resisting force for the 20 mm rivets was of 70.40 kN and for the 101.4kN. The curve was then limited to these values for the respective rivet size. In addition, since the diagonals were simplified in the model, only one line of the rivets was modelled instead of the pair of rivets along the diagonals due to time constraints. The

original detail should have one row of three rivets on the top angle and one row of 4 on the bottom angle. In order to account for this simplification, the rivet strength in the diagonal was modified with a ratio of 7/4 multiplied by 2 for the 24 mm diameter curve. This ratio takes into account the 7 rivets present in reality with the 4 rivets modelled and the factor of 2 represents the two existing shear planes modelled only as one due to the use of a simplified beam element. In terms of the small eccentricities for the existing rivets, they could not be modelled due to the simplification. Furthermore, in order to ensure the friction via contact elements between the shell elements for the plates and angles, a prestressing load based on a temperature of -400 degrees Celsius was imposed on the rivets. From this, the experiment conducted in the previous studies was reproduced via modelling and compared to the experimental data to confirm and to adjust the real behaviour of the rivets as modelled beam elements (Figure 33).

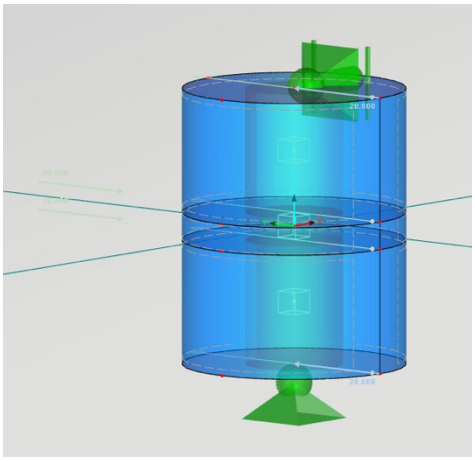

Figure 32. Modelled Behaviour of the Rivets as a Beam Element.

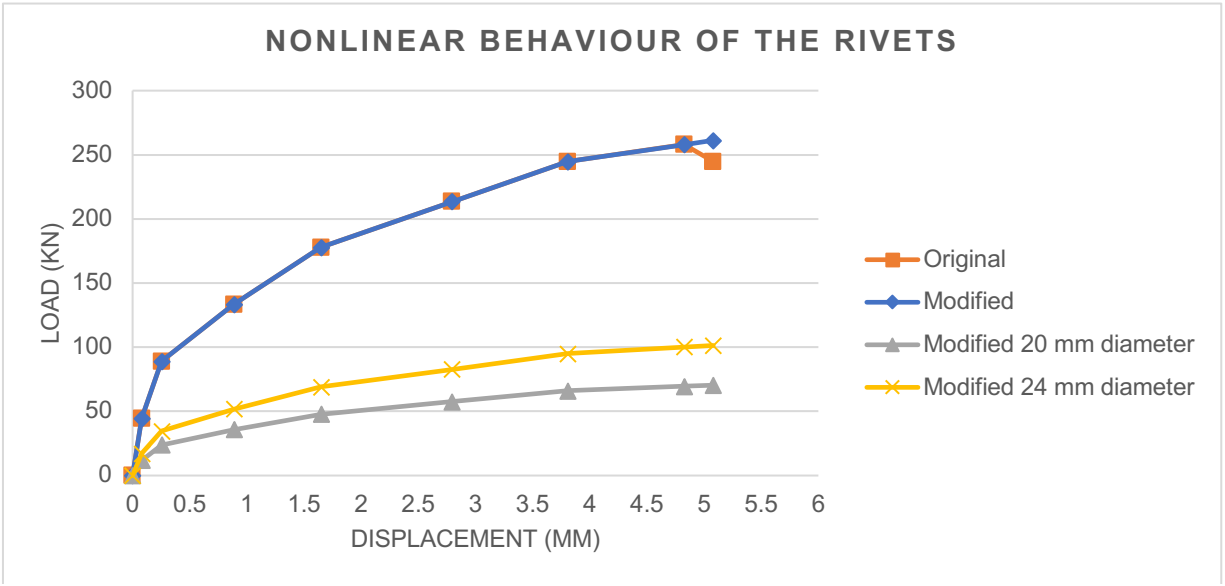

Figure 33. Behaviour at the Interface of the Rivets. (Kulak et al., 2001; Munse & Cox, 2007)

In addition, as an update to the original model, the asphalt and gravel layers were introduced as a shell element replacing only a dead load acting on the bridge deck. The shell element corresponding to the layer of both asphalt and gravel layers merged together is connected via rigid connections to the beam elements, including the ZORES sections and the cross-beams. A spring constant of 1 MN/m as a simplification for the member hinge was used to recreate the bond between the deck and the cross-beams. As it can be observed, the asphalt and gravel layers were assumed to be uncoupled to the rest of the structure.

In terms of mesh size for the whole model, a different mesh size was used for the beam and rigid elements as an update from the preliminary models. The shorter members were divided in 3 for the mesh when the longer members such as the truss elements as well as the cross-beams, stringers and bracing were separated in 10 divisions since more detailed information was required for these members. For the shell and solid elements at the detailed connection, a mesh size of 30 mm was used and in areas with a higher number of nodes, a reduced mesh size of 20 mm was used. The size of the mesh was critical to be similar to the rivet size as it permits to establish an appropriate distribution of the stresses near the rivets on the plates. For the asphalt shell elements, a mesh size of 200 mm was used.

Once the mesh was generated, a non-linear analysis was used using the Picard method up until convergence. The final updated model for the unstrengthen bridge is presented in Figure 34 below.

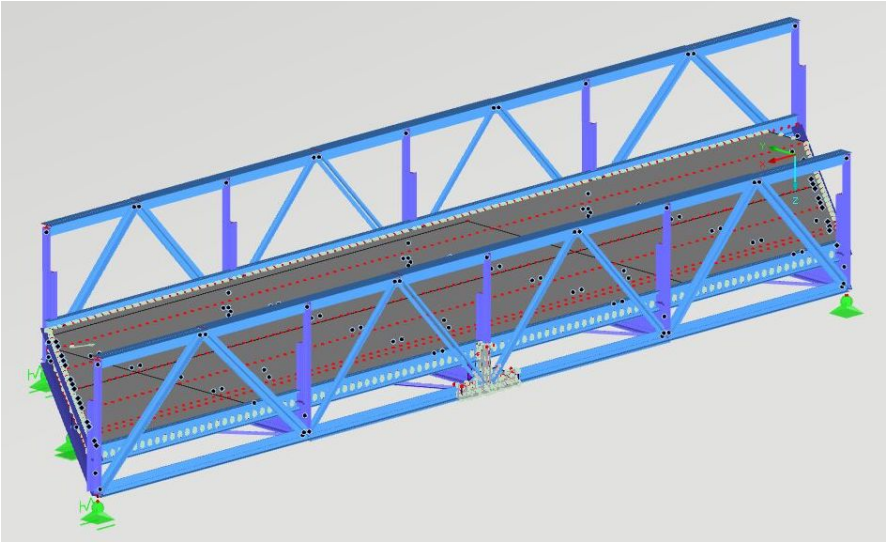

Figure 34. Unstrengthen Bridge Model with Detailed Connection.

5. VALIDATION OF THE MODEL

Two techniques were used in order to calibrate and therefore, validate the model prior and after the strengthening of the bridge. The models of the strengthened and of the unstrengthen bridge were updated based on monitoring data obtained via static load tests and dynamic testing.

5.1 According to Monitoring Data

A monitoring system was introduced on the bridge to better collect information on the real traffic and micro-seismicity of the bridge. Such system was then used to collect information during the static load tests and then later, for the testing of the ultimate capacity of the bridge.

5.1.1 Monitoring System

Based on the initial model that was selected as the most representative of the load-carrying capacity of the bridge, critical locations were selected for the monitoring as well as for both the static and dynamic testing of the bridge. The monitoring system includes 72 strain gauges, four potentiometers or displacement sensors in the z direction (x2) and in the y direction (x2), nine accelerometers in the z (x6) and y direction (x3) and eight temperature sensors. In addition, measurements of the river flow is also recorded. Figures 35 to 39 present the location of the sensors as well as their identification number: presented in blue are the strain gauges, in red are the accelerometers and in green are the displacement sensors.

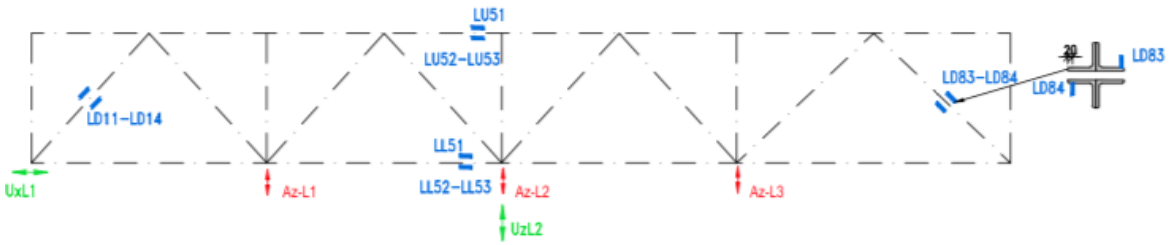

Figure 35. Monitoring Plan: North Elevation or Left Girder (Not to Scale).

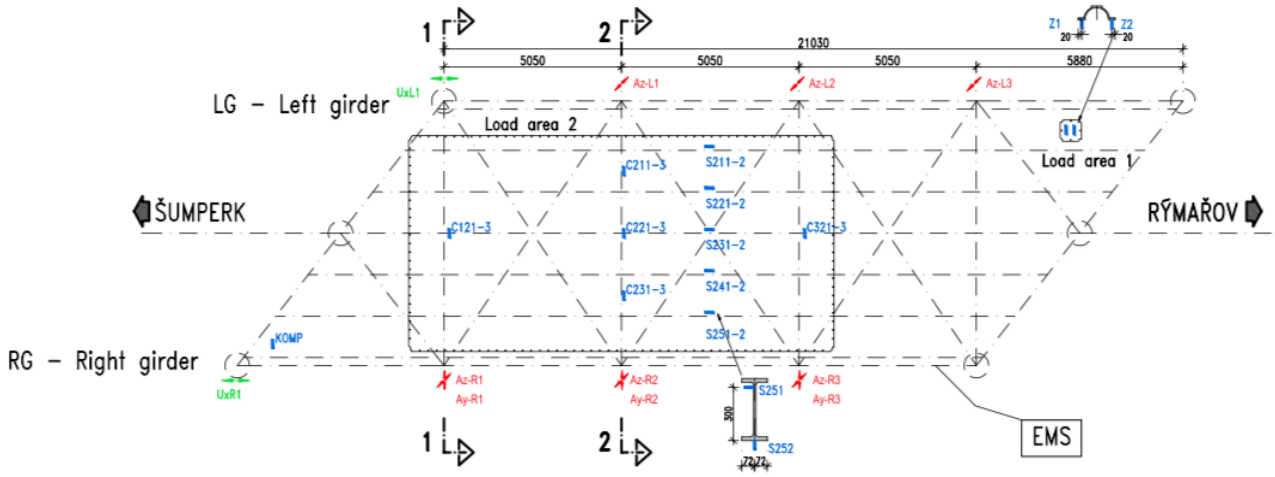

Figure 36. Monitoring Plan: Plan View (Not to Scale).

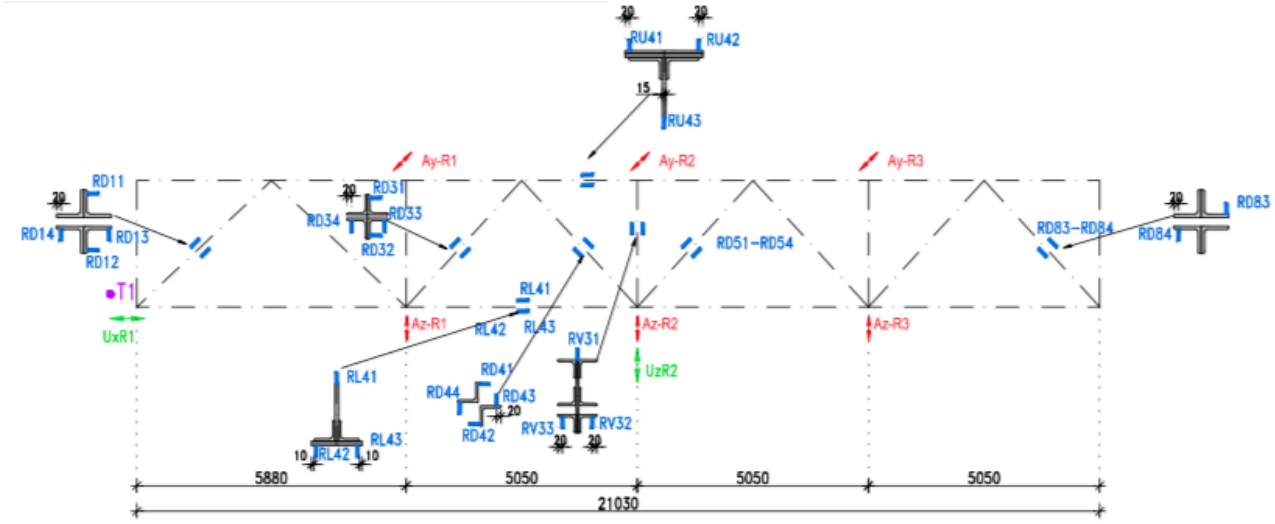

Figure 37. Monitoring Plan: South Elevation or Right Girder (Not to Scale).

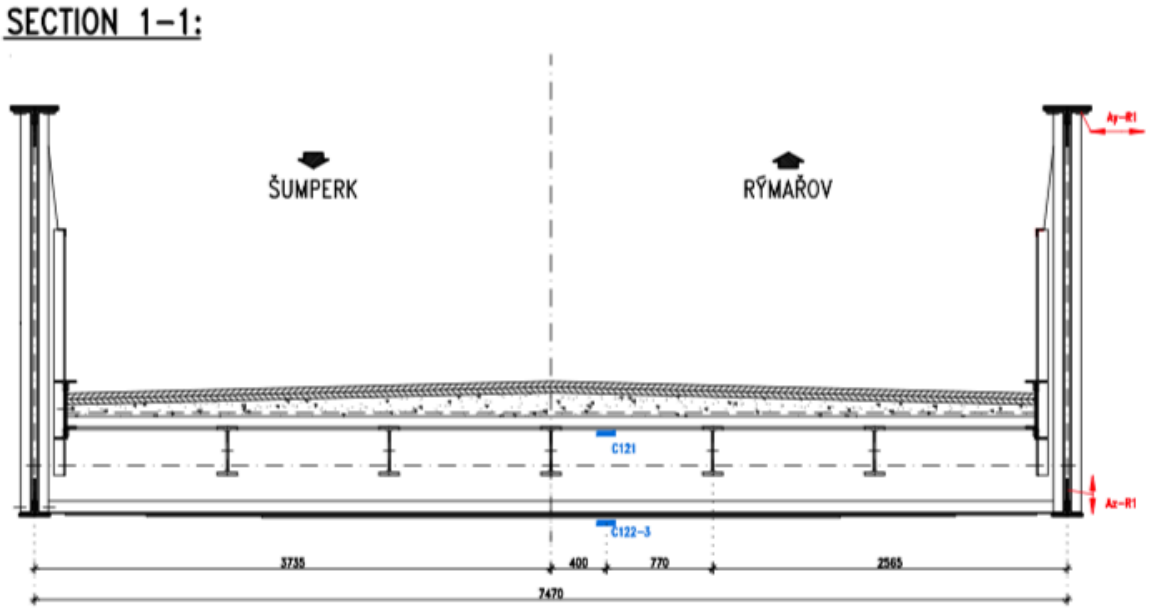

Figure 38. Monitoring Plan: Section 1-1 (Not to Scale).

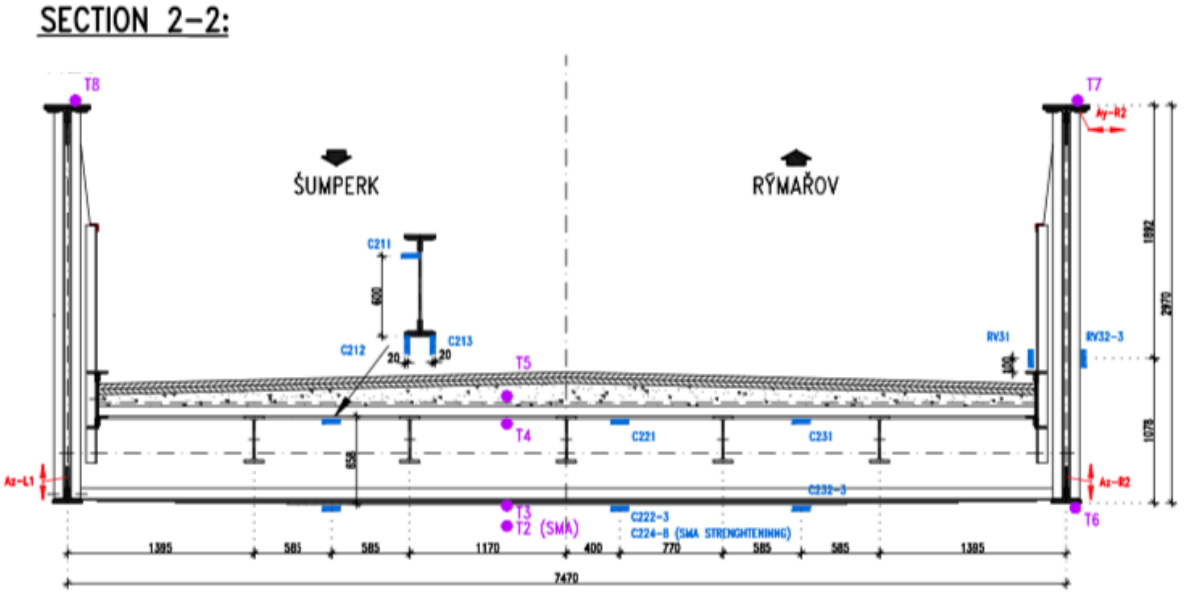

Figure 39. Monitoring Plan: Section 2-2 (Not to Scale).

The monitoring helped to obtain real traffic and micro-seismicity data regarding the bridge which also helped for the calibration of the numerical model in addition to obtain additional information during the conducted tests. Figures 40 and 41 present some of the monitoring devices used for this project.

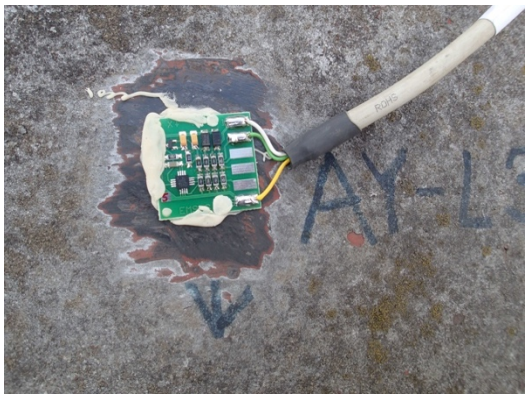

Figures 40 and 41. Monitoring Equipment: Strain Gauge (left); Accelerometer (right) (Ryjáček, 2019).

5.1.2 Load Test on Existing Bridge

The first load test was performed in the morning of May 20, 2019, on the bridge using a mobile crane LTM 1055-3.2 by Liebherr (Figure 42). The load of the crane was of 45.34 tons in total with 14.69 tons on the first axle and 29.46 tons for the combined second and third axles. Figures 43 and 44 depict two of the passages of the crane across the bridge.

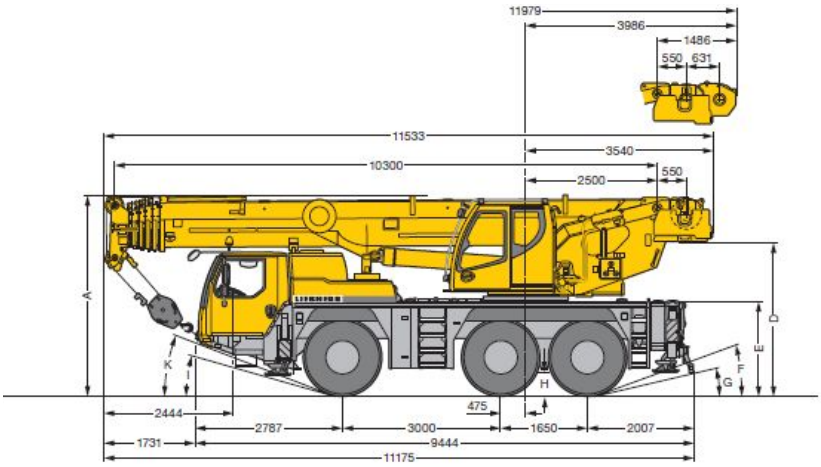

Figure 42. LTM1060 Crane (LIEBHERR, 2013).


Figures 43 and 44. Load Test Being Performed: In the Lane (left); On the Axis (right) (Ryjáček, 2019).

In total, 9 passages across the bridge were completed, including one that failed and that was, then, repeated at last. The crane was positioned in the lanes of both directions and also along the axis of the bridge. The testing was performed at various speeds including 5 km/h, 20 km/h, 30 km/h and 40 km/h. The different set ups are presented in Table 14 below.

Table 14. Load Test 1: Load Cases.

Load Case	Time	Speed	Direction	Location	Status
1	8:11:30	5 km/h	Šumperk	In the lane	Failed
2	8:14:00	5 km/h	Petrov	In the lane	Completed
3	8:17:00	5 km/h	Šumperk	Along the axis	Completed
4	8:22:00	40 km/h	Petrov	In the lane	Completed
5	8:23:30	40 km/h	Šumperk	In the lane	Completed
6	8:25:30	30 km/h	Petrov	Along the axis	Completed
7	8:28:00	40 km/h	Šumperk	Along the axis	Completed
8	8:31:00	20 km/h	Petrov	In the lane	Completed
9	8:33:30	5 km/h	Šumperk	In the lane	Completed, LC1 repeated

In order to obtain results from the load test, only the quasi-static or 5 km/h drive through were considered and compared to the results from the model. In addition, since the bridge is symmetric the model was only calibrated for one of the in-lane passages. From the monitoring system, the strains measured by the strain gauges along the critical members were recorded and then converted into stresses by multiplying with the modulus of elasticity of the mild steel. Then, on the model, the load per axle of the crane was modelled following the same path as per during the load test using the RMOVE add-on module from Dlubal to create moving point loads at intervals of 1.0 m along the bridge span. This resulted in more than a point per second. The faster speeds were only considered in order to better observe the dynamic properties of the bridge during the passage of the crane.

As part of the calibration a spring constant of 800 MN/m was added to the two monitored support according to the monitoring data presenting a movement of 0.2 mm of the bridge at the support. Moreover, the spring constant of 1 MN/m remained at the interface of the asphalt layer modelled as a shell element and of the steel deck and cross-beams modelled as beam elements. This resulted in the observation of an uncoupled behaviour between the asphalt and gravel layers to the rest of the steel structure.

The resulting stresses were then compared with the experimental data based on the strain gauges' readings. The complete results can be found in Appendix 2.1 for the passage in the lane going to Šumperk and Appendix 2.2 for the passage in the centre of the bridge also in the direction of Šumperk. In general, the shape of the curves of the models are similar to the experimental data and the values fit quite well. However, it can be observed that some discrepancies are present between the model and the experimental data. Most smaller lack of accuracy can be assumed to be caused by the limited number of nodes in the model for each cross-section of the beam elements and the mesh size or division of the members, therefore, in areas of great moments a small error in location and the results can be quite different. Moreover, the exact location of the crane is also unknown and may affect the resulting stresses. Furthermore, another observation is that the stresses tend to generally be higher for the stringers and cross-beams in the model which can be caused by the simplifications in terms of member hinges, i.e. fixed versus hinge connections, when truly the connection showcases a semi-rigid behaviour that is closer to a fixed connection than to a hinged connection. For the purpose of this study, six groups of strain gauges representing each member group will be compared in terms of experimental and modelled data and general observations will be made on the members' stresses.

It can be observed that the largest stresses can be found in the cross-beams for the unstrengthen case, in particular in the two central cross-beams. Based on this observation, the strengthening of the bridge was focused on reinforcing one of the cross-beams with the SMA technology. In terms of behaviour, the stresses near the top flange tend to be less accurate than the lower flange stresses. This can be explained by the condition seen between the asphalt and gravel layers. During the calibration, it was observed that by changing the connection between the top flange and the asphalt, the best assessment of the bond was to be uncoupled. The examples in Figures 45 and 46 showcases the typical behaviour of the cross-beam at mid-span, which illustrates this difference at the top flange. For the bottom flanges, the shape and magnitude for the stresses are quite accurate and in some instances, almost exact. However, it is to be noted that a greater difference can be observed for the strain gauges located closer to the support along the beam. This is estimated to be due to the lack of nodes from the mesh along the member making it difficult to select the exact location of the strain gauge. This is even more critical in areas of high moments which is characteristic of the cross-beams. A comparison can be made between the location of the crane between the two graphs where it can be observed that when the crane is in the centre of the bridge, this creates the highest amount of

stresses at the centre of the cross-beam as when being offset to one of the lanes, the amount of stresses if reduced.

In summary for the cross-beams, a difference between the top of the web experimental and modelled data at the peaks generally is of about 25%- 50% and for the bottom flange is 0%-30%. In addition, the values for the top of the web peaks around -11 to -17 MPa and for the bottom flange around 15 to 50 MPa.

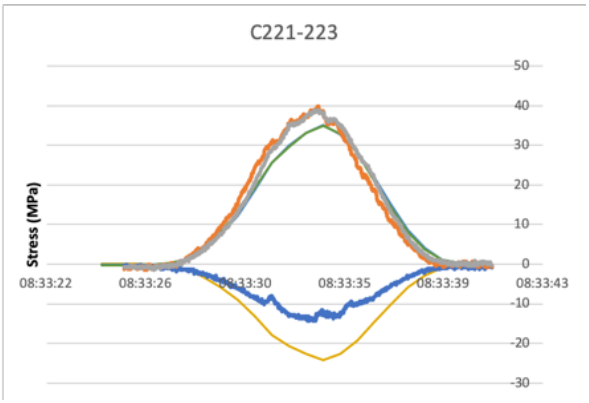

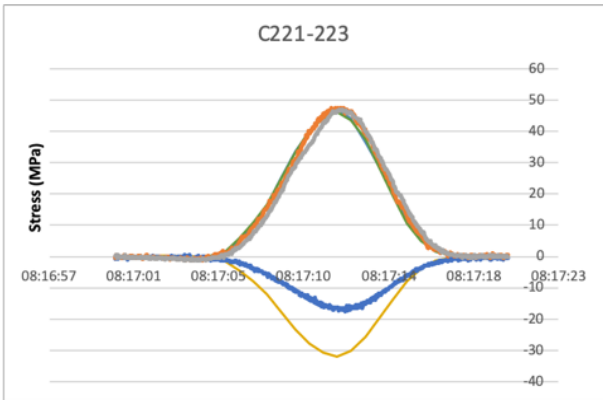

Figures 45 and 46. Calibration of the C221-C223 Cross-beam for the Unstrengthen Bridge: in the Lane (left); on the Axis (right).

In general, the stringers showcase a good response in terms of the calibration of the model. It can be observed on some of the stringers' response that in certain locations the stresses caused by the three axles are visible and that the central axle tends to lead to the highest stresses on this type of member. This response is also normally seen in the model. However, the stresses in the top chord tend to be less accurate than the lower chord stresses. The stringers showcase the same behaviour as per the cross-beams in this regard. This therefore also appears to be caused by the condition seen between the asphalt and gravel layers which was determined to be uncoupled. In addition, for most of the stringers model response, a lag of the shapes can be observed even if well-fitting and this can simply be caused by the change in speed of the driver (Figures 47 and 48).

In summary, for the stringers, a difference between the top flange experimental and modelled data at the maximums and minimums generally is of about 50%-60% and for the bottom flange is 5%-35%. It is to be noted that high percentage stresses in this case are often related to small stresses difference, i.e., the difference between -1.6 MPa and 2.8 MPa. In addition, the values for the top flange peaks around -2 to -17 MPa and for the bottom flange around 10 to 44 MPa.

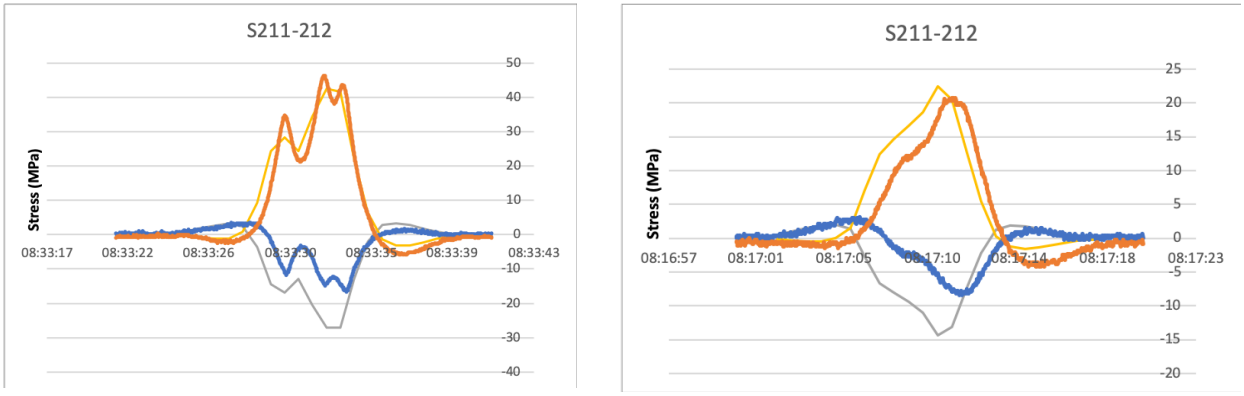

Figures 47 and 48. Calibration of the S211-S212 Stringer for the Unstrengthen Bridge: in the Lane (left); on the Axis (right).

Looking at the truss elements as a whole, the behaviour of the members is adequate in terms of shapes with a few exceptions. Looking first at the lower chords, the modelled lower chords exhibit a behaviour that is quite similar in terms of shape and stresses magnitude. The bottom flange behaviour is quite nicely fitting with a percentage difference of only 5% to 12%. However, in this case, the web behaviour is inadequate and result in a discrepancy with a percent difference of about 200%. This could be due to improper distribution of the moments across the member. This behaviour only occurs for the bottom chord on the left girder and is not being observed for the right girder (Figures 49 to 50).

As a summary, in general, a difference between the bottom flange experimental and modelled data at the peaks is only 5% to 12% as previously mentioned and for the web is 15%. Such difference is calculated by excluding the presented outlier in the figures below. In addition, the values for the bottom flange as per the experimental data peaks around to 6.5 to 13 MPa and for the web around 10.5 to 23 MPa.

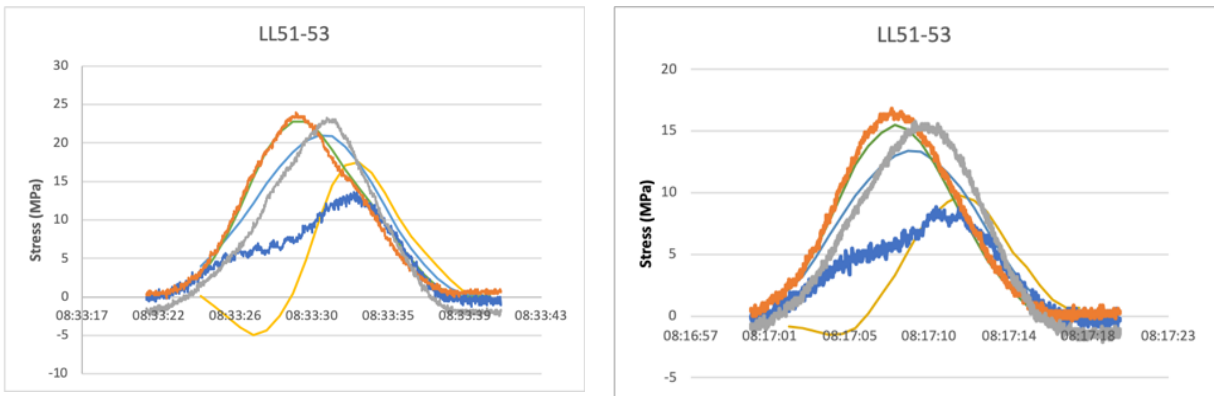

Figures 49 and 50. Calibration of the LL51-LL53 Lower Chord for the Unstrengthen Bridge: in the Lane (left); on the Axis (right).

Regarding the upper flange, a trend that was observed is that when the crane is located on the same side of the strain, the modelled stresses are greater than the experimental ones as when it is one the opposite side, the opposite phenomenon occurs. This might be due to the fact that the exact location of the crane in the lane is unknown and the chosen location for the calibration might be slightly offset to the true location of the crane. When looking at the behaviour of the modelled data according to the experimental data, it can be observed, in this case, that the position of the crane as an impact on the accuracy of the results. The percentage difference for when the truck is in the lane is at a maximum of 17% in this case and when on the axis, it is of maximum 7% (Figures 51 to 52). In terms of the shape of the stress curve, the results are quite satisfying. In general, a difference between the top flange experimental and modelled data at the maximums and minimums is 0%-20% and for the web is 0%-30%. In addition, the values from the experimental data for the top flange peaks around -17 to -36 MPa and for the web around 2 to 11 MPa.

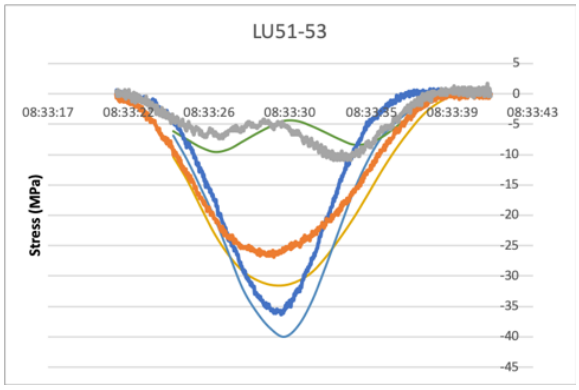

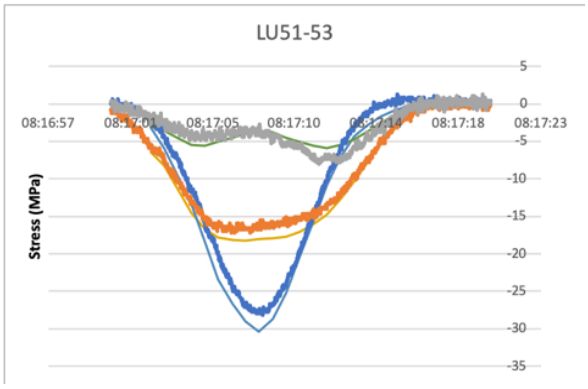

Figures 51 and 52. Calibration of the LU51-LU53 Upper Chord for the Unstrengthen Bridge: in the Lane (left); on the Axis (right).

Looking at the diagonals, there is a wide range of behaviour and disparities depending on the type of diagonal and their location across the truss. Mostly, the stress curves for the diagonals are similar from the model to the experimental data and the main differences occur in the accuracy of the peak values in some instances. From the calibration, it can easily be observed that the members of the truss next to the lane being driven by are more stressed than the ones on the opposite side and that a passage on the axis permit a more equal distribution of the stresses between the two trusses. For example, Figures 53 and 54 present a mid-span diagonal which represents the typical behaviour of the diagonals. Stresses across the angles forming will slightly vary often being over or underestimated by a small percentage. Some other diagonals such as RD83-84 presents larger discrepancies as its mirrored diagonal LD83-84 behaves very closely to the true behaviour collected on site (Appendices 2.1 and 2.2). This different behaviour might be induced by the fact that the bridge is skewed providing therefore different results in this case. In general, a difference between the experimental and modelled data at the peaks is 0%-190%, therefore, highlighting the wide range of behaviour, and the peak values from the experimental data range from -19 to 27 MPa.

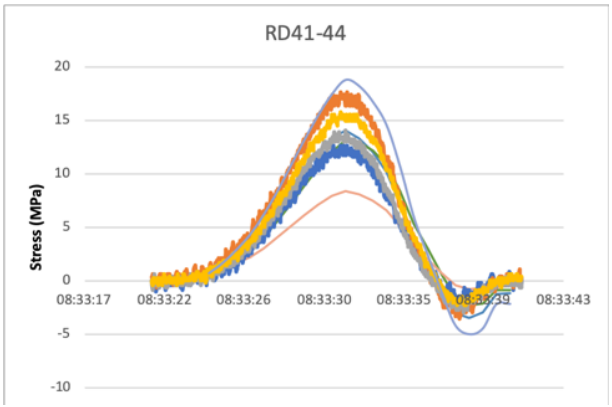

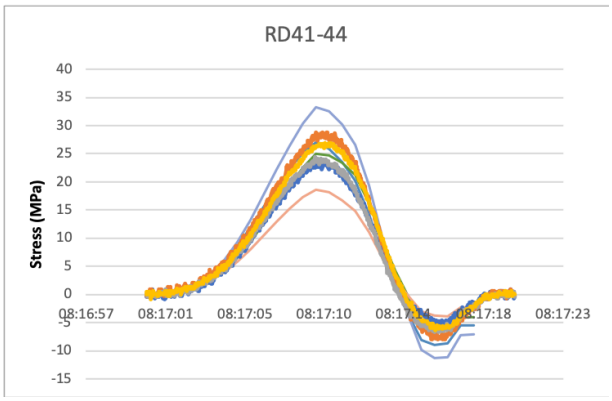

Figures 53 and 54. Calibration of the RD83-RD84 Diagonal for the Unstrengthen Bridge: in the Lane (left); on the Axis (right).

In summary, based on the observation of the experimental results and the comparison of the model's response to them, a few conclusions can be made. For example, f the crane is close to the member, normally greater stresses can be observed as a comparison between the two passages. The axis passage tend to provide more accurate resulting from a better knowledge of its location on the bridge. Additionally, the top flange of the cross-beams and stringers display a greater percentage error due to the lack of understanding of the bond between the asphalt and the steel structure and therefore as s a recommendation, it would be interesting to further investigate on the topic with destructive testing. It can therefore be concluded that the general behaviour of the model according to the experimental data is adequate since the stress curves are almost identical with a few exceptions.

5.1.3 Load Test after the Bridge Strengthening

SMA's or Shape memory alloys were used for the strengthening of the bridge on June 6, 2019, on the cross-beam with strain gauges C211-223, C221-223 and C231-233 (Figures 55 and 56). The application of such a product for the reinforcement of steel constructions and bridges up to this date had actually only been done in a laboratory context, but for the first time with this project, we assisted to its installation on a real structure. The reinforcement of the member was recommended following the preliminary study of the bridge by the project team in order to ensure that the collapse of the bridge would not first be led by the failure of this particular cross-beam, but instead by the failure of the main trusses. The strengthening consisted in the installation of strips of 6 layers of 1.5 mm thick and 120 mm tall of SMA. The reinforcing system was anchored using two back-to-back L150x80x10 with M20 bolts between the angles and the SMA and between the angles and the cross-beam with the whole system measuring 5.0 metres on the centre of the cross-beam. This material was chosen due to its ease of anchorage in comparison to other prestressing strengthening techniques which ought to increase either the fatigue resistance or the load capacity of the members. This material has the particular ability to restore its original shape after heating it and can be more simply anchored via the

use of prestressed screws. The procedure first started by exposing the SMA's to normal environmental temperatures and to then anchor it to the structure to be reinforced with the previously prescribed anchorage system. Then, the SMA was heated to an activation temperature of 260 degrees Celsius reaching 431 MPa followed by a cooling period. Once fully cooled, a new strain gauge, C224, was installed on the SMA strip for further monitoring. (Stančík, 2019)

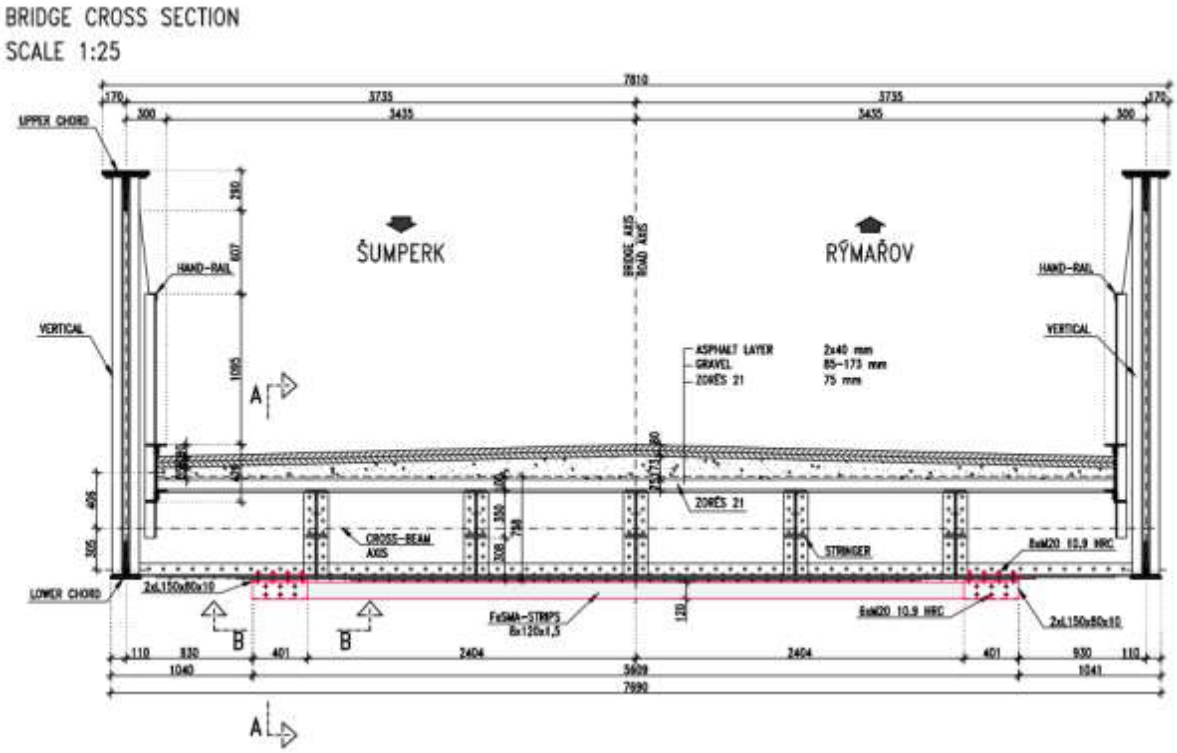

Figure 55. Location of the SMA Strengthening at the Cross-beam on the Bridge (Stančík, 2019).

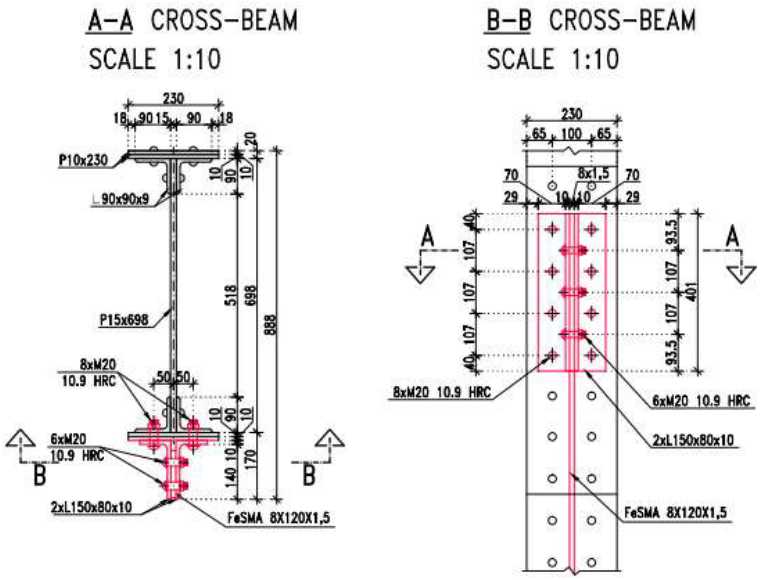

Figure 56. SMA Strengthening Anchorage System (Stančík, 2019).

Prior to the on-site installation, a laboratory testing conducted on May 30-31, 2019 was performed to verify the SMA's applicability under real operating conditions. In addition, the testing permitted to establish the best activation technique for once on site. Figure 57 presents the test setup which consisted of a small scale representation of what would be performed on the bridge. A test I beam was used onto which the same anchoring system as for the bridge was anchored to the beam. In this case, the SMA was first activated at 140 degrees Celsius and then, finally, activated at 260 degrees Celsius. The time of heating was recorded in order to know better on what to expect on site. The system was heated with ceramic pads on both sides of the SMA covered by thermal insulation up to the desired temperature which was monitored by thermocouples. At the same time, strain gauges were also used to measure the strain in the test beam and track sensors were also used to measure the vertical deflections occurring in the beam. (Stančík, 2019)

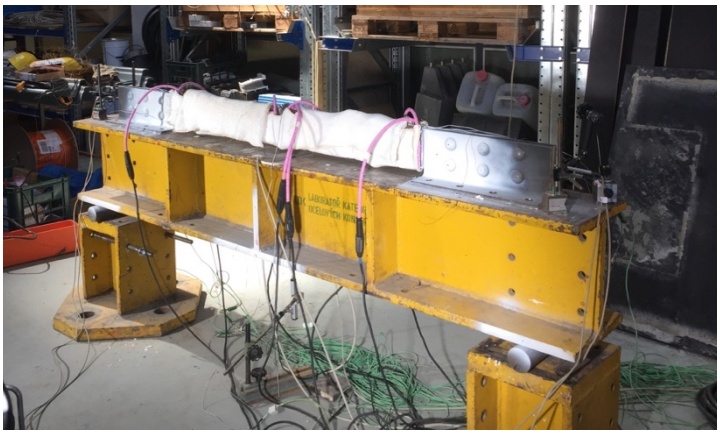

Figure 57. SMA Strengthening Laboratory Testing.

In order to take into account the installation of the strengthening in the updated model, three more elements were added to the model. A new beam element was used to depict the SMA strips merged all together and two rigid elements at the end of the beam element were added to connect the SMA to the reinforced cross-beam. The rigid elements for the link between the cross-beam and of the SMA permitted the simplification of the model (Figure 58). A prestressing load due to a temperature of -260 degrees Celsius should normally be applied to the SMA, however, since only the live load of the crane was being considered in this calibration and since the strain gauge on the SMA was only activated after its heating, the prestressing force was only used for the last step, i.e. determining the ultimate capacity of the bridge model. Figure 59 presents the reinforced bridge model with the SMA below the cross-beam in green.

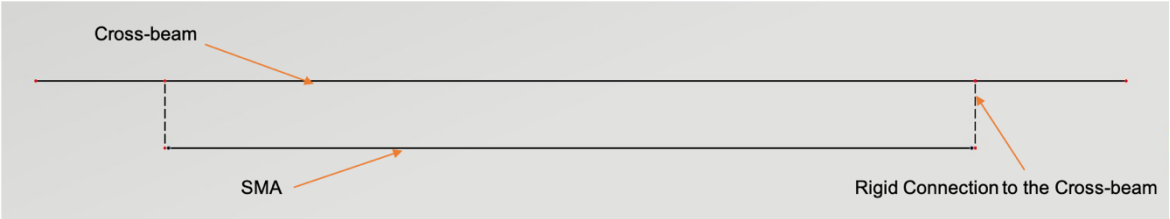

Figure 58. SMA Model.

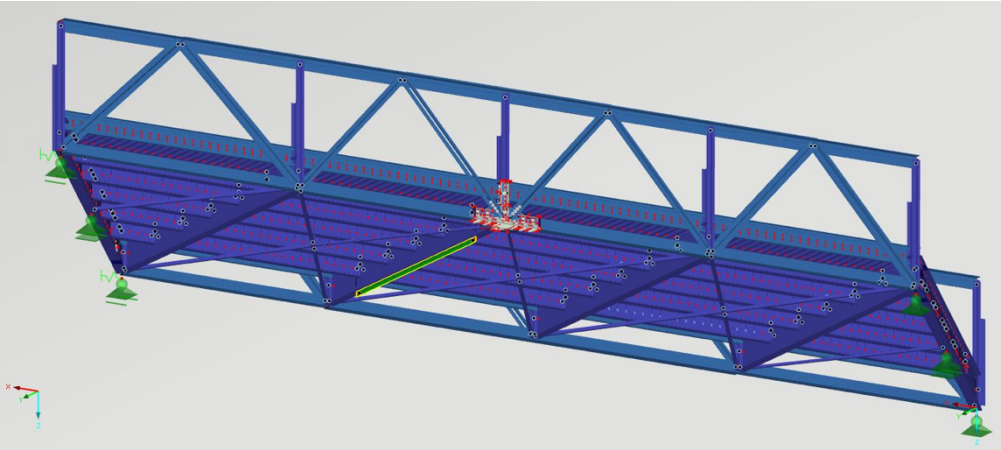

Figure 59. Strengthened Bridge Model (SMA in green).

Once the installation of the strengthening system was completed and full cooled and any additional measuring devices installed, an additional load test was performed again using the same crane. Additionally to the similar load cases from the previous load test, break and acceleration cases were also performed in this instance. Table 15 below showcases the load cases for this load test.

Table 15. Load Test 2: Load Cases.

Load Case	Time	Speed	Direction	Location	Status
1	8:17:00	5 km/h	Šumperk	In the lane	Completed
2	8:20:00	5 km/h	Petrov	In the lane	Completed
3	8:26:00	5 km/h	Šumperk	Along the axis	Completed
4	8:28:50	34 km/h	Petrov	In the lane	Completed
5	8:31:30	40 km/h	Šumperk	In the lane	Completed
6	8:34:10	40 km/h	Petrov	Along the axis	Completed
7	8:40:00	40 km/h	Šumperk	In the lane	Completed, LC4 repeated
8	8:47:50	Break + acceleration	Petrov	Along the axis, first axle 0.6m before the lane	Completed
9	8:52:20	Break + acceleration	Šumperk	Along the axis	Completed
10	8:55:10	Break + acceleration	Petrov	Along the axis	Completed, LC8 repeated

The full calibration based on the second load test is presented in Appendix 2.3 for the passage in the lane going to Šumperk and Appendix 2.4 for the passage on the axis going to Šumperk. In this section, the same strain groups attached to a member as for the first load test will be analyzed based on experimental data from the strain gauges' readings and on the model response. Similar observations can be made on the response of the model. For examples, in most cases, the shape of the curves of the models is similar to the experimental data and the values fit quite well. However, discrepancies can still be noted between the model and the experimental data. This lack of accuracy can again be assumed to be caused by the limited number of nodes in the model for each cross-section of the beam elements and the mesh size or division of the members. In addition, the exact location of the crane is also unknown and may affect the resulting stresses.

In general, one can observe that with the strengthening, the cross-beam with the strain gauges C121-C123 and C321-C323 now have the highest stress concentrations depending on where the second and third axles of the crane are located. It is the most critical when the axles are located just over the cross-beams. Figures 60 and 61 showcases the results from the strain gauges at the mid-span of the now reinforced cross-beam. In general, the stresses in this member are almost the same as for the previously unreinforced beam. This can be explained by the fact that the member is still not loaded enough to rely on the strengthening system and instead it works together with the SMA. This is showcased by a very similar stress distribution between the cross-beam and the SMA. Again as previously mentioned as for the unreinforced beam, the stresses near the top flange are on average less corresponding to the experimental data than the lower flange stresses. This appears to be due to the type of existing bond that can be found between the asphalt and gravel layers. For the bottom flanges, the shape and magnitude for the stresses remain quite accurate. An exception can still be seen in the graph C231-233 for the in-lane passage, where the strain gauges are located about 2 m away from the mid-span, during the passage in the lane where the top flange behaviour is more corresponding to the bottom flange. In this particular case a percentage error for the bottom flange is of 70% when for the top flange of about 10% (Figure 62). Furthermore, on the opposite side of the bridge axis, C211-213 also presents a different behaviour where the model also assumes a similar amount of stress in the top flange and the bottom flange when it is quite dissimilar. This might be caused by the simplification of the connection of the SMA to the cross-beam via only one rigid connection at each end of the beam element representing the SMA and such behaviour is not reflected when the crane is on the axis of the bridge (Figure 63).

In summary for the cross-beams, a difference between the top of the web experimental and modelled data at the peaks generally is of about 0%-25% and for the bottom flange is 0%-30% with disregard to the aggravated cases previously discussed. In addition, the values for the top of the web peaks around -9 to -17 MPa and for the bottom flange around 30 to 52 MPa. Such results, showcase quite a

similar behaviour to the unstrengthen model with the exception of a higher range of peak values at the bottom flange for the reinforced bridge.

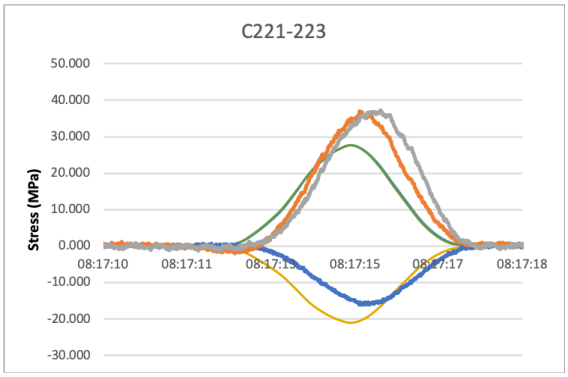

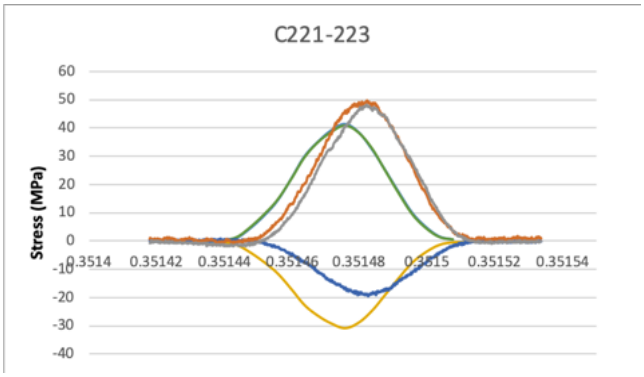

Figures 60 and 61. Calibration of the C221-C223 Cross-beam for the Strengthened Bridge: in the Lane (left); on the Axis (right).

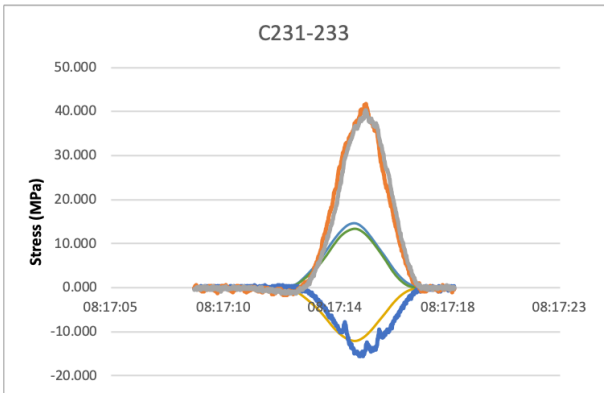

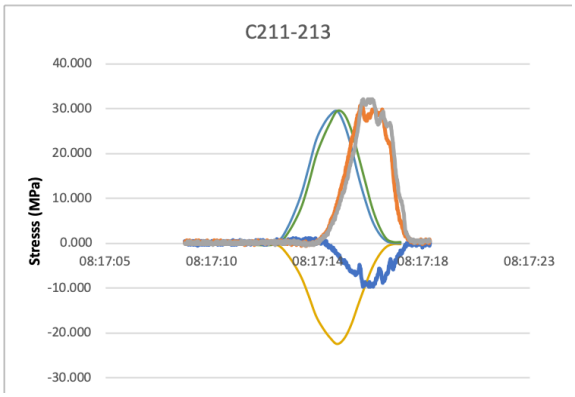

Figures 62 and 63. Calibration of the Reinforced Cross-beam for the Strengthened Bridge: C231-C233 in the Lane (left); C211-C213 in the Lane (right).

In terms of the behaviour of the SMA, it can be observed that it is quite accurate and varies from 10 to 20%. This could be explained by the simplification of the anchorage system via the simple use of two rigid elements at the end of the SMA strip instead of the installed angles and prestressing bolts on-site. (Figures 64 and 65)

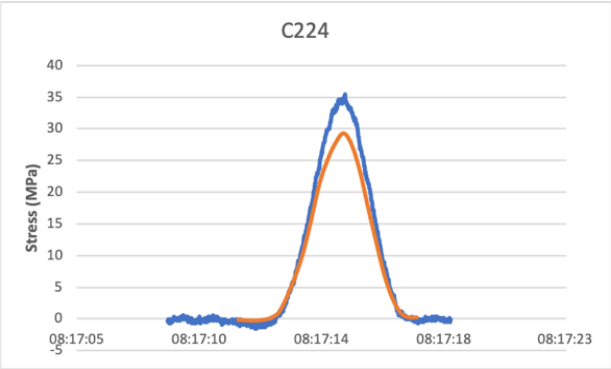

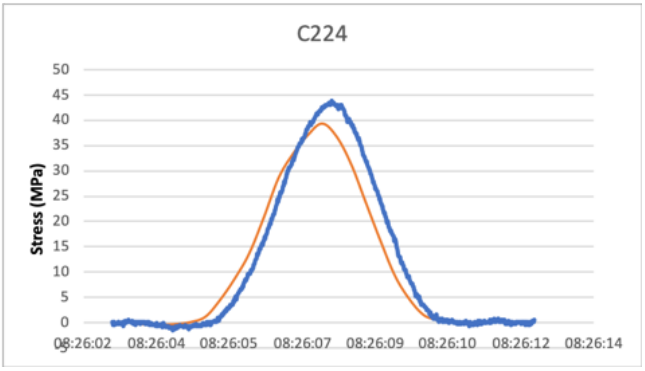

Figures 64 and 65. Calibration of the C224 SMA for the Strengthened Bridge: in the Lane (left); on the Axis (right).

In general, the stringer response from the strengthened model is quite adequate. The misalignment of the shape as for the Figure 67 can simply be caused by the inconstant speed of the moving crane during its passage. All the shapes of the stringer appear to be corresponding, but a difference in between the stresses for both the top flange and lower flange can still be observed as shown in Figures 66 and 67. In general, a difference between the bottom flange experimental and modelled data for the peak values is 0%-35% as previously mentioned and for the top flange is 20%-50%. In addition, the values for the bottom flange as per the experimental data peaks around to 17 to 46 MPa and for the top flange around -2.5 to -19 MPa.

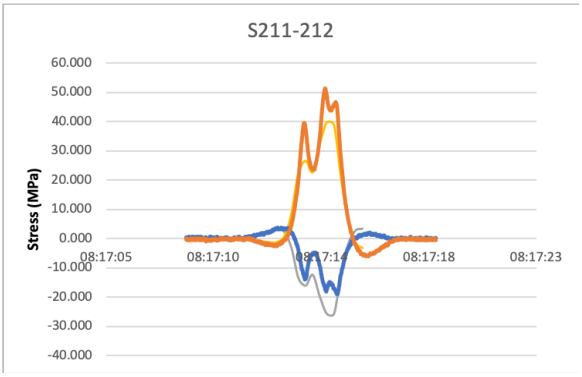

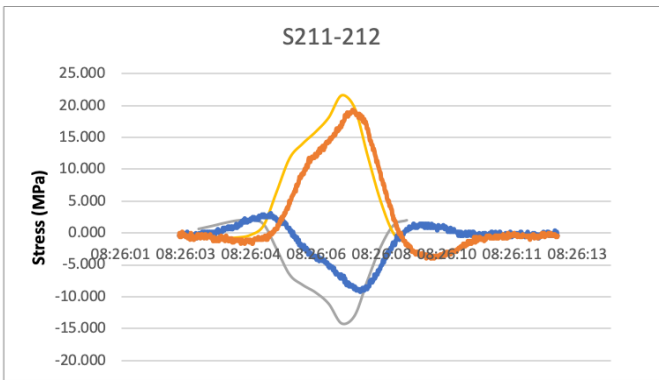

Figures 66 and 67. Calibration of the S211-S212 Stringer for the Strengthened Bridge: in the Lane (left); on the Axis (right).

In terms of the lower chord of the trusses, a similar behaviour can be observed with the reinforcement of the bridge. The correspondence between the shapes related to the experimental readings remains the same as shown in Figures 68 and 69. In general, a difference between the bottom flange experimental and modelled data at the peaks is of 12%-30% and for the web is 10-40%. Such difference is calculated by excluding the presented outlier in the figures below. In addition, the values for the bottom flange as per the experimental data peaks around 9 to 19 MPa and for the web around 5.5 to 11.5 MPa.

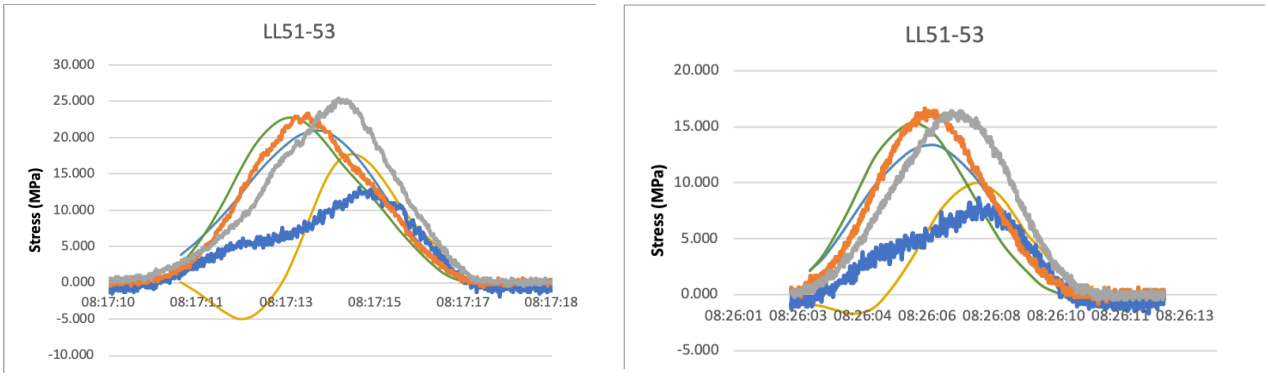

Figures 68 and 69. Calibration of the LL51-LL53 Lower Chord for the Strengthened Bridge: in the Lane (left); on the Axis (right).

Regarding the upper flange, the behaviour of the modelled data according to the experimental data is very comparable to the unstrengthen bridge. As per the lower chord graphs, the shape of the stress curve, the results are quite satisfying and no real discrepancies were observed (Figures 70 and 71). In general, a difference between the bottom flange experimental and modelled data at the peaks for the upper chords of is 10%-40% and for the web is 0%-20%. Such difference is calculated by excluding the presented outlier in the figures below. In addition, the values for the bottom flange as per the experimental data peaks around to -10.5 to -40 MPa and for the web around -3.4 to -10.5 MPa.

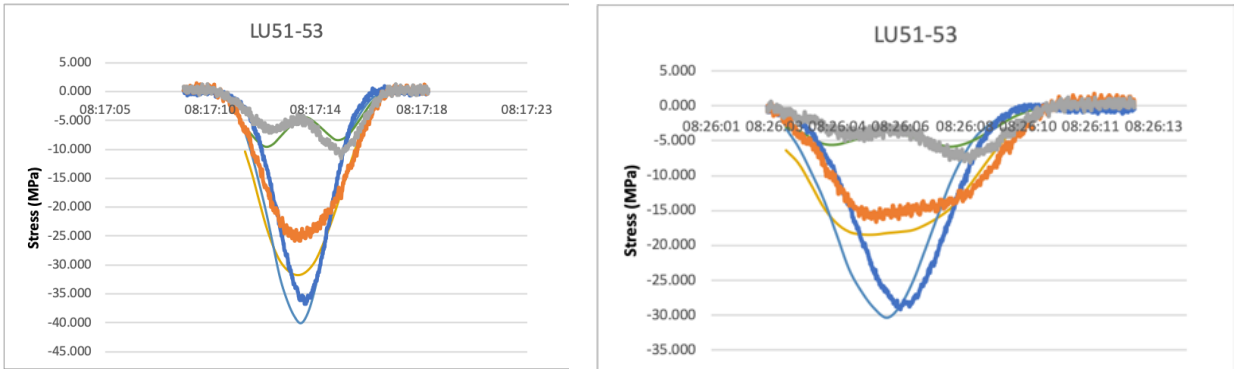

Figures 70 and 71. Calibration of the LU51-LU53 Upper Chord for the Strengthened Bridge: in the Lane (left); on the Axis (right).

In terms of the diagonals, there is a still a great variability in terms of behaviour and disparities depending on the type of diagonal and their location across the truss. The stress curves for the diagonals are similar from the model to the experimental data as well as comparable to the unreinforced bridge data (Figures 72 to 73). The main discrepancies still remain in terms of the accuracy of the peak stresses. In general, a difference between the experimental and modelled data at the peaks is 0%-60%, therefore, highlighting the wide range of behaviour, and the peak values from the experimental data range from -19 to 27.5 MPa.

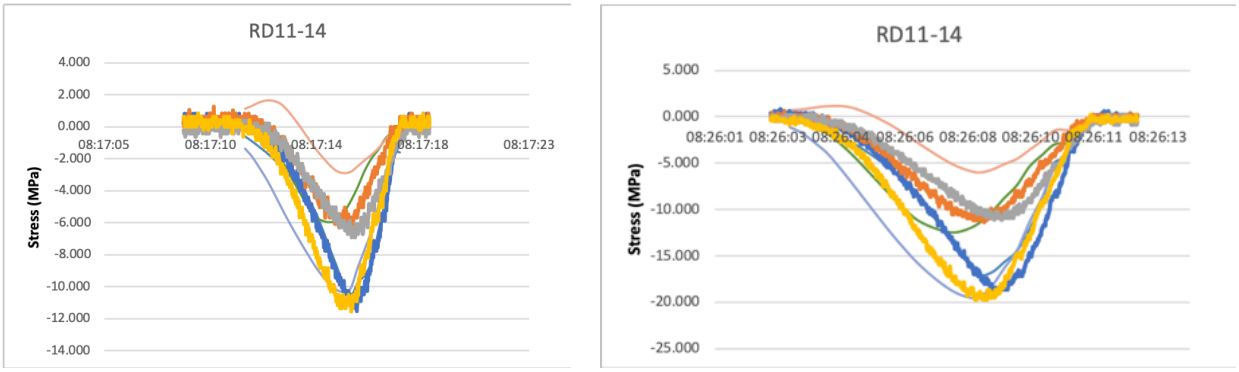

Figures 72 and 73. Calibration of the RD83-RD84 Diagonal for the Strengthened Bridge: in the Lane (left); on the Axis (right).

In summary, the addition of the SMA to the previously calibrated model leads to the main following observations. The stress curve shapes appear to remain very similar to the ones of the unreinforced bridge with a few exceptions. The response of the model for the SMA curve to the experimental data is positive in terms of calibration. It can therefore be concluded that the model behaviour is adequate for giving a good estimate of the true bridge behaviour under static loads.

5.2 According to Dynamic Testing

Dynamic testing for both the unstrengthen and strengthened bridge was planned. However, to this date, only the operational modal analysis for the unstrengthen bridge has been conducted. This was due to delays with the project.

5.2.1 Operational Modal Analysis on Unstrengthen Bridge

An operational modal analysis (OMA) was performed by Tomáš Plachy on May 20, 2019. From the results obtained from the dynamic testing of the bridge, six mode shapes were recorded based on the ambient vibrations, the traffic as well as from a few isolated impacts. For the purpose of this analysis, only the first five were selected for comparison. For the test, the accelerometers were positioned along the upper and lower chord of the truss only as per Figure 74.

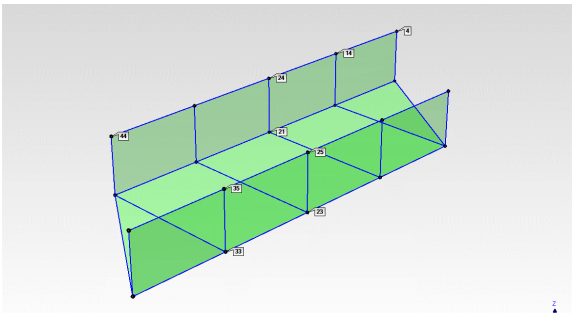

Figure 74. Accelerometers Positioning.

The mode shapes and their associated frequencies are presented in Table 16 below and the accuracy of the measurements is of +/- 0.03 Hz. It is to be noted that the ambient vibrations used for the bridge were quite low and that therefore, the mode shapes could be providing a less accurate correspondence to the one from the model prepared using the Dlubal RFEM software. In addition, it is to be noted that since the evaluation of the dynamic behaviour was only limited to the truss, this does not provide a complete assessment of the properties of the bridge, but more of a preliminary understanding on how the trusses behave under ambient vibrations. It would be recommended for the next dynamic test to also take into account other structural elements such as the cross-beams and the stringers to better understand the global movement of the structure.

Table 16. Operational Modal Analysis: Mode Shapes.

Frequency	Mode Shapes
6.56 Hz	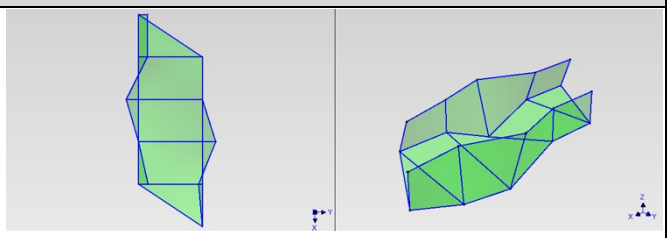
9.91 Hz	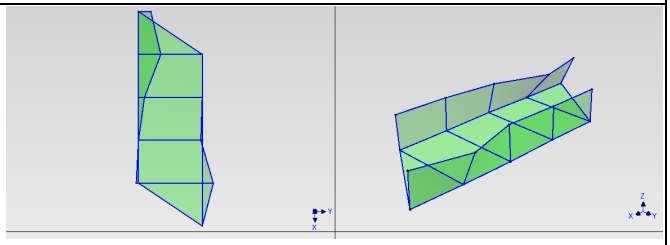
10,91 Hz	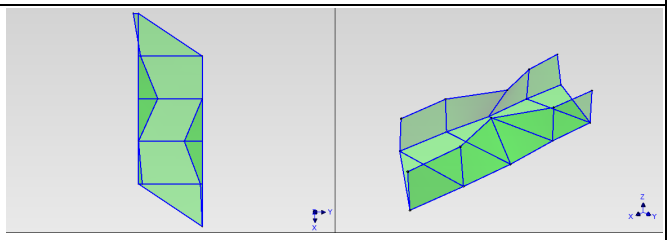
12.16 Hz	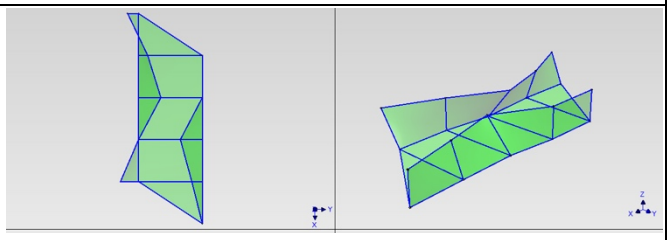
16.05 Hz	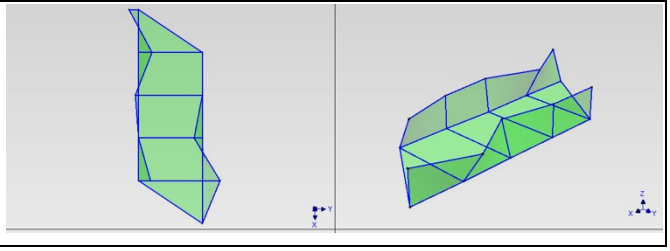

In general, when comparing the OMA results to the model, one can observe a divergence in terms of the frequencies of the mode shapes associated with the bridge and this could be explained by the use of small ambient vibrations for the experiment (Table 17). However, the mode shapes themselves are quite well corresponding from the experimental data confirming the true behaviour of the bridge.

Table 17. Model Dynamic Analysis: Mode Shapes of the Unstrengthen Bridge.

Frequency	Mode Shapes	Frequency	Mode Shapes
7.08 Hz	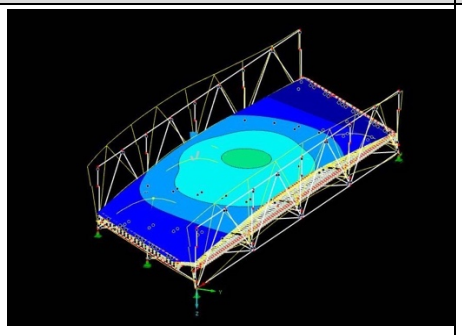	13.04 Hz	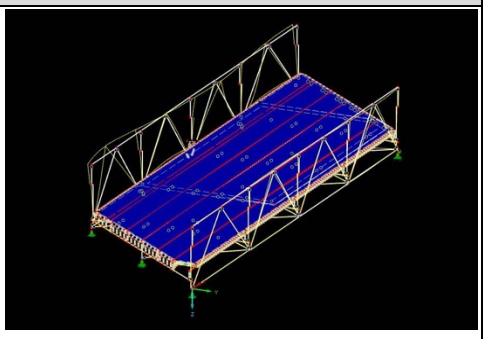
10.13 Hz	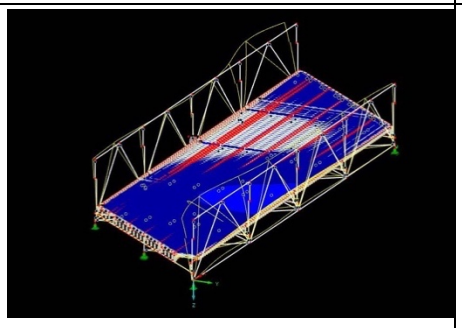	16.20 Hz	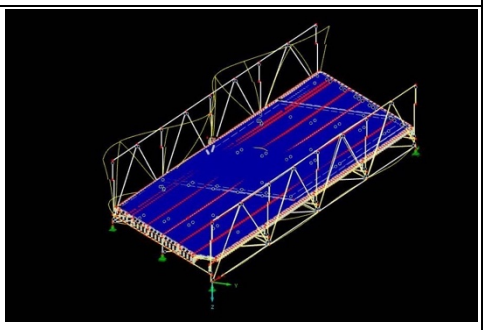
11.21 Hz	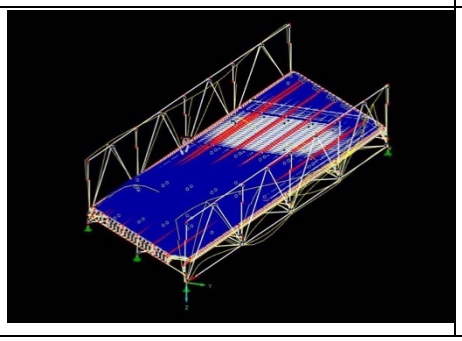		

Looking at the first global mode, the frequency for the OMA is of 6.56 Hz and for the model is of 7.08 Hz leading to an acceptable percentage difference of 8%. For the mode shapes, they are appear to be a bit different. The movement of the central middle span of both trusses by translation in the y-direction can be observed in addition to the movement of the central portion of the deck of the bridge. The difference is that the movement from the trusses from the model is in a joined motion as for the OMA, it is moving in the opposite direction from opposite sides from OMA. This might be caused by the small ambient vibrations used for the OMA since the mode shapes forward are quite similar to the OMA. For the second mode, natural frequencies were recorded as 9.91 Hz for the OMA and 10.31 Hz

for the model resulting in a difference of 4%. In terms of the mode shape, the bridge presents a translation in the y-direction at the ends of the trusses with a small displacement of the deck of the bridge. The trusses open in the opposite direction in both the model and from the OMA. For the third mode shape, the OMA obtains natural frequencies of 10.91 Hz when the model of 11.21 Hz therefore leading to a 3% difference. The trusses' central section move inwards as a mode shape with a small movement from the deck for both analyses. For the fourth mode, the OMA obtains natural frequencies of 12.16 Hz when the model of 13.04 Hz therefore leading to a 7% difference. For both analyses, a translation mainly in the y-direction of the trusses with the central section moving towards the inside is showcased, however, the movement from the OMA appears to be greater on the trusses than for the model. In terms of the deck, a small oscillation of the deck in two parts is common to both. Finally, the fifth analyzed natural frequency presents a magnitude of 16.05 Hz for the OMA and of 16.20 Hz for the model resulting in a 1% difference which is again adequate knowing that for the OMA only the trusses were monitored. For the modal shape, a translation of the trusses moving together in the same direction under the form of an oscillation can be recorded. However, one can observe a difference where a greater movement from the deck from the model is present in comparison to a very limited from the OMA. This might be caused by the oscillation of the substructure of the deck, i.e. cross-beams, which have a lower natural frequency than the global structure.

Based on this analysis of the mode shapes and natural frequencies, it can be determined that the behaviour is quite corresponding even when only considering the truss elements from the OMA. Therefore, the calibration via dynamic testing was determined to be still be quite effective. Furthermore, due to the limited collection of data by the accelerometers, the model provides additional information on the behaviour of the bridge in terms of local natural frequencies of some of the members. In fact, the bracing is the first to oscillate locally with a frequency at 4.916 Hz and then, the global oscillation of the bridge only occurs at 7.083 Hz as shown in the Table 17 above. As previously recommended, it would be valuable to obtain some more information from the OMA from the cross-beams, stringers and cross-bracing.

5.2.1 Operational Modal Analysis on Strengthened Bridge

The dynamic analysis of the bridge after the strengthening was delayed due to unforeseen events and will not be part of this thesis work. However, the results as per the strengthened model can still be observed below, but no calibration nor comparison can be made at this point (Table 18).

Table 18. Model Dynamic Analysis: Mode Shapes of the Strengthened.

Frequency	Mode Shapes	Frequency	Mode Shapes
7.09 Hz	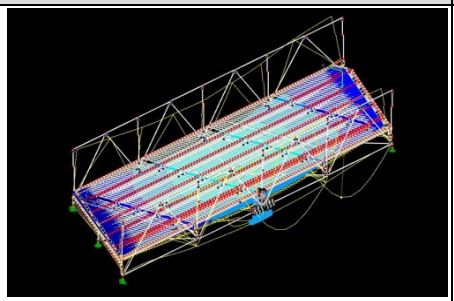	13.04 Hz	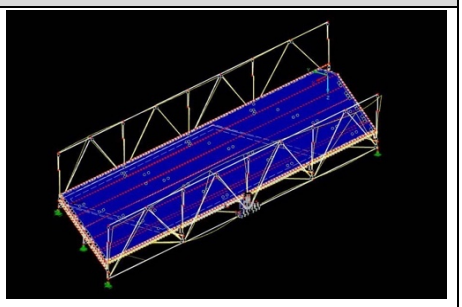
10.33 Hz	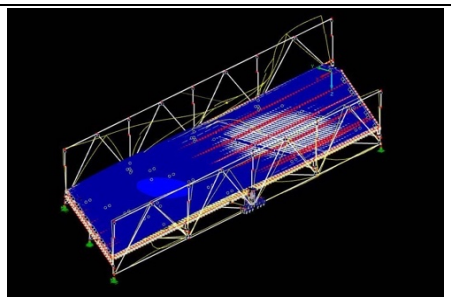	16.20 Hz	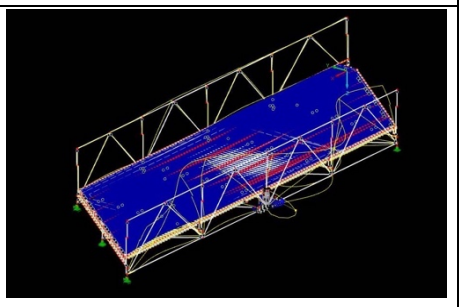
11.22 Hz	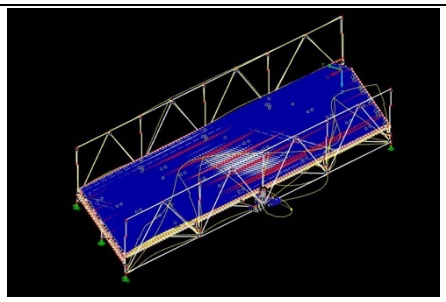		

Looking at the first global mode, the natural frequency is of 7.09 Hz, which is almost equivalent to the unstrengthen bridge. For the mode shape, they are quite similar. There is a movement of the central middle span of both trusses in the y-direction in addition to the upward and downward movement of the central portion of the deck. For the second mode, the natural frequency was recorded as 10.33 Hz. In terms of the mode shape this leads to a translation in the y-direction at the ends of the trusses in the form of an opening with a small displacement of the deck of the bridge. For the third mode, a frequency of 11.22 Hz was assessed. In terms of mode shape, centre part of the trusses moves inwards as per the OMA with a small movement from the deck for both analyses. For the fourth mode, the frequency is of 13.04 Hz with a mode shape presenting a translation in the y-direction of the trusses with the central section moving towards the inside and a movement of the deck in the form of an oscillation alternating from one end of the bridge to the other. The fifth natural frequency presents a of 16.20 Hz as per the reinforced model. For the modal shape, a translation of the trusses moving together in the same direction under the form of an oscillation can be recorded with an oscillation of the deck too.

Based on the results, it can be observed that the unstrengthen bridge in comparison to the strengthened bridge showcases a very similar behaviour with the exception of the addition of the SMA. Such result is normally desired when a continuous use is planned for. A high change in stiffness could lead to the detriment of the structure by changing its dynamic properties. From the model, it can also be observed that some members have lower natural frequencies than for the global structure. In this case, the SMA vibrates locally at a low frequency of 1.74 Hz prior to the rest of the structure to vibrate globally. Similarly to the unstrengthen model, the bracing starts vibrating locally at low frequency of 4.92 Hz and a global behaviour is only noticed at 7.09 Hz.

It is recommended to complete the dynamic analysis of the strengthened bridge. This will permit further calibration of the model to obtain the most accurate behaviour of the bridge model.

6. EVALUATION OF THE MODEL CAPACITY

In order to estimate the capacity of the ultimate capacity of the bridge, the calibrated strengthened model was tested to its ultimate load-bearing capacity. In order to assess any weaknesses coming from the bridge due to corrosion, a few members were replaced from their original cross-section to a reduced cross-section. This is the case of the two side cross-beams where a hole in the web near the support was recorded. Based on this, a whole of approximately 300 mm in the centre of the beam was created for a distance of 300 mm. In addition, heavy corrosion was also observed at some of the horizontal gusset plates at the junction between the lower chord, the cross-beam, the vertical, and the bracing. In these cases, the corrosion was so advanced that most of the concerned gusset plates were lost to corrosion and such level of corrosion was also reflected in the diagonal bracing. Since the model is a simplified model, the corrosion within the gusset plated could not be modelled, however, the impact on the bracing was possible to model. Therefore, for a length of 300 mm, which is the length on which the bracing is anchored on the gusset plates, the cross section of the bracing was reduced by approximately half in order to take into consideration the corrosion weakening. This weakening of the structure within the model helps address additional instabilities or potential failure modes from the bridge, which might be disregarded without inputting a reduction in the cross-section of such weakened members.

Once the weakening of some of the members in the model was completed, a series of incremental loads was applied on the calibrated model of the bridge to assess its ultimate load carrying capacity up until an instability in the structure was recorded. Such loads were modelled based on the loading materials, which will be used on site and loaded on the loading area of 6.5 m wide by 12.3 m long (Figure 75). In this area, a grid of 6 by 4 concrete panels of 3 m long and 1 m wide spaced by 0.10 m intervals will be used for the test on site. The concrete panels were estimated to have a density of about 25 kN/m^3 and are 0.215 m thick, however, since six panels will be placed on top of each other this will lead to a total thickness of 1.29 m for a total area load of 32.25 kN/m^2. On top of the concrete panels, gravel bags with an approximate density of 15 kN/m^3 are to be stacked on top of each other with an approximate maximum filling height of 0.8 m.

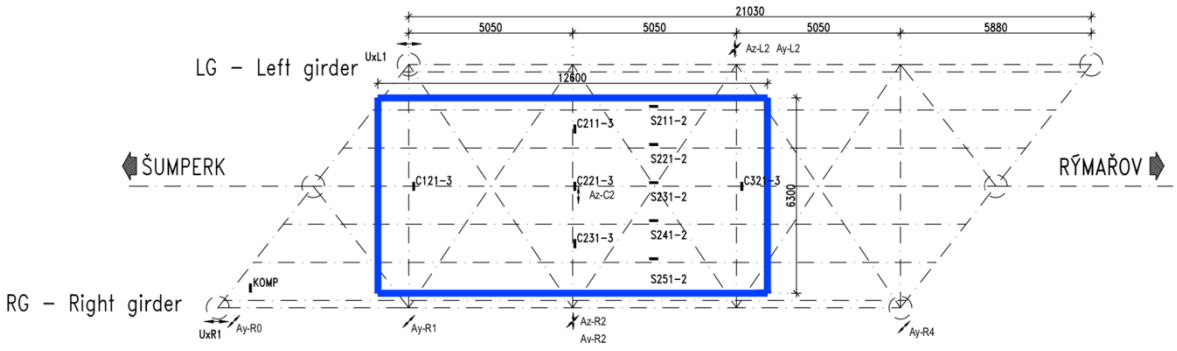

Figure 75. Loading Area for Ultimate Capacity (in Blue).

As previously mentioned an incremental approach was used in order to obtain the ultimate load capacity of the bridge. The concrete panels area load was first modelled and then, additional loading from the gravel bags was performed. Table 19 presents the last loading steps, their corresponding deformed shape. Figures 76 to 78 showcases such deflections of the model based on the different load increases. As it can be observed, as the loading increase in increments of approximately 6 kN/m^2, the deflections would increase of about 7.5 mm or 10%.

Table 19. Load Increments and Corresponding Maximum Deflections.

Steps	Load	Maximum Deflection
80% of the load	32.25 kN/m^2 + 16.67 kN/m^2	64.8 mm
90% of the load	32.25 kN/m^2 + 22.79 kN/m^2	72.3 mm
Ultimate load (61 kN/m^2)	32.25 kN/m^2 + 28.9 kN/m^2	80.1 mm

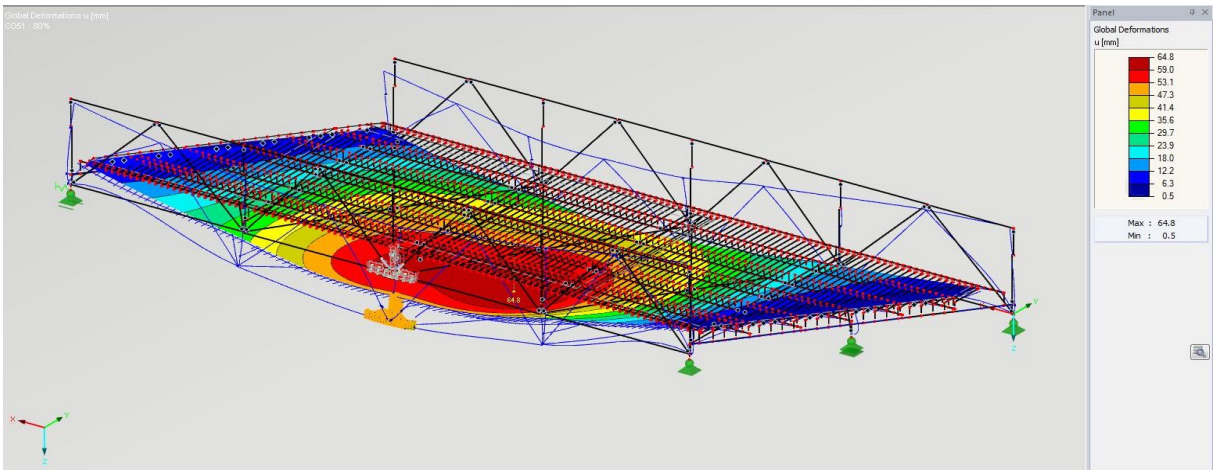

Figure 76. Deformed Shape: 80% of the Load.

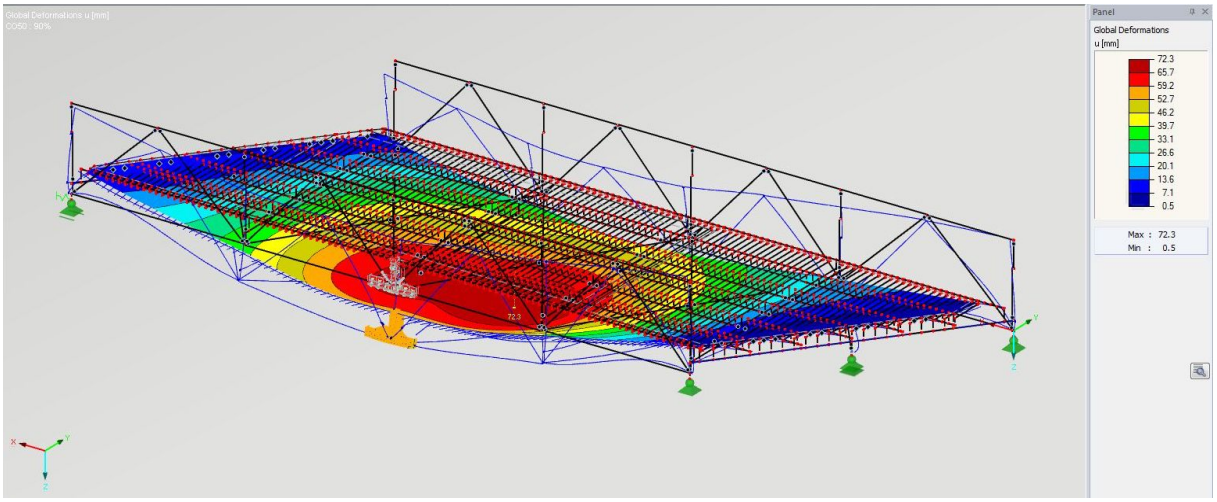

Figure 77. Deformed Shape: 90% of the Load.

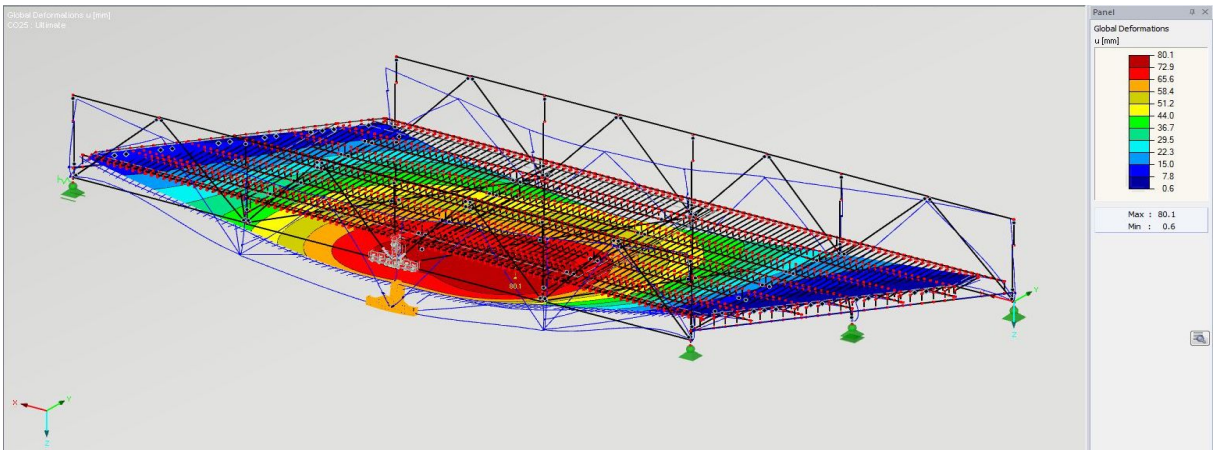

Figure 78. Deformed Shape: Ultimate Capacity Loading.

It is interesting to also compare the evolution of the stresses in the modelled connection as well as the strains in the whole structure as the model approaches its maximum loading capacity. In terms of strain for the whole model, a general increase of approximately 9 to 10% can be observed between the load steps in terms of maximum strains. This increase appears to be corresponding and consistent with the deflections of the structure (Figures 79 to 81).

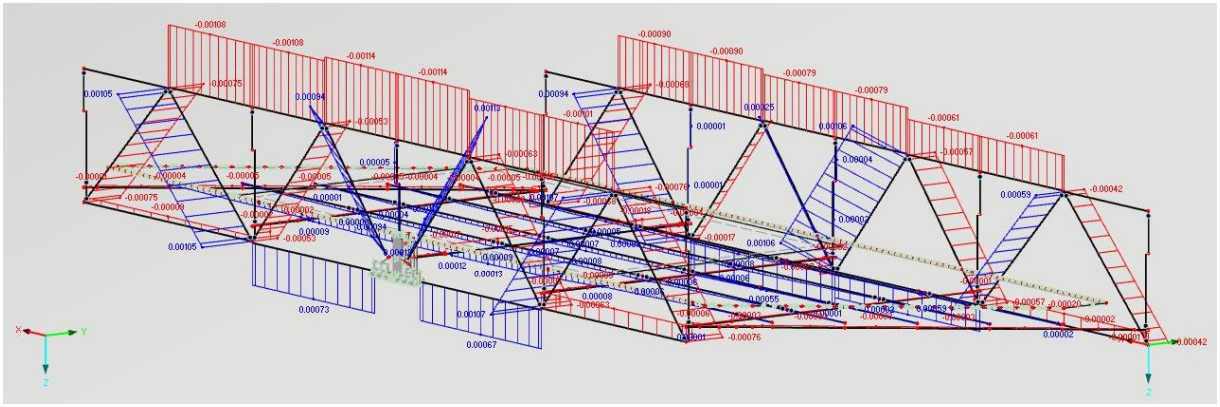

Figure 79. Strains: 80% of the Load.

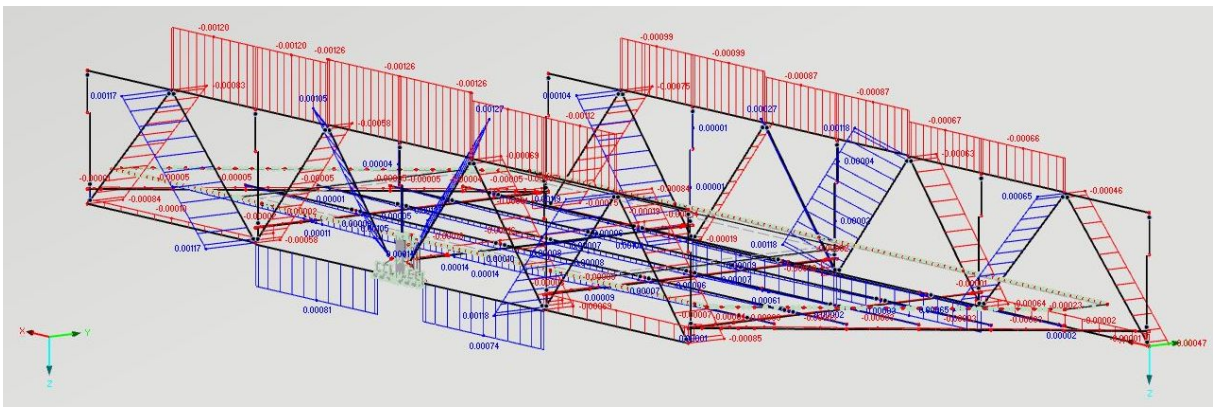

Figure 80. Strains: 90% of the Load.

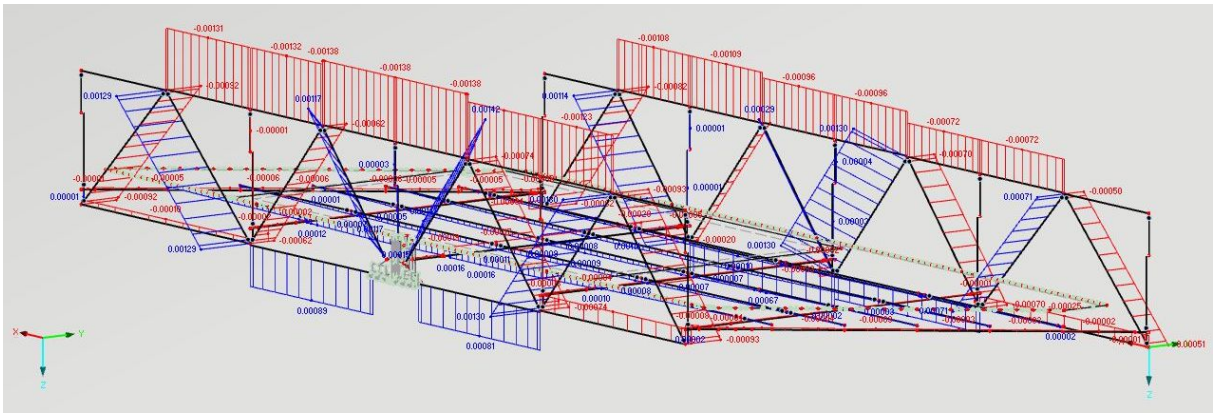

Figure 81. Strains: Ultimate Capacity Loading.

In regards to the stresses in the detailed connection at the centre bottom chord (Figures 82 to 84). An increase in stress of approximately 2% from 80% to 90% loading and from 90% to the ultimate loading can be observed. The stress distribution appears to be spreading as the load increases with a higher concentration near and at the rivets. High compressive stresses are forming at the junction of the top of the gusset plate and of the vertical. In addition, the stresses can be observed to be rising in the vertical gusset plate from the bottom chord and also spreading around the rivets of the two smaller shear vertical plates framing the gusset plate on each side. Higher stress concentrations, in between the diagonals and the vertical are also being observed. It is to be noted that in the areas where rivets are located, the gusset plate is reaching beyond its ultimate strength especially at the node. It is estimated that the elevated peak stresses at the node reaching over the ultimate capacity of are caused by the extrapolation of the values at the nodes. This is even reflected in the model when only the self-weight is being considered at the nodes which is a small fraction of the ultimate capacity of the bridge. This therefore shows that the material non-linearity is working and that in the instance where a linear analysis would be conducted, even higher stresses would be recorded.

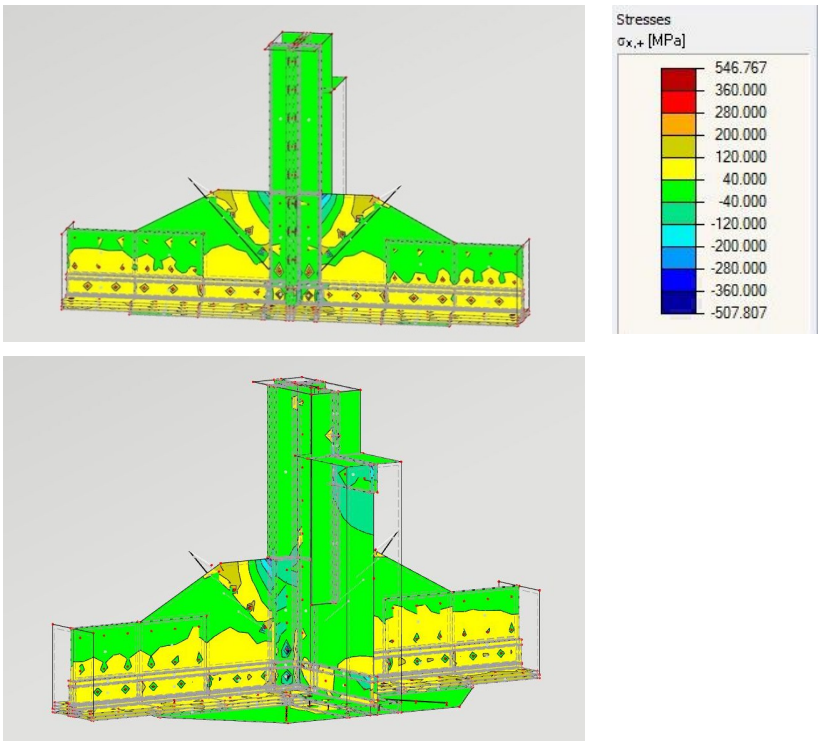

Figure 82. Stresses in the Detailed Connection: 80% of the Load.

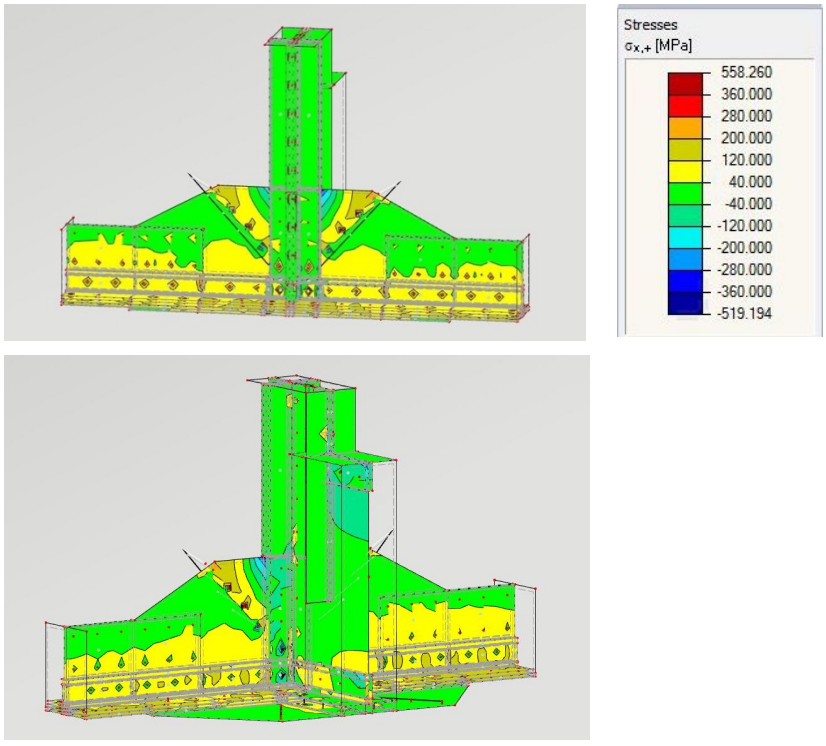

Figure 83. Stresses in the Detailed Connection: 90% of the Load.

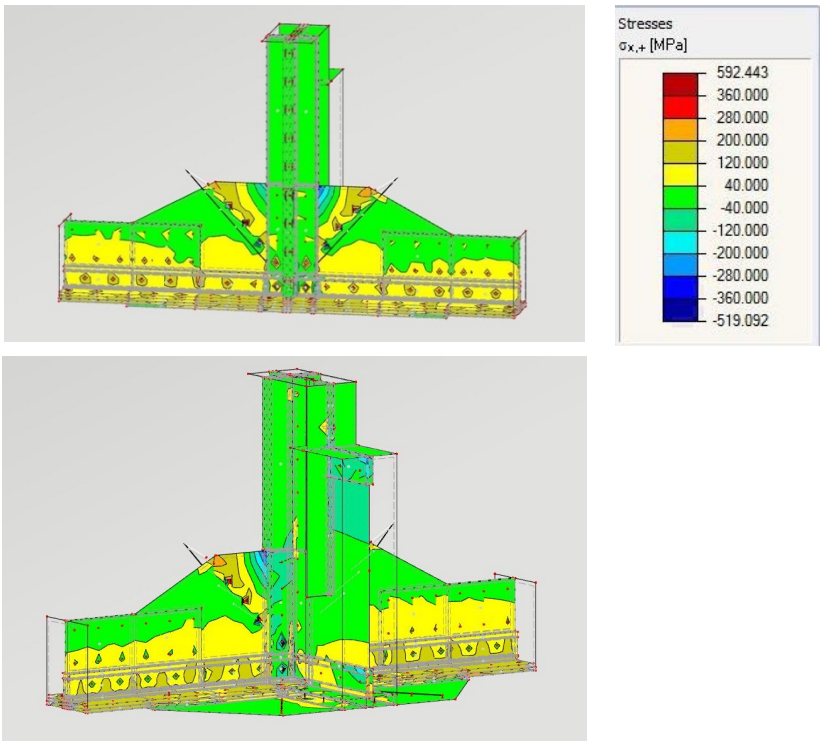

Figure 84. Stresses in the Detailed Connection: Ultimate Capacity Loading.

Once the ultimate load on the bridge was determined, the results of the loading actions on the bridge at its ultimate capacity were recorded and assessed in regards to the predicted failing connection. In this case, the maximum loading in terms of axial forces is concentrated at the top chord with a maximum of 3.62 MN (Figure 85). The strains are also at their peaks in this particular at the top chord members (Figure 81). In general, the internal forces tend to be higher on the members of the right truss since the load is non-symmetrically resting closer to this particular. In terms of moments, the cross-beams have the greatest moments at the y-axis where 1.24 MNm are recorded for the C211-213 cross-beam, 1.85 MNm for the C221-C223 and 1.42 MNm for the C231-233 (Figure 86). In terms of moments in z, the diagonals, the top chords and the base of the verticals have the highest moments (Figure 87). In terms of the verticals, the highest moments are found at their base at the ends of the bridge -101.9 kNm on the Šumperk side and of 117.7 kNm on the Rýmařov. In addition, the end diagonals on the right girder present moments approximate to 63.03 kNm at their base and -41.20 kNm at their top.

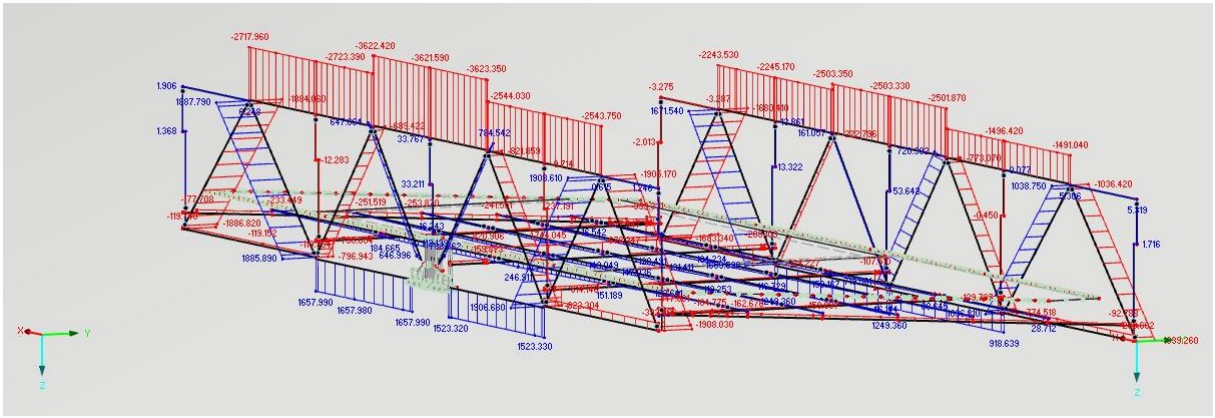

Figure 85. Axial Loads: Ultimate Capacity Loading.

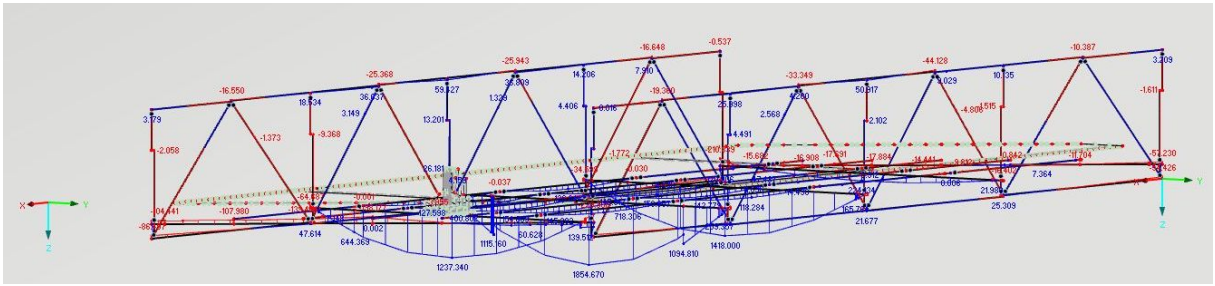

Figure 86. Moments in y: Ultimate Capacity Loading.

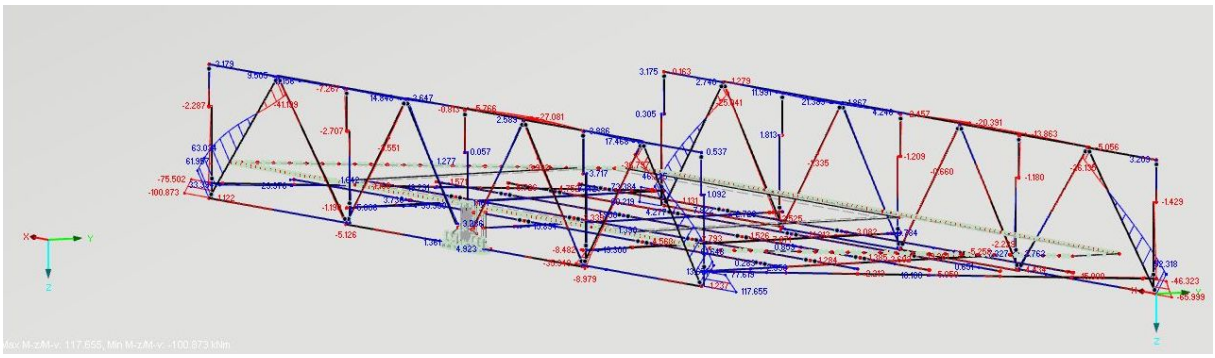

Figure 87. Moments in z: Ultimate Capacity Loading.

Based on the modelling of these actions on the reinforced bridge modelled, the ultimate critical load of the model was determined to be 61.15 kN/m^2 of the loading area. This load would result in using the whole amount of concrete panels on the designated loading area, which is equivalent to an approximate load of 32.25 kN/m^2 for each panel area, in addition to a total of 28.9 kN/m^2 of gravel bags is then to be placed on top of the concrete panels. Such load can be estimated as 3 layers of bags over the concrete area filled at 0.64 m each.

By applying this load to the bridge, it is expected that the centre-left top chord connection on the right girder will be the first to fail. This can be seen in the results from the strains for the members, mainly

the top chord and diagonals, surrounding the connection. Such behaviour is controlled by the fact that the one of the main cross-beams, which was of concern in terms of stability under ultimate loading, was strengthened using SMA's as recommended by a previous report on the preliminary assessment of the bridge. (Stančík, 2019) This therefore permitted to redirect the failure towards the main trusses at first. In general, as per the model, the top chords and diagonals are weakest members, which is showcased by the predicted first failure mode of the bridge via the centre-left top chord connection on the right girder. In addition, it was observed that some of the weakened bracing is also susceptible to a lower resistance and an early failure during the loading of the bridge, however, the impact of the reduced section for the cross-beam does not seem to be as critical. Therefore, the top chord connection and its connecting members should be monitored as well as the bottom chord connections with corroded gusset plates and the weakened bracing. Lastly, it is also recommended to monitor during the loading the stringer to cross-beam connections as well as the detailed connection which were raised in the previous preliminary report as a potential weaker connection. (Stančík, 2019)

Furthermore, based on the ultimate loading of the bridge, some displacements at the supports and deformations near the mid-span of the bridge are to be expected. In order to avoid the uncontrolled collapse of the bridge, temporary supports will be provided during the ultimate capacity loading test. In order to better design such a temporary structure, the displacements at the supports are necessary to be considered. Table 20 presents the displacements at the node support and Figures 88 to 90, the displacements of the structure as a whole. It can be observed that the Šumperk side moves towards the road in +x as when the Rýmařov side moves towards the river in -x. On the Rýmařov side only a small movement in the direction of the river, in y, can be observed as for the Šumperk side greater movement up to 3.5 mm can be observed. In addition, since deformations up to 80 mm downwards are to be expected near the mid-span as per Figure 78, the temporary support should be distant enough from this estimated deformation so they do not become a support therefore changing the load paths of the bridge. It is therefore recommended to leave a space up to 200 mm to avoid this situation. In locations, near the support, a smaller spacing is adequate since the deflections were assessed to be much lower, i.e. around 10 mm.

Table 20. Support Displacements.

Support	Location: Side of the River	
	Rýmařov Side	Šumperk Side
At the Right Girder	-2 mm in x, 0.5 mm in y	4 mm in x, -0.5 mm in y
On Center	-4 mm in x, 0.5 mm in y	5 mm in x, -3.5 in y mm in y
At the Left Girder	-2 mm in x, 1 mm in y	2.5 mm in x, -2 mm in y

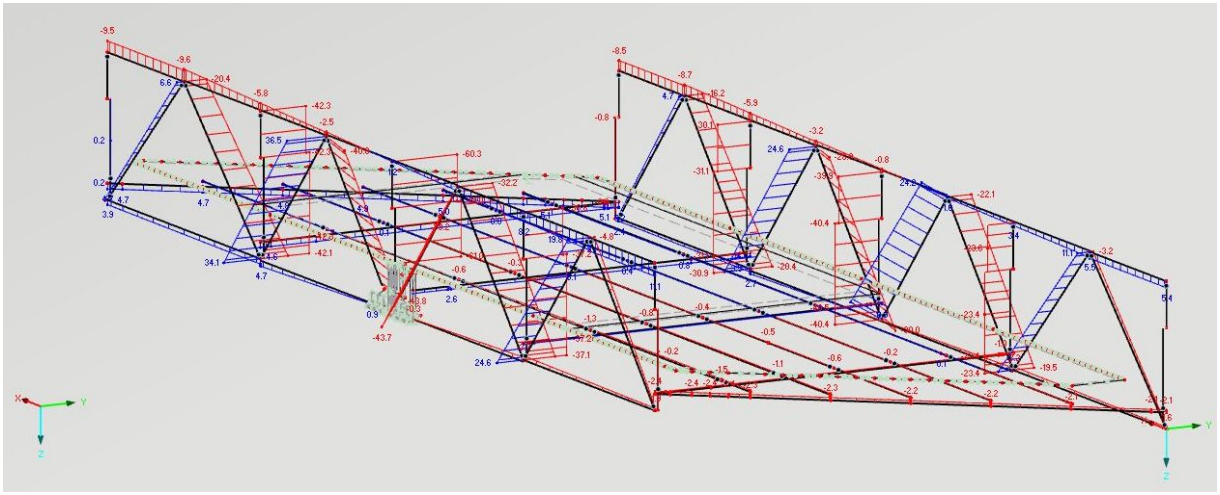

Figure 88. Displacements in x: Ultimate Capacity Loading.

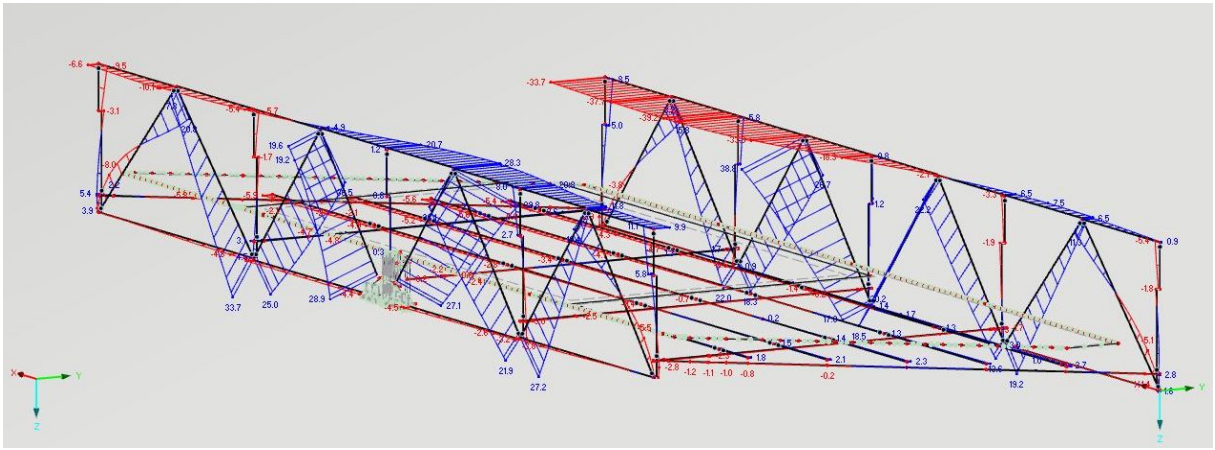

Figure 89. Displacements in y: Ultimate Capacity Loading.

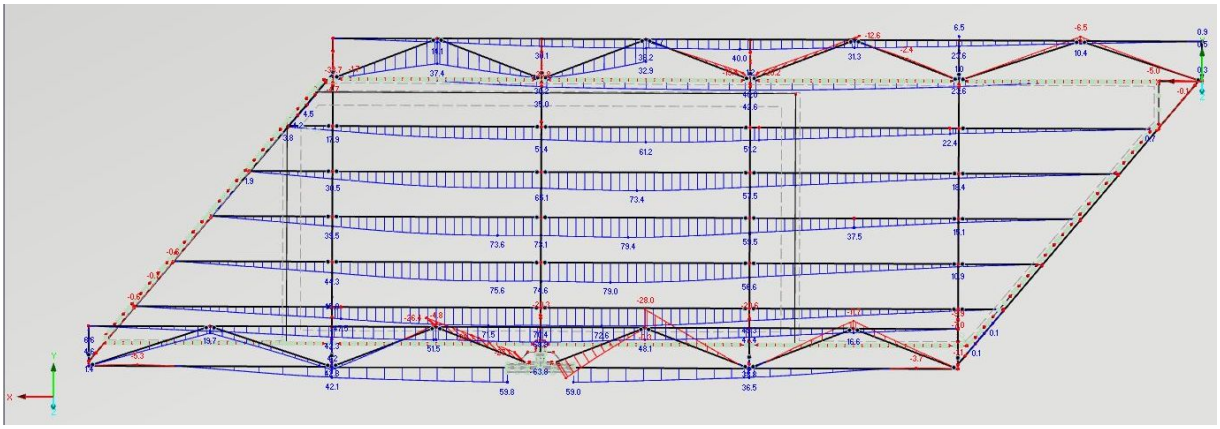

Figure 90. Displacements in z: Ultimate Capacity Loading.

Based on the movement observed from the model, it is therefore recommended to load the bridge with the sum of the concrete panels (32.25 kN/m^2) on the designated area with 3 layers of bags over the

concrete area filled at 0.64 m each (28.9 kN/m^2) in order to reach the ultimate capacity of the bridge. In addition, it is recommended to build a temporary structure in such a way that any slipping of the supports does not occur and that the bridge does not collapse in the river just underneath.

7. NEXT STEPS

Due to unforeseen circumstances in terms of closing roads and building a temporary replacement bridge, part of the testing planned for this thesis was impossible to be completed prior to its due date. In this spirit, the model could not be compared with the experimental ultimate capacity of the bridge for this thesis. In Table 21 below, the methodology used can be observed with their status of completion.

Table 21. Methodology and Task Status.

Tasks	Status
Parametric study	Completed prior to this thesis
Material testing	Completed
Construction of a model with a detailed connection	Completed
Load test with a crane	Completed
Dynamic testing	Completed
Calibration of the model with the load test	Completed
Calibration of the model with the dynamic test	Completed
Strengthening of the bridge with SMA's	Completed
Update of the model with strengthening	Completed
Load test of the strengthened bridge with a crane	Completed
Dynamic testing of the strengthened bridge	To be completed
Calibration of the model with the load test	Completed
Calibration of the model with the dynamic test	To be completed
Testing of the model to its ultimate capacity	Completed
Testing of the model bridge to its ultimate capacity	To be completed
Final calibration of the model and Comparison of the experimental and model results	To be completed
Publication of the results	To be completed

Based on the table above, the next steps therefore include the dynamic testing of the bridge with the strengthening system in place as for the unstrengthen bridge, the testing of the bridge up until its ultimate capacity based on the predicted ultimate load from the model, the comparison between the model and the experimental data and the calibration of the model based on the true ultimate capacity of the bridge. Finally, the results can then be published in order to better share the results for the assessment of similar historical bridge typologies.

8. CONCLUSION

In conclusion, the bridge should be loaded up to approximately 61.15 kN/m^2 in the designated loading area in order to lead to the failure of some of its members and then, to its collapse. This can be done by placing 6 by 4 concrete panels of 3 m long and 1 m wide spaced by 0.10 m intervals to avoid any arch action for the concrete. Then, 3 layers of 0.64 m tall gravel bags are to be placed on top of the concrete panels. The critical members to be monitored are the diagonals and the top chord and in terms of connections the second top chord connection as well as the connections of the cross-beam to the stringer and the modelled connection with shell elements at the bottom chord. In addition, a temporary support system should be put into place to prevent the collapse of the bridge in the river based on the support displacements calculated with the model. With the information obtained by the collapse of the bridge, further data will be collected and the strengthened model will be again calibrated to showcase a behaviour closest the true behaviour of the bridge. This will then later in the future be useful of similar typologies of bridges found in the Czech Republic or in its surrounding countries as the available data on the topic of the ultimate capacity of historical steel bridges is quite limited and is still quite recent. It is recommended that this area of study be more investigated when a structure is to be replaced in order to provide data on historical structures of its typology for future assessment of similar typologies. This can be a critical aspect for historical bridges which, even if they have reached their service life, may still have a residual capacity still acceptable for today's codes and standards, but due to the lack of understanding of their construction technique and of the capacity of their connections might be disregarded as functional and capable.

9. REFERENCES

Blanksvärd, T., Häggström, J., & Collin, P. (2016). Fullscale testing and assessment of a steel truss bridge (pp. 1220–1227). Luleå, Sweden. https://doi.org/10.14264/uql.2016.627

Caglayan, O., Ozakgul, K., & Tezer, O. (2012). Assessment of existing steel railway bridges. *Journal of Constructional Steel Research*, *69*(1), 54–63. https://doi.org/10.1016/j.jcsr.2011.08.001

Costa, B. J. A., Magalhães, F., Cunha, Á., & Figueiras, J. (2014). Modal Analysis for the Rehabilitation Assessment of the Luiz I Bridge. *Journal of Bridge Engineering*, *19*(12), 05014006. https://doi.org/10.1061/(asce)be.1943-5592.0000632

Cunha, Á., Caetano, E., & Calçada, R. (2002). Dynamic Measurements in Bridges. In Harry Grundmann & G. I. Schuëller (Eds.), *Structural Dynamics: EURODYN 2002* (pp. 367–372). Lisse: Balkema.

ČVUT v Praze. (2019). *Zkušební protokol č. 19/12133/xxx*. Praha.

Dreher, R. C., & Batterson, S. A. (1962). *COEFFICIENTS OF FRICTION AND WEAR CHARACTERISTICS FOR SKIDS MADE OF VARIOUS METALS ON CONCRETE, ASPHALT, AND LAKEBED SURFACES*. Washington D.C.

Historic American Engineering Record. (1976). Trusses: A Study by the Historic American Engineering Record. Washington D.C. Retrieved from https://www.nps.gov/hdp/samples/HAER/truss poster.pdf

Institute for Steel Development & Growth. (1998a). Steel Bridges - I. In *Teaching Materials* (pp. 43-1-43–20). Retrieved from http://www.steel-insdag.org/TeachingMaterial/chapter43.pdf

Institute for Steel Development & Growth. (1998b). Steel Bridges - II. In *Teaching Materials* (pp. 44-1-44–15).

Institute for Steel Development & Growth. (1998c). Trusses. In *Teaching Materials* (pp. 27-1-27–46).

Kim, H., & Buttlar, W. G. (2009). Discrete fracture modeling of asphalt concrete. *International Journal of Solids and Structures*, *46*(13), 2593–2604. https://doi.org/10.1016/j.ijsolstr.2009.02.006

Kulak, G. L., Fisher, J. W., & Struik, J. H. A. (2001). *Guide to Design Criteria for Bolted and Riveted Joints* (Second Edi). Chicago, IL: AMERICAN INSTITUTE OF STEEL CONSTRUCTION.

Larsson, T., & Lagerqvist, O. (2019). Material properties of old steel bridges. *NSCC2009*, 120–127.

LIEBHERR. (2013). Mobilkran - Mobile Crane LTM 1055-3.2. Retrieved June 1, 2019, from https://www.hanys.cz/galerie/tinymce/PDF Jeraby/ltm-1055-3-2.pdf

Munse, W. H., & Cox, H. L. (2007). The Static Strength of Rivets Subjected to Combined Tension and Shear. *University of Illinois Bulletin*, *Engineerin*(437), 1–28.

Plachý, T., Polák, M., & Ryjáček, P. (2017). Assessment of an Old Steel Railway Bridge Using Dynamic Tests. In *Procedia Engineering* (Vol. 199, pp. 3053–3058). https://doi.org/10.1016/j.proeng.2017.09.555

Ryjáček, P. (2019). On-site Pictures. Rapotin.

Seznam.cz. (2019). Mapy.cz. Retrieved June 29, 2019, from https://en.mapy.cz/zakladni?x=15.6531438&y=49.9904570&z=7

Sparks, S. P. (2008). Evaluation of Iron & Steel in Historic Bridges. In *Proceedings of the Sixth International Conference on Structural Analysis of Historical Constructions*. Bath, UK.

Stančík, V. (2019). *Bridge no. 11-097 Petrov nad Desnou – Use of demolition for research purposes – assessment of critical loading*. Prague.

Stančík, V. (2019). *Ověření nové technologie SMA pro zesílení mostu - most 11- 097 přes řeku Desná v obci Petrov nad Desnou Obsah*. Pra.

Waddell, J. A. L. (1916). *Bridge Engineering* (First Edit). New York: John Wiley & Sons, Inc. Retrieved from https://archive.org/details/bridgeengineerin01wadd/page/n5

Wright, K. (2015). *Steel Bridge Design Handbook Selecting the Right Bridge Type* (Vol. 5). Washington D.C. Retrieved from https://www.fhwa.dot.gov/bridge/steel/pubs/hif16002/volume05.pdf

APPENDIX 1. DETAILED DRAWINGS OF THE BRIDGE

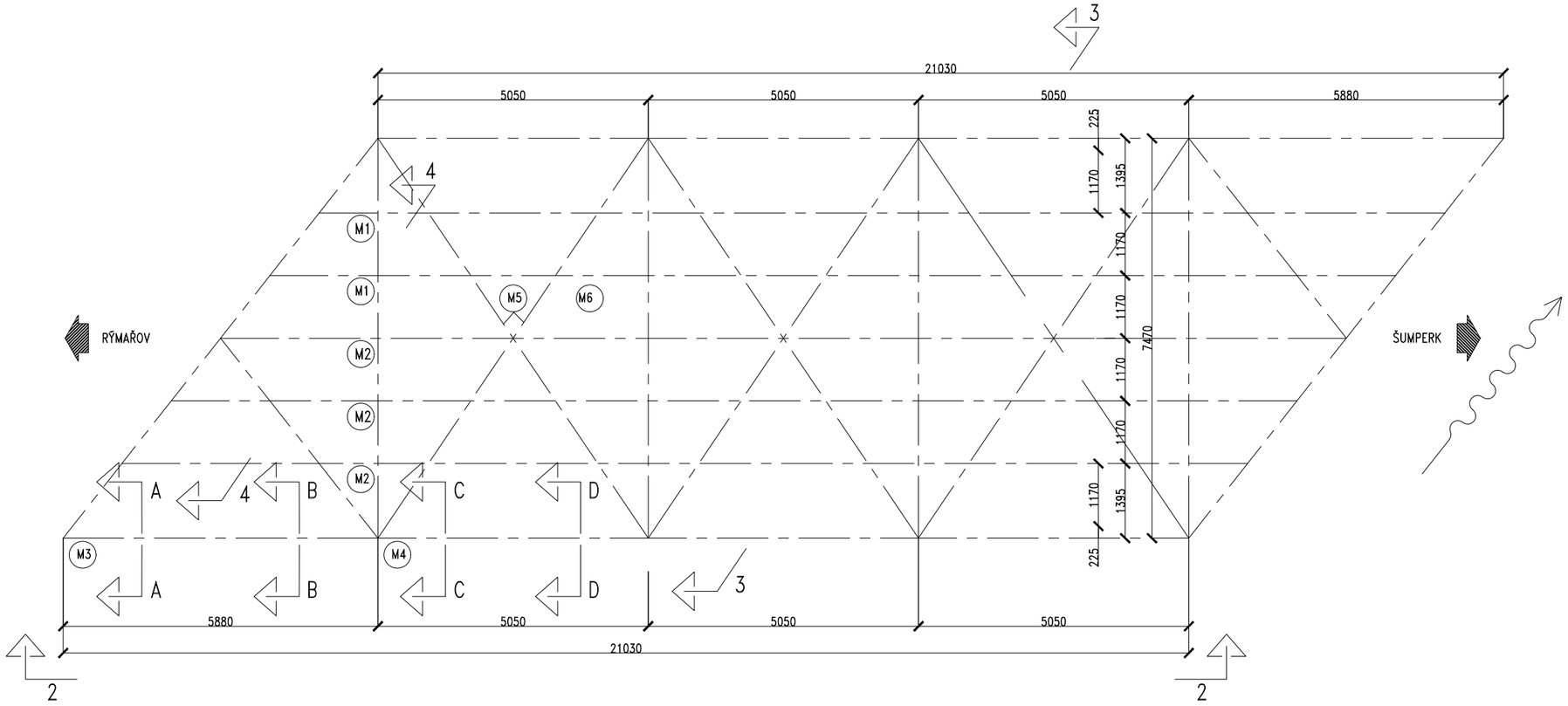

1 / A1 PLAN VIEW: SCHEMATIC

SCALE: 1:100

PICTURE OF THE SITE

LOCATION MAP OF THE SITE

Název akce: The Ultimate Load Capacity of the Road Historic Steel Bridge	
Název části: AS-FOUND DRAWINGS	
Název přílohy: 11-097 PETROV BRIDGE - PLAN AND LOCATION	Číslo přílohy: A1/A7

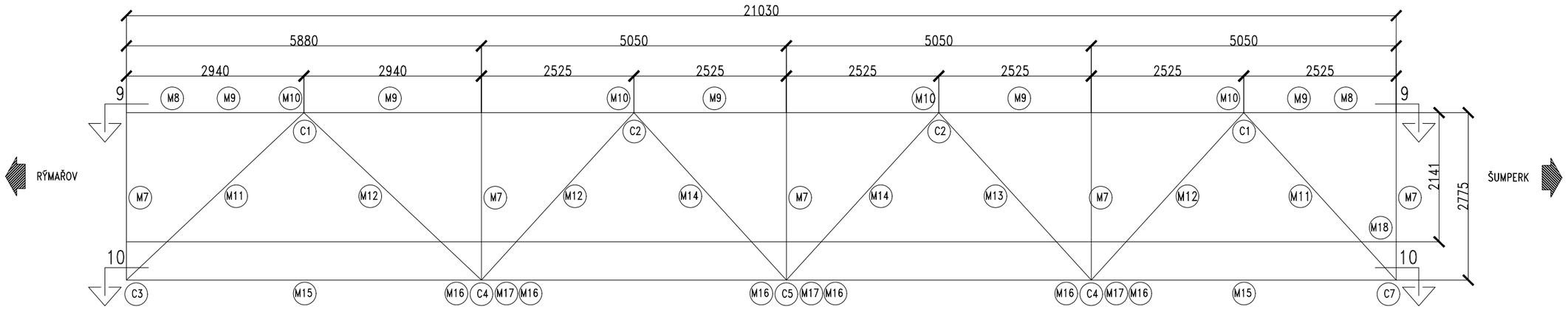

2A A1 A2 NORTH AND SOUTH ELEVATIONS: SCHEMATIC

SCALE: 1:75

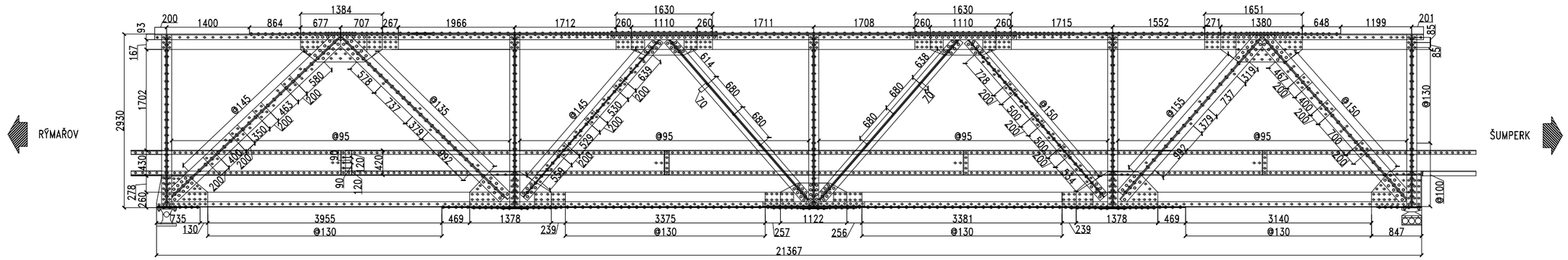

2B A1 A2 NORTH AND SOUTH ELEVATIONS: DETAILED

SCALE: 1:75

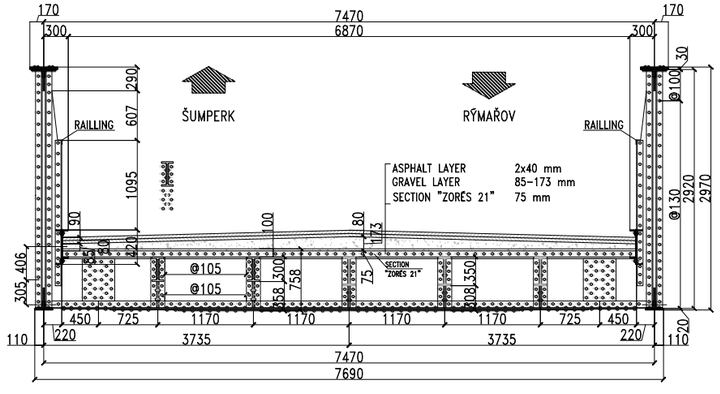

3 A1 A2 EAST AND WEST ELEVATIONS: DETAILED

SCALE: 1:75

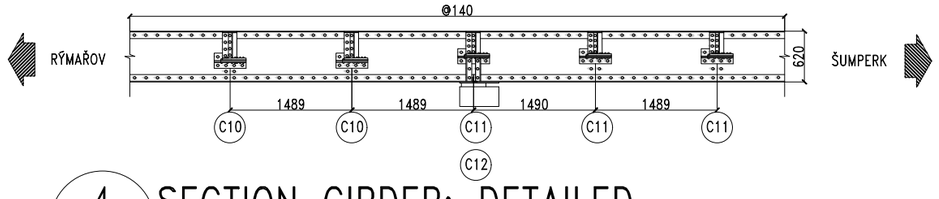

4 A1 A2 SECTION GIRDER: DETAILED

SCALE: 1:75

LEGEND

- 24mm HEAD DIAMETER FOR 16mm RIVET DIAMETER
- 30mm HEAD DIAMETER FOR 20mm RIVET DIAMETER
- 40mm HEAD DIAMETER FOR 24mm RIVET DIAMETER

Název akce: The Ultimate Load Capacity of the Road Historic Steel Bridge	
Název části: AS-FOUND DRAWINGS	
Název přílohy: 11-097 PETROV BRIDGE - ELEVATIONS	*Číslo přílohy:* A2/A7

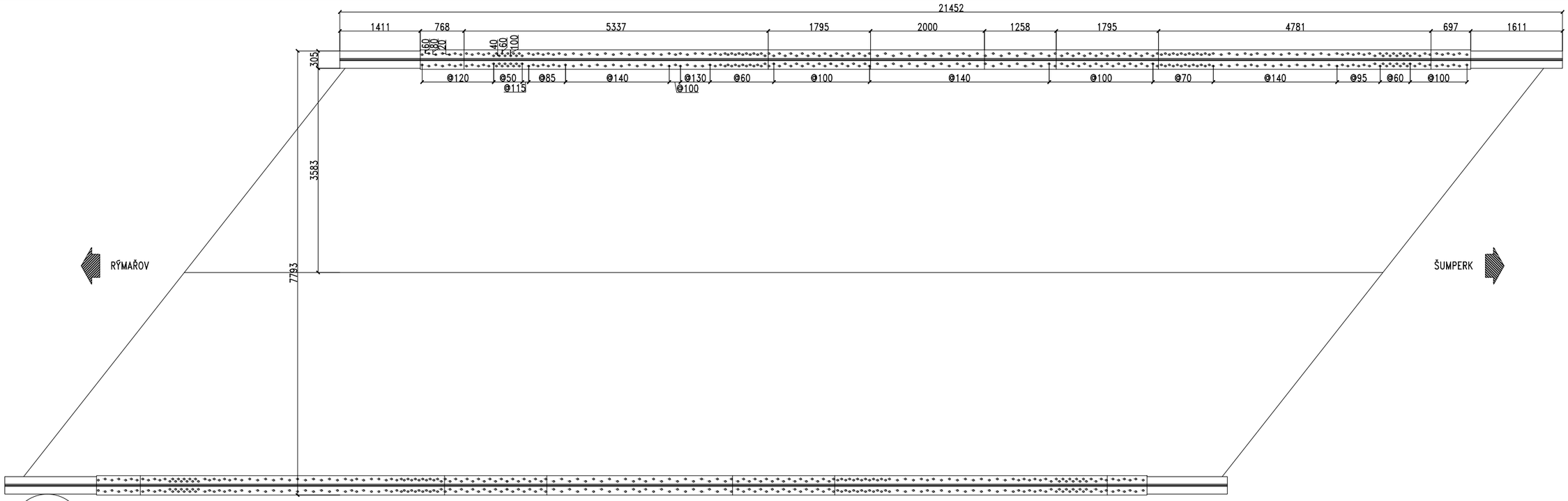

9 A2 A3 **UPPER CHORD PLAN VIEW**

SCALE: 1:75

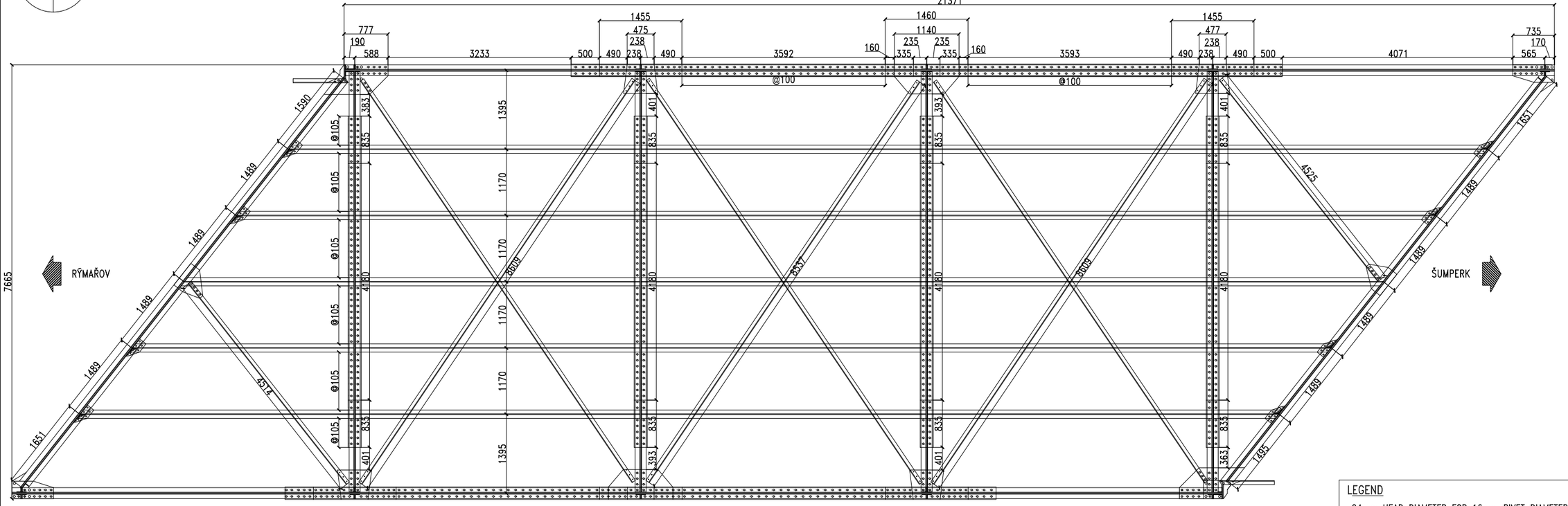

10 A2 A3 **LOWER SECTION PLAN VIEW**

SCALE: 1:75

LEGEND

- 24mm HEAD DIAMETER FOR 16mm RIVET DIAMETER
- 30mm HEAD DIAMETER FOR 20mm RIVET DIAMETER
- 40mm HEAD DIAMETER FOR 24mm RIVET DIAMETER

Název akce: The Ultimate Load Capacity of the Road Historic Steel Bridge	
Název části: AS-FOUND DRAWINGS	
Název přílohy: 11-097 PETROV BRIDGE - PLANS	*Číslo přílohy:* A3/A7

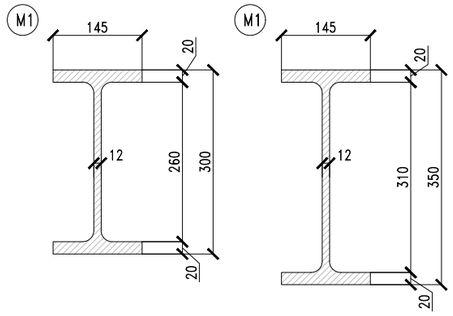

M1–M2 A1 A2 DETAIL STRINGERS
SCALE: 1:10

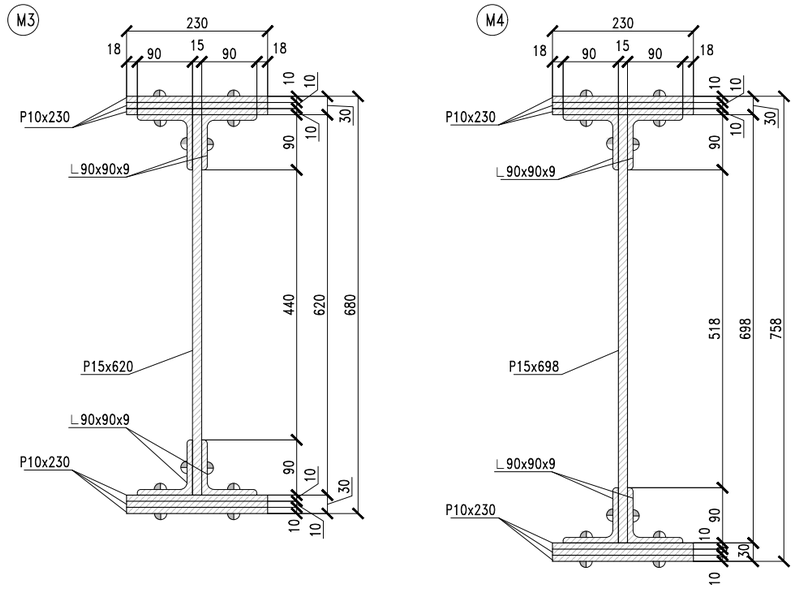

M3–M4 A1 A2 DETAILS CROSS BEAM AND GIRDER
SCALE: 1:10

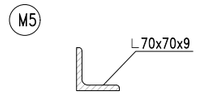

M5 A1 A2 DETAIL BRACING
SCALE: 1:10

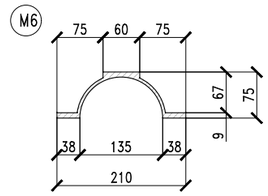

M6 A1 A2 DETAIL "ZORES 21"
SCALE: 1:10

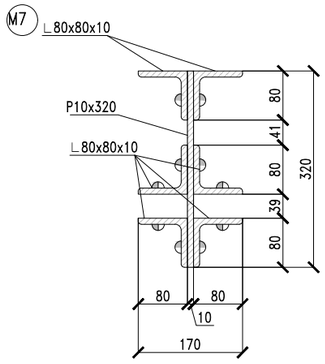

M7 A1 A2 DETAIL VERTICALS
SCALE: 1:10

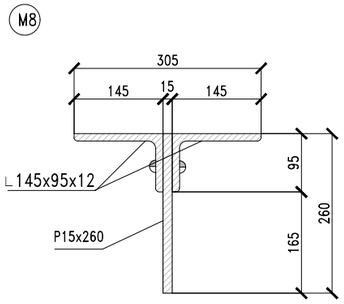

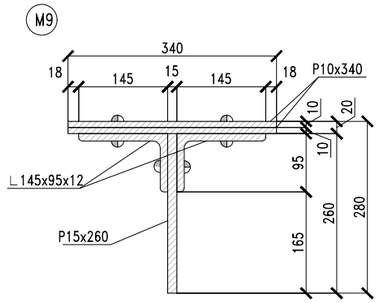

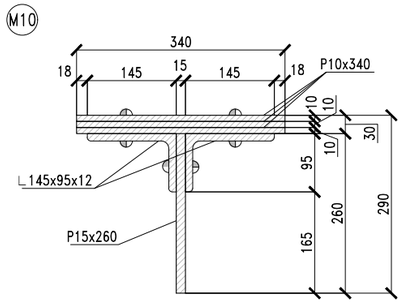

M8–M10 A1 A2 DETAILS UPPER CHORD
SCALE: 1:10

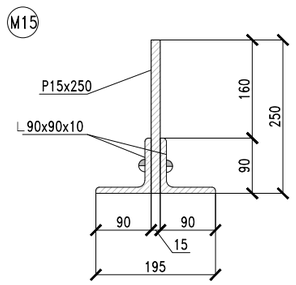

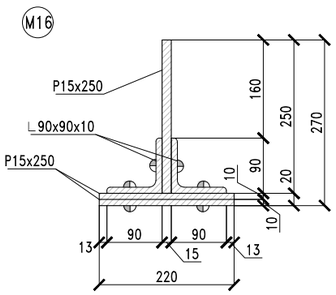

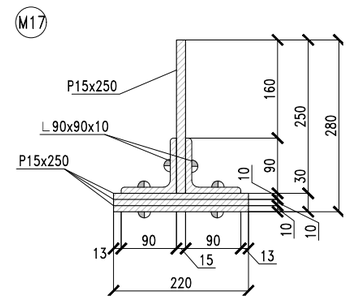

M15–M17 A1 A2 DETAILS LOWER CHORD
SCALE: 1:10

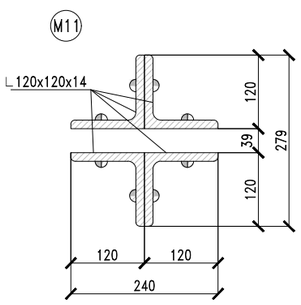

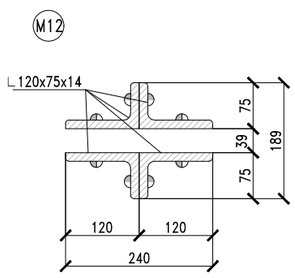

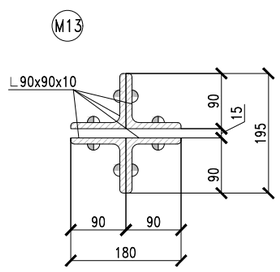

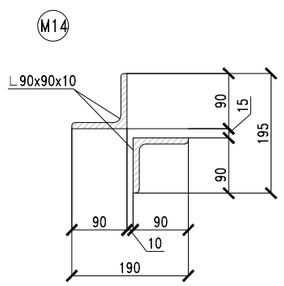

M11–M14 A1 A2 DETAILS DIAGONALS
SCALE: 1:10

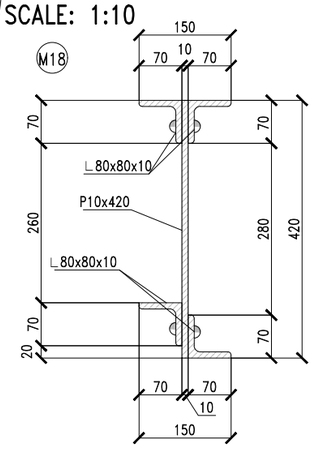

M18 A1 A2 DETAIL ROAD BEAM
SCALE: 1:10

LEGEND
- 24mm HEAD DIAMETER FOR 16mm RIVET DIAMETER
- 30mm HEAD DIAMETER FOR 20mm RIVET DIAMETER
- 40mm HEAD DIAMETER FOR 24mm RIVET DIAMETER

Název akce: The Ultimate Load Capacity of the Road Historic Steel Bridge	
Název části: AS-FOUND DRAWINGS	
Název přílohy: 11-097 PETROV BRIDGE - CROSS-SECTION DETAILS	Číslo přílohy: A4/A7

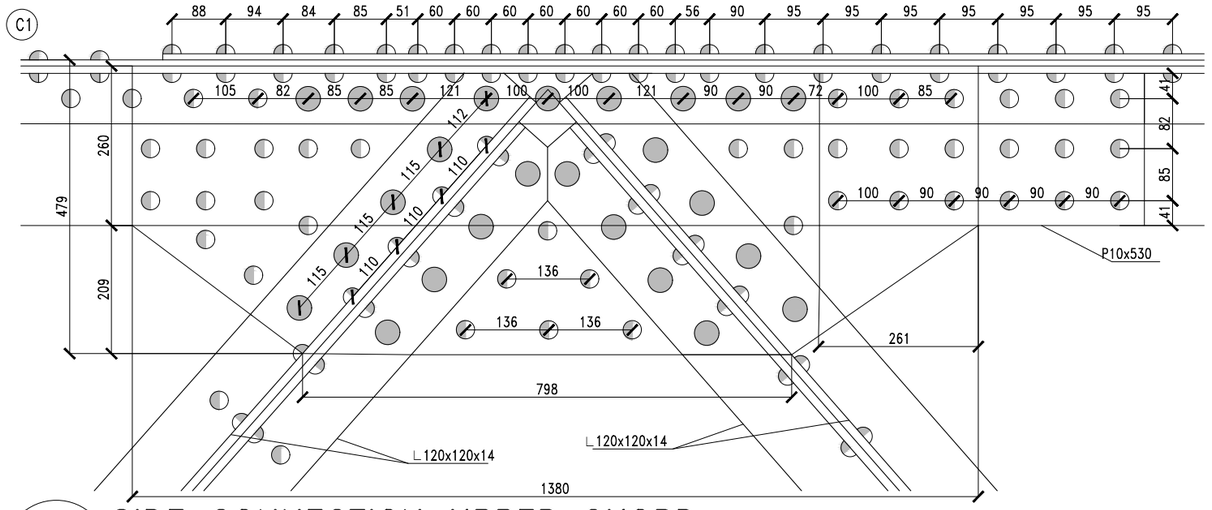

C1 | A2 | A5

SIDE CONNECTION UPPER CHORD

SCALE: 1:10

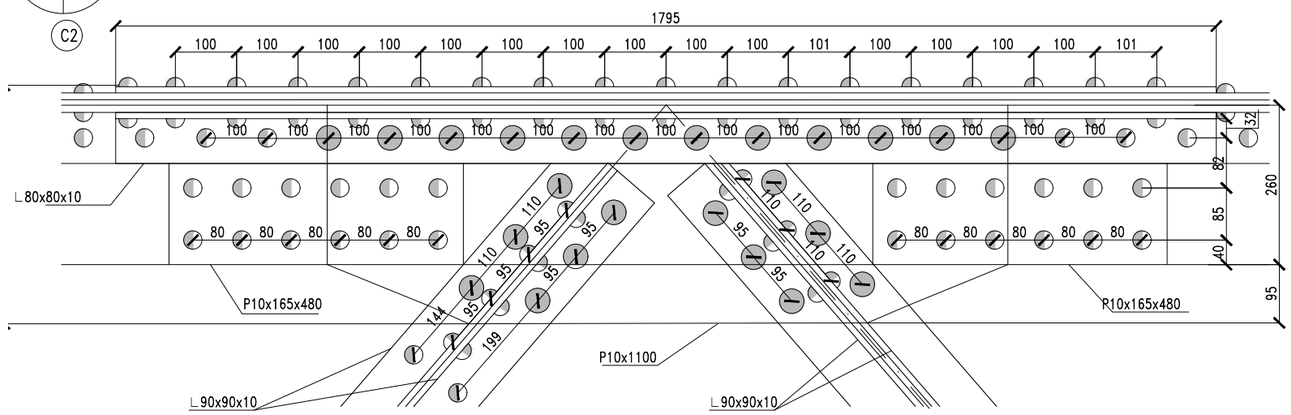

C2 | A2 | A5

CENTER CONNECTION UPPER CHORD

SCALE: 1:10

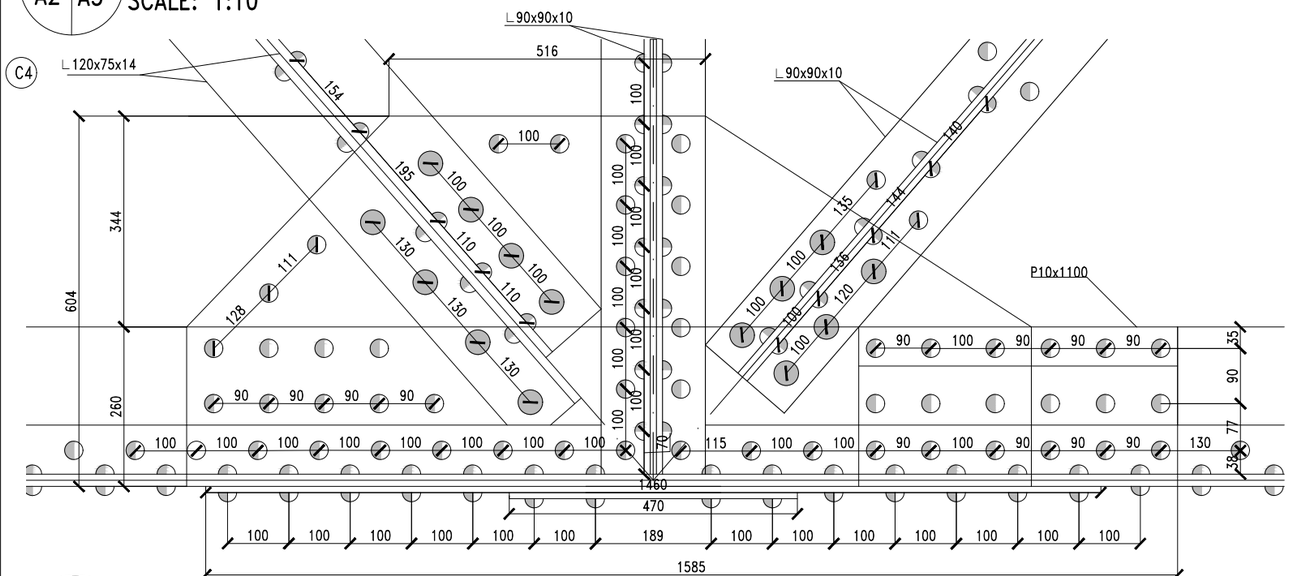

C4a | A2 | A5

SIDE CONNECTION LOWER CHORD: ELEVATION

SCALE: 1:10

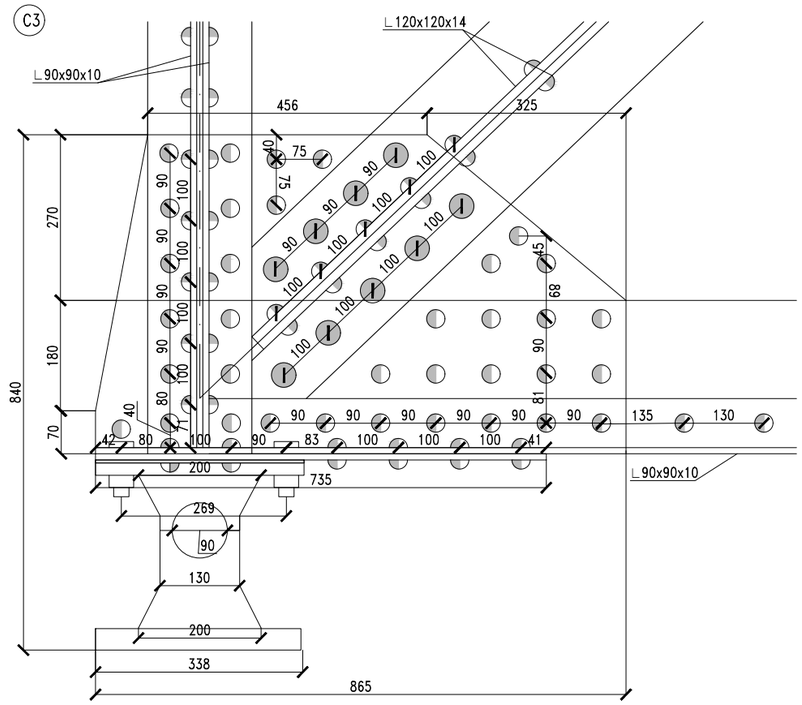

C3a | A2 | A5

HINGED CONNECTION: ELEVATION

SCALE: 1:10

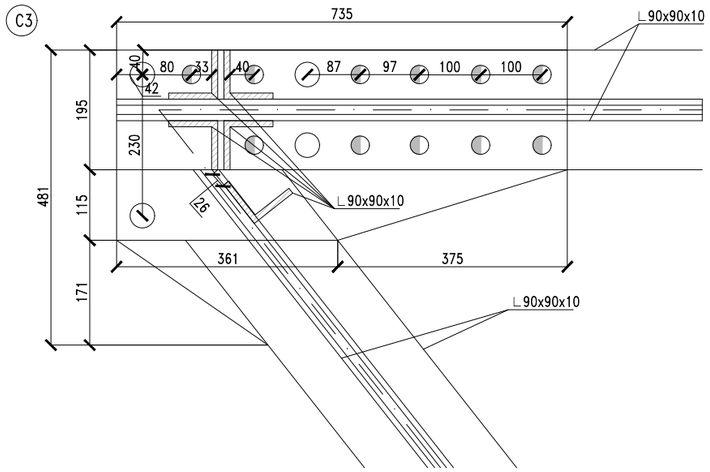

C3b | A2 | A5

HINGED CONNECTION: PLAN

SCALE: 1:10

LEGEND

- 24mm HEAD DIAMETER FOR 16mm RIVET DIAMETER
- 30mm HEAD DIAMETER FOR 20mm RIVET DIAMETER
- 40mm HEAD DIAMETER FOR 24mm RIVET DIAMETER

Název akce: The Ultimate Load Capacity of a Historical Road Steel Bridge	
Název části: AS-FOUND DRAWINGS	
Název přílohy: 11-097 PETROV BRIDGE - CONNECTION DETAILS 1/3	Číslo přílohy: A5/A7

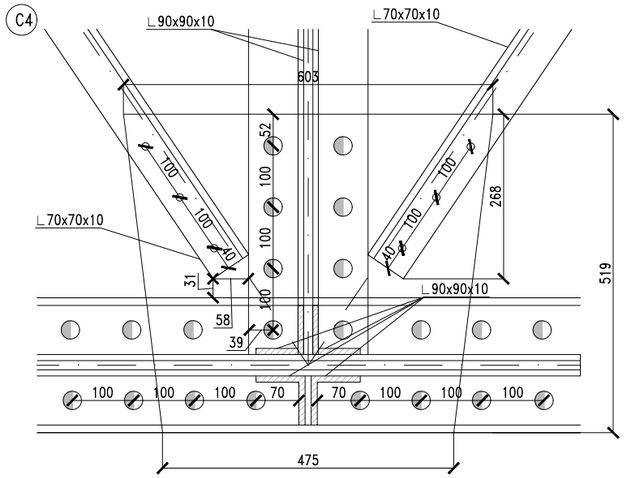

C4b SIDE CONNECTION LOWER CHORD: PLAN

A2 | A6

SCALE: 1:10

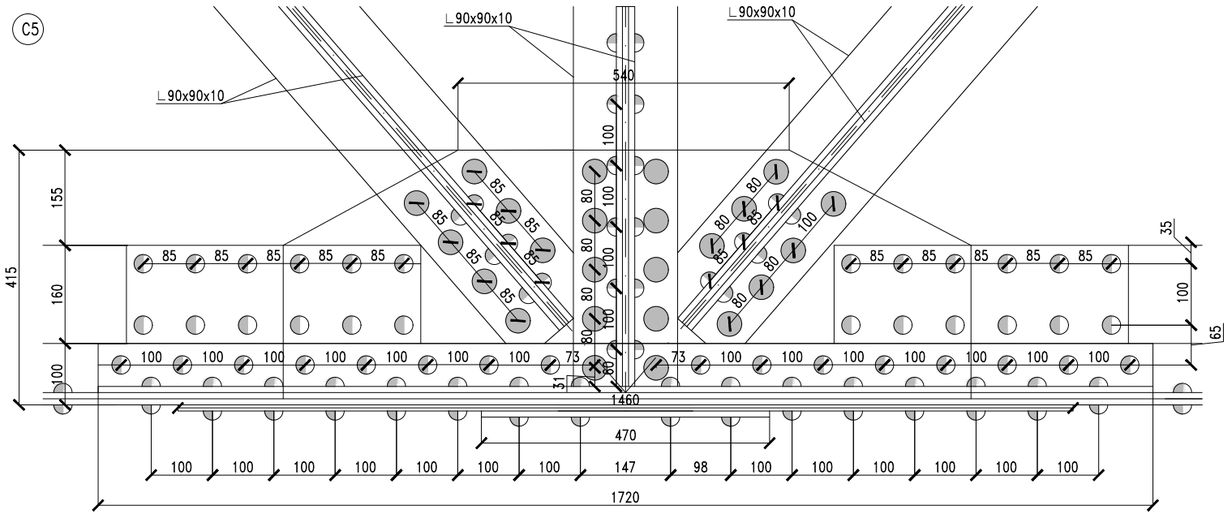

C5a CENTRE CONNECTION LOWER CHORD: ELEVATION

A2 | A6

SCALE: 1:10

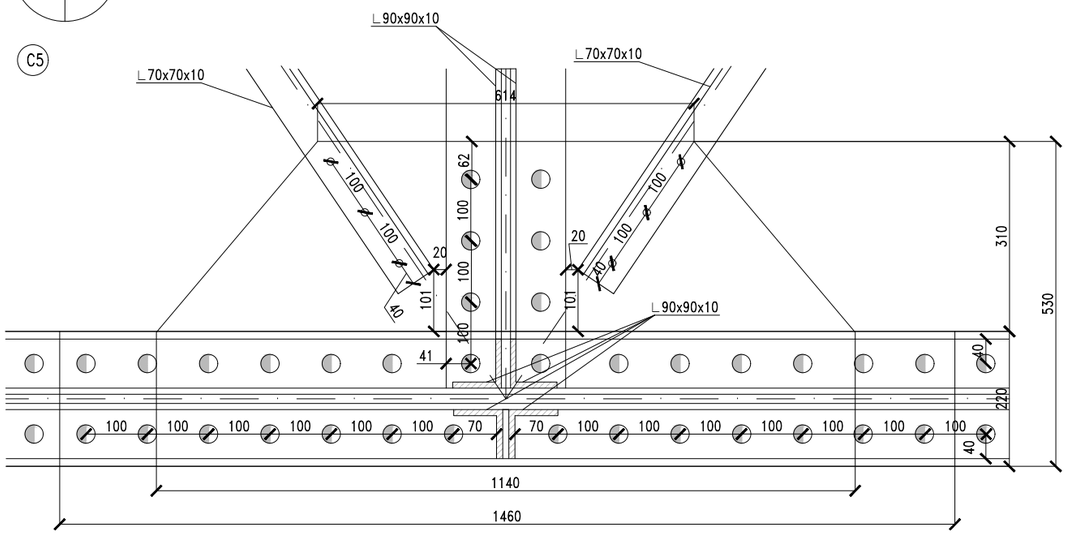

C5b CENTRE CONNECTION LOWER CHORD: PLAN

A2 | A6

SCALE: 1:10

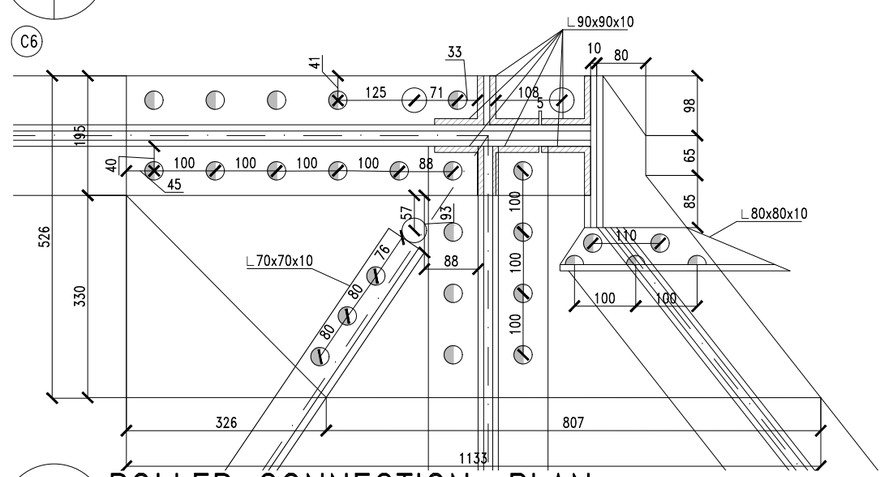

C6b ROLLER CONNECTION: PLAN

A2 | A6

SCALE: 1:10

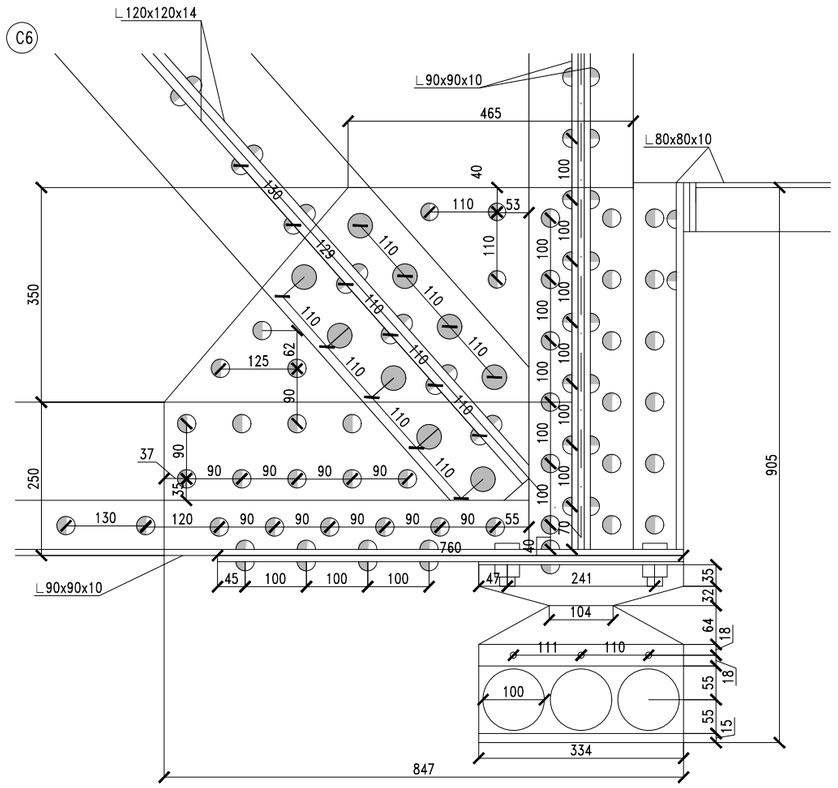

C6a ROLLER CONNECTION: ELEVATION

A2 | A6

SCALE: 1:10

LEGEND

- 24mm HEAD DIAMETER FOR 16mm RIVET DIAMETER
- 30mm HEAD DIAMETER FOR 20mm RIVET DIAMETER
- 40mm HEAD DIAMETER FOR 24mm RIVET DIAMETER

Název akce: The Ultimate Load Capacity of the Road Historic Steel Bridge	
Název části: AS-FOUND DRAWINGS	
Název přílohy: 11-097 PETROV BRIDGE - CONNECTION DETAILS 2/3	Číslo přílohy: A6/A7

C7

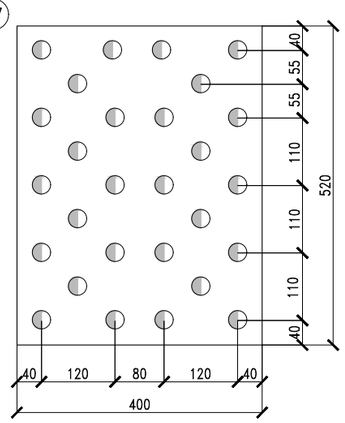

C8

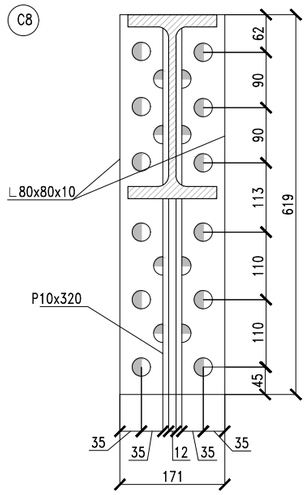

C9

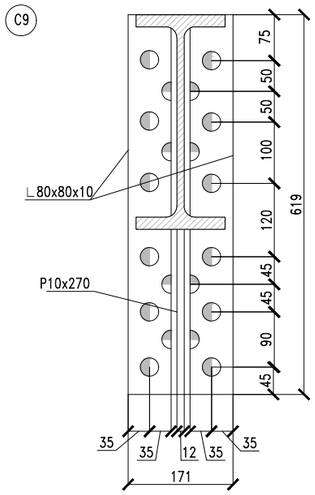

C7 GUSSET PLATE

A2 | A7 SCALE: 1:10

C8–C9 CROSS BEAM AND STRINGER CONNECTION

A2 | A7 SCALE: 1:10

C10

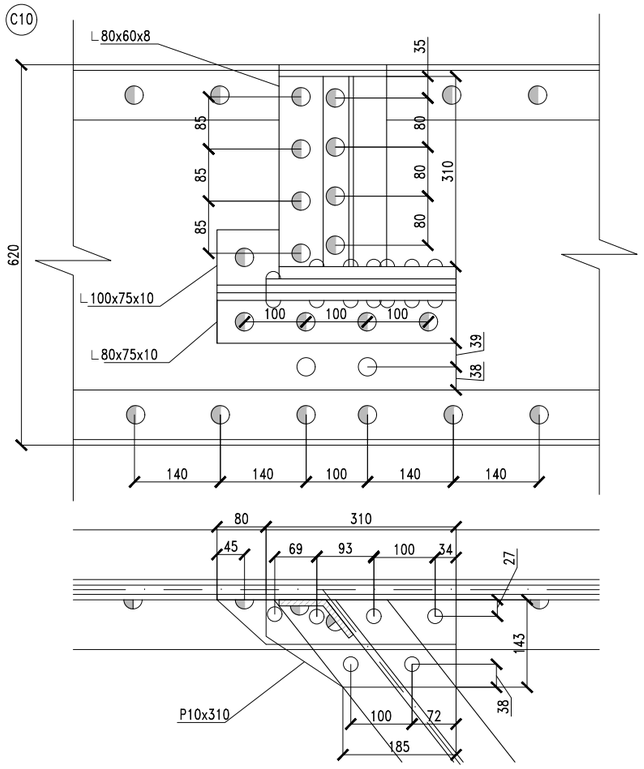

C11

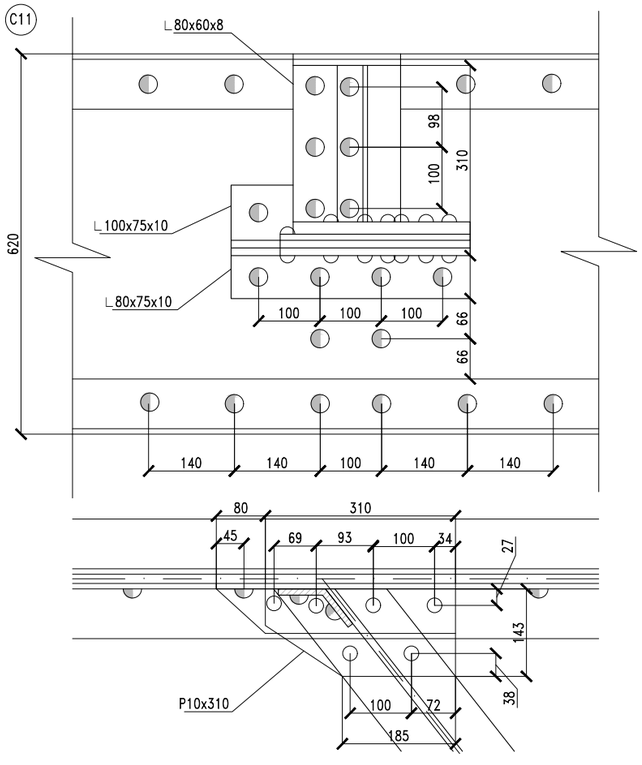

C12

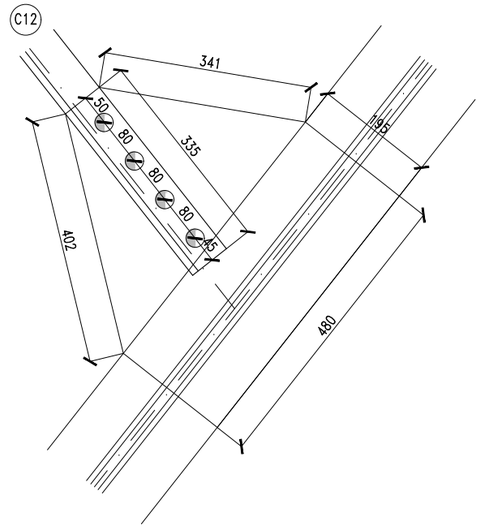

C10 GIRDER AND STRINGER CONNECTION

A2 | A7 SCALE: 1:10

C11 GIRDER AND STRINGER CONNECTION

A2 | A7 SCALE: 1:10

C12 SECONDARY SUPPORT CONNECTION

A2 | A7 SCALE: 1:10

LEGEND

- 24mm HEAD DIAMETER FOR 16mm RIVET DIAMETER
- 30mm HEAD DIAMETER FOR 20mm RIVET DIAMETER
- 40mm HEAD DIAMETER FOR 24mm RIVET DIAMETER

Název akce: The Ultimate Load Capacity of the Road Historic Steel Bridge	
Název části: AS-FOUND DRAWINGS	
Název přílohy: 11-097 PETROV BRIDGE - CONNECTION DETAILS 3/3	*Číslo přílohy:* A7/A7

APPENDIX 2. MODEL CALIBRATION BASED ON EXPERIMENTAL DATA

Appendix 2.1. Model Calibration of the Unstrengthen Bridge: in the Lane.

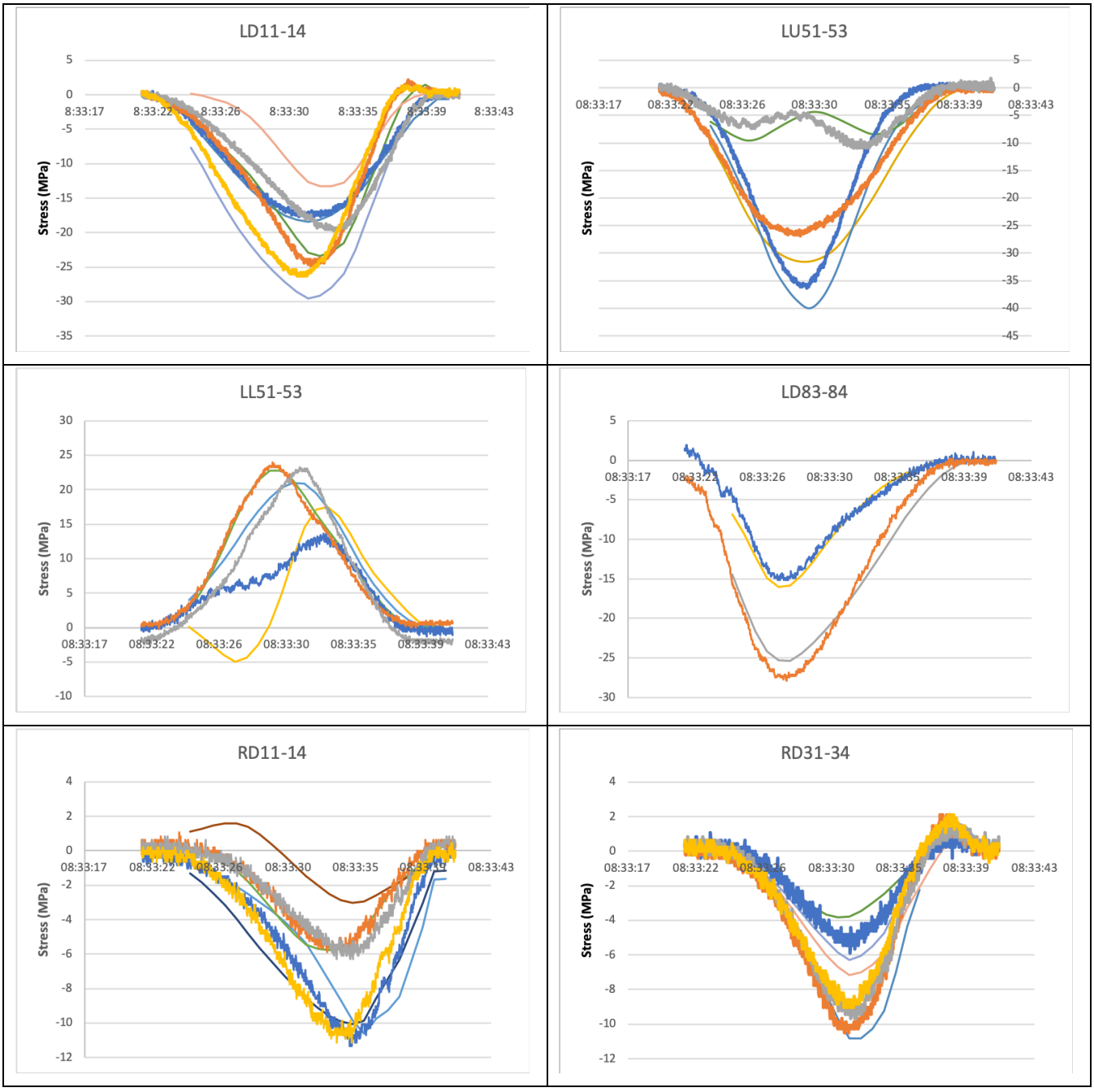

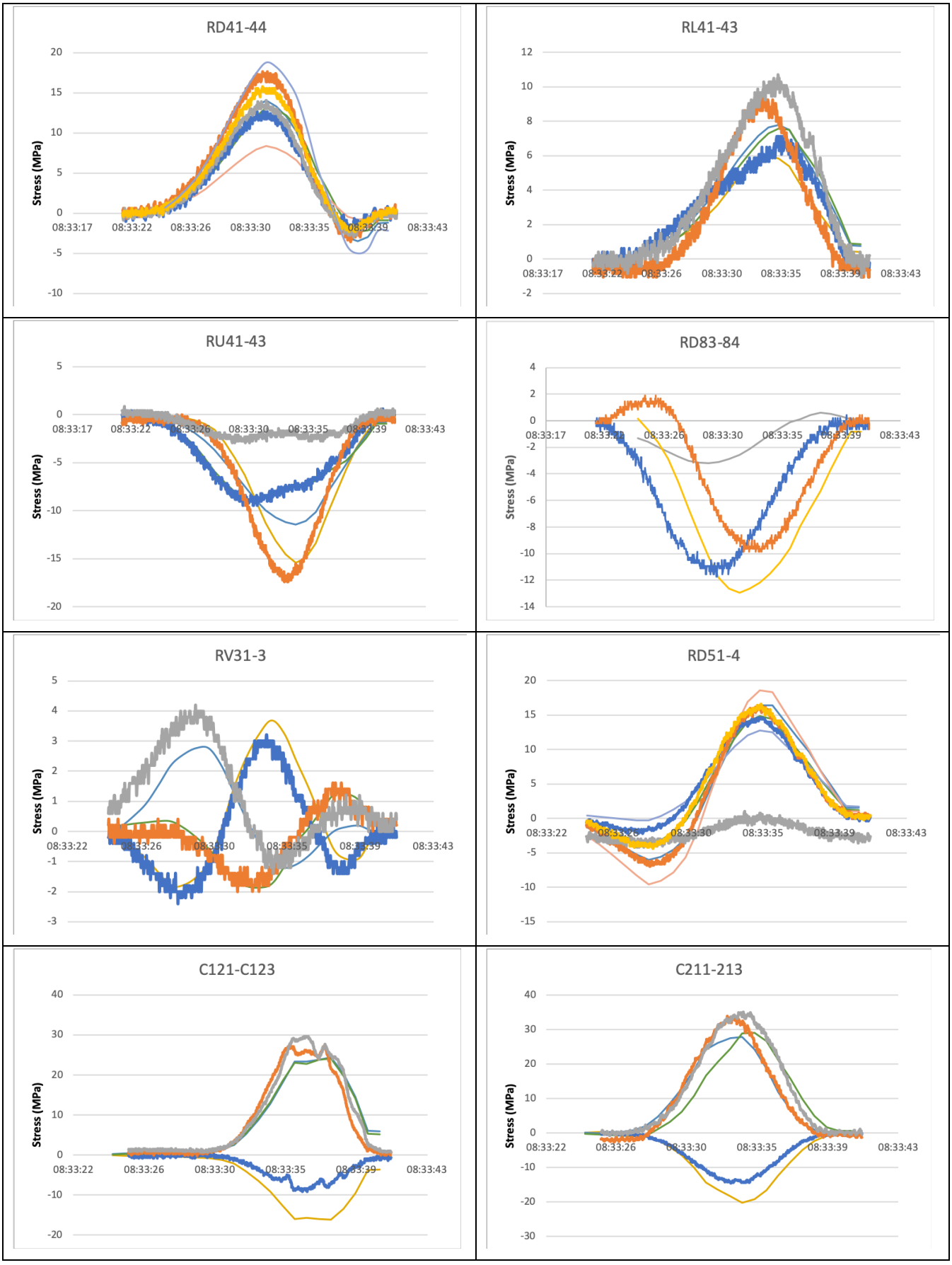
RD41-44
Stress (MPa)
RL41-43
Stress (MPa)
RU41-43
Stress (MPa)
RD83-84
Stress (MPa)
RV31-3
Stress (MPa)
RD51-4
Stress (MPa)
C121-C123
Stress (MPa)
C211-213
Stress (MPa)

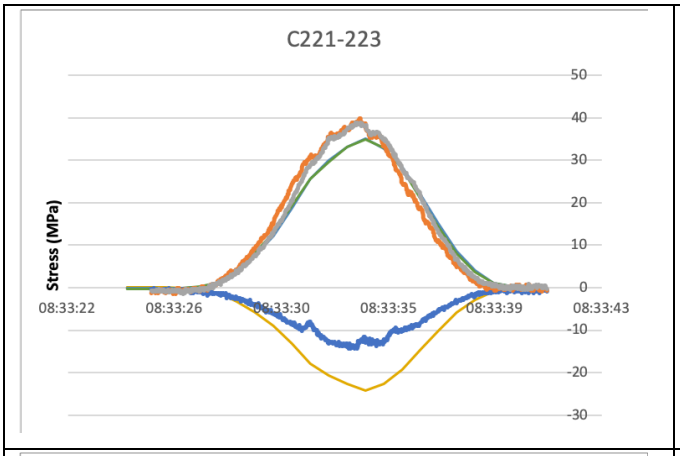
C221-223
Stress (MPa)
50
40
30
20
10
0
-10
-20
-30
08:33:22
08:33:26
08:33:30
08:33:35
08:33:39
08:33:43

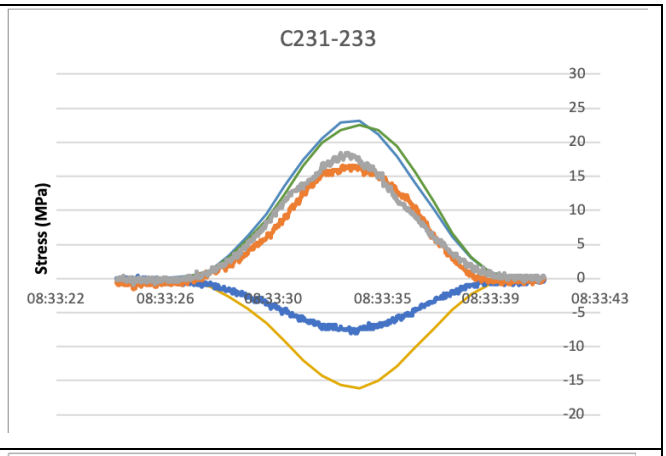
C231-233
Stress (MPa)
30
25
20
15
10
5
0
-5
-10
-15
-20
08:33:22
08:33:26
08:33:30
08:33:35
08:33:39
08:33:43

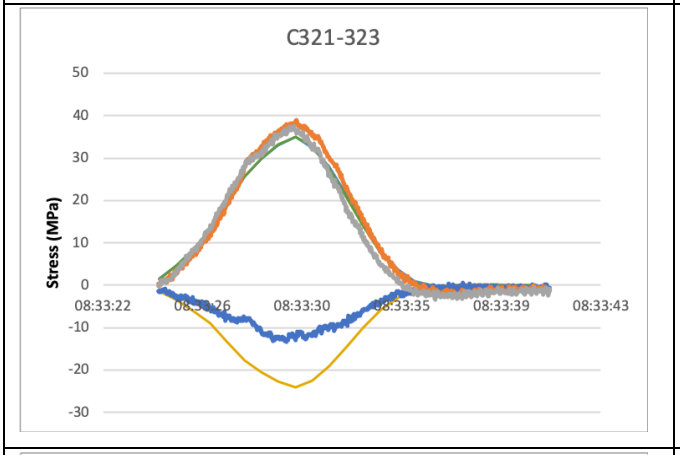
C321-323
Stress (MPa)
50
40
30
20
10
0
-10
-20
-30
08:33:22
08:33:26
08:33:30
08:33:35
08:33:39
08:33:43

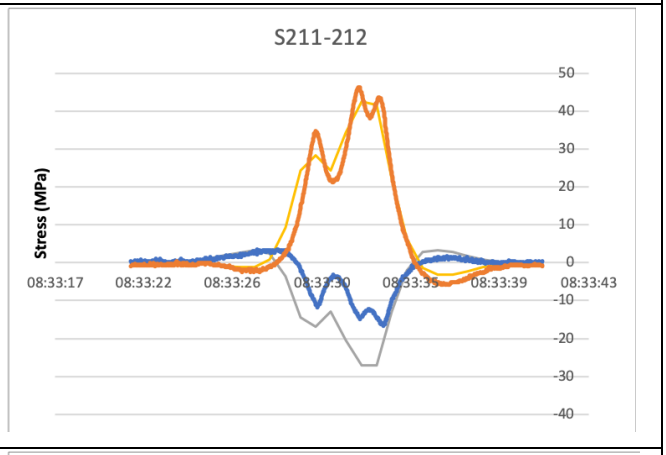
S211-212
Stress (MPa)
50
40
30
20
10
0
-10
-20
-30
-40
08:33:17
08:33:22
08:33:26
08:33:30
08:33:35
08:33:39
08:33:43

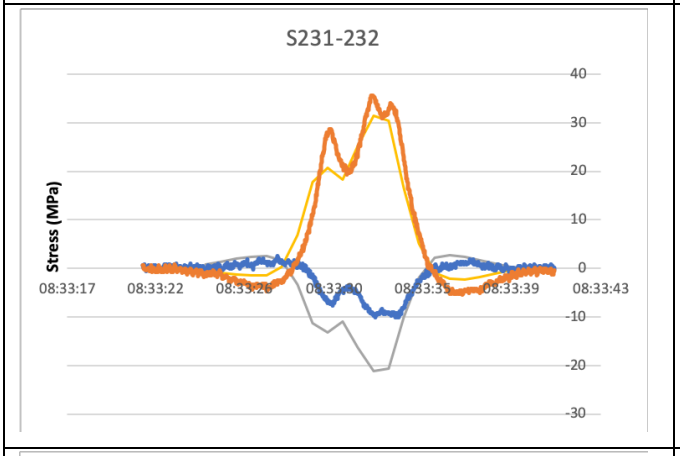
S231-232
Stress (MPa)
40
30
20
10
0
-10
-20
-30
08:33:17
08:33:22
08:33:26
08:33:30
08:33:35
08:33:39
08:33:43

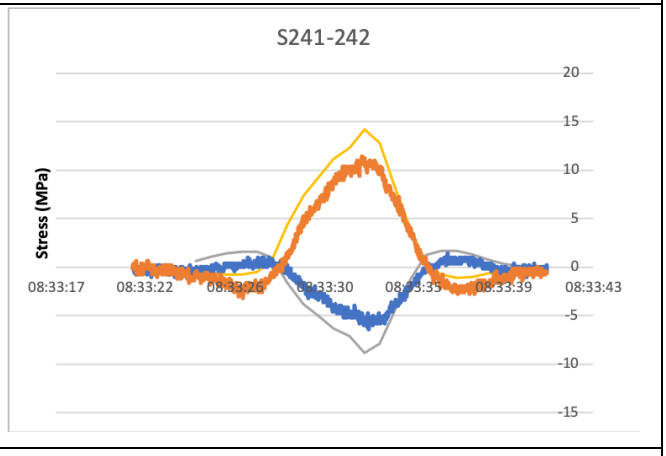
S241-242
Stress (MPa)
20
15
10
5
0
-5
-10
-15
08:33:17
08:33:22
08:33:26
08:33:30
08:33:35
08:33:39
08:33:43

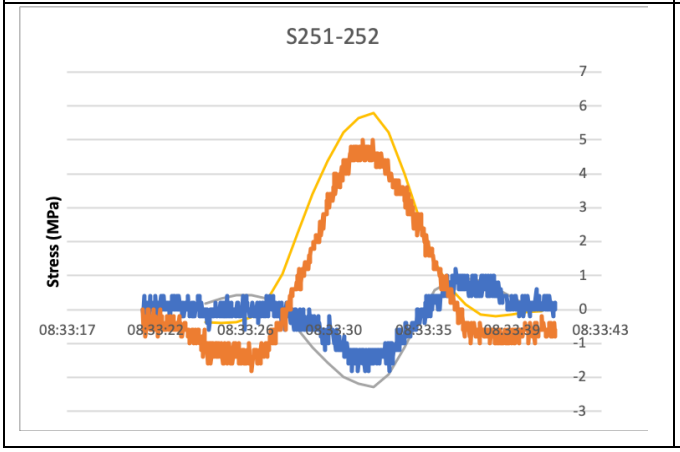
S251-252
Stress (MPa)
7
6
5
4
3
2
1
0
-1
-2
-3
08:33:17
08:33:22
08:33:26
08:33:30
08:33:35
08:33:39
08:33:43

Appendix 2.2. Model Calibration of the Unstrengthen Bridge: on the Axis.

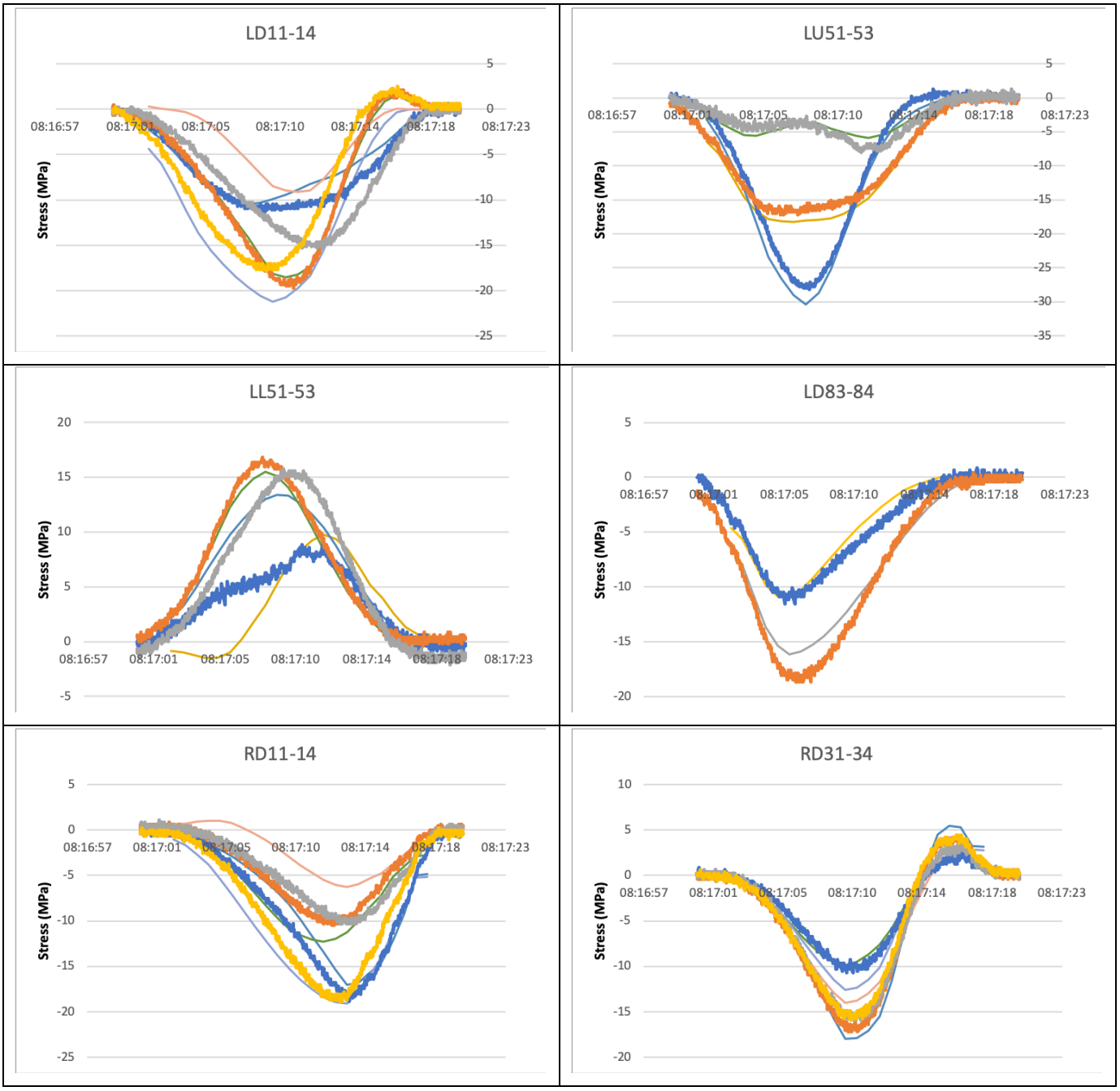

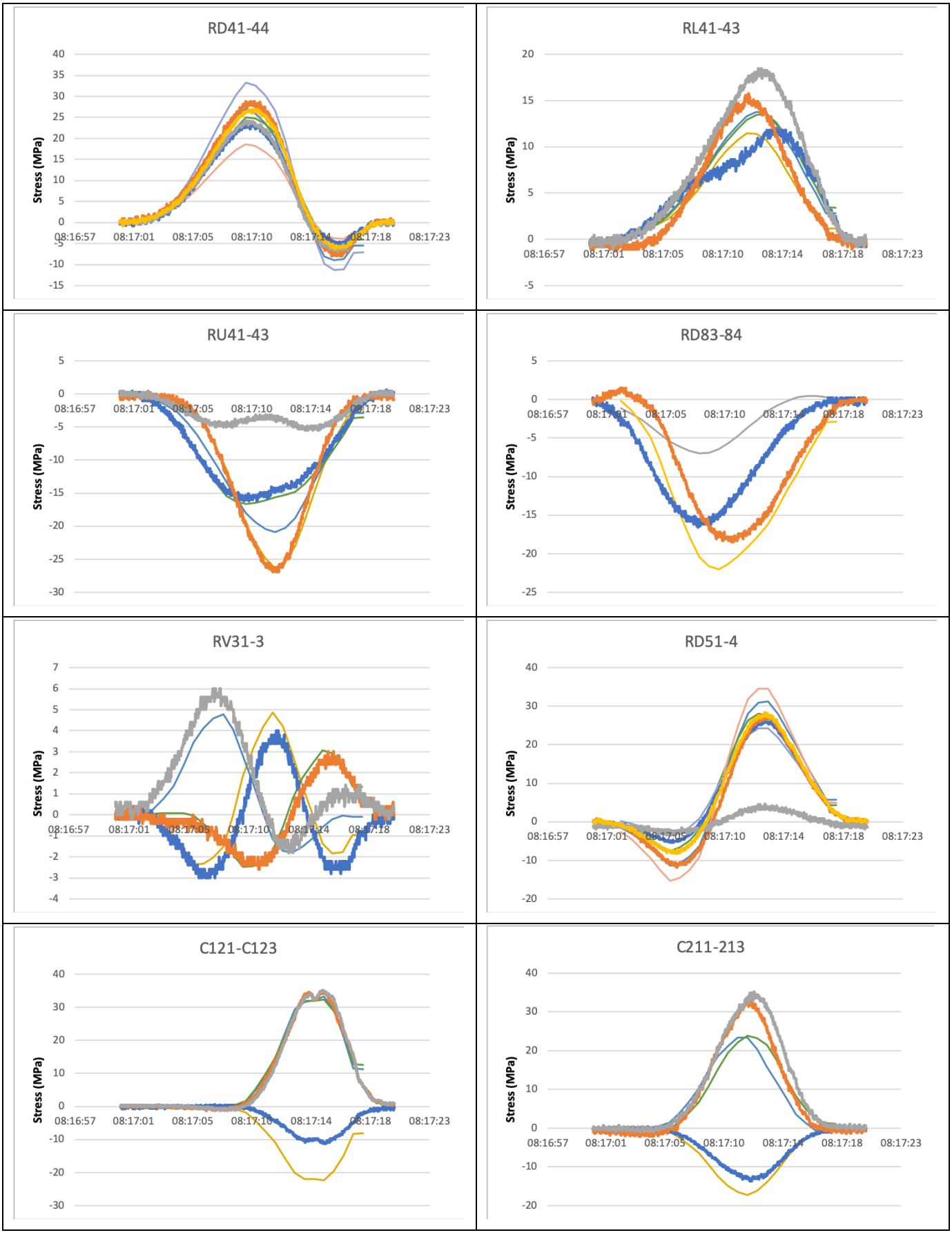
RD41-44
Stress (MPa)
40
35
30
25
20
15
10
5
0
-5
-10
-15
08:16:57
08:17:01
08:17:05
08:17:10
08:17:14
08:17:18
08:17:23
RL41-43
Stress (MPa)
20
15
10
5
0
-5
08:16:57
08:17:01
08:17:05
08:17:10
08:17:14
08:17:18
08:17:23
RU41-43
Stress (MPa)
5
0
-5
-10
-15
-20
-25
-30
08:16:57
08:17:01
08:17:05
08:17:10
08:17:14
08:17:18
08:17:23
RD83-84
Stress (MPa)
5
0
-5
-10
-15
-20
-25
08:16:57
08:17:01
08:17:05
08:17:10
08:17:14
08:17:18
08:17:23
RV31-3
Stress (MPa)
7
6
5
4
3
2
1
0
-1
-2
-3
-4
08:16:57
08:17:01
08:17:05
08:17:10
08:17:14
08:17:18
08:17:23
RD51-4
Stress (MPa)
40
30
20
10
0
-10
-20
08:16:57
08:17:01
08:17:05
08:17:10
08:17:14
08:17:18
08:17:23
C121-C123
Stress (MPa)
40
30
20
10
0
-10
-20
-30
08:16:57
08:17:01
08:17:05
08:17:10
08:17:14
08:17:18
08:17:23
C211-213
Stress (MPa)
40
30
20
10
0
-10
-20
08:16:57
08:17:01
08:17:05
08:17:10
08:17:14
08:17:18
08:17:23

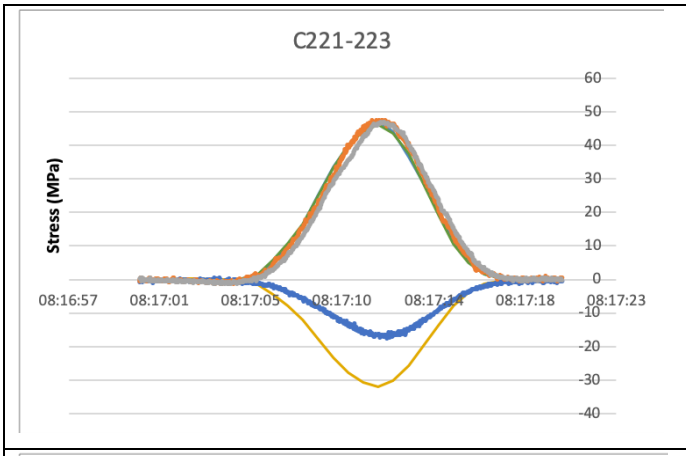
C221-223
Stress (MPa)
60
50
40
30
20
10
0
-10
-20
-30
-40
08:16:57
08:17:01
08:17:05
08:17:10
08:17:14
08:17:18
08:17:23

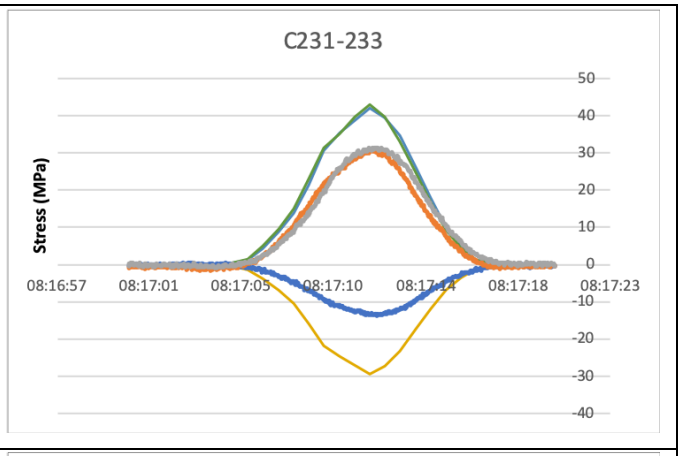
C231-233
Stress (MPa)
50
40
30
20
10
0
-10
-20
-30
-40
08:16:57
08:17:01
08:17:05
08:17:10
08:17:14
08:17:18
08:17:23

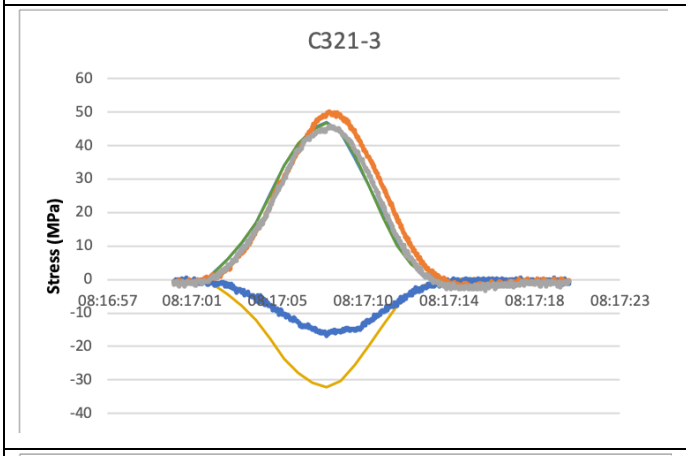
C321-3
Stress (MPa)
60
50
40
30
20
10
0
-10
-20
-30
-40
08:16:57
08:17:01
08:17:05
08:17:10
08:17:14
08:17:18
08:17:23

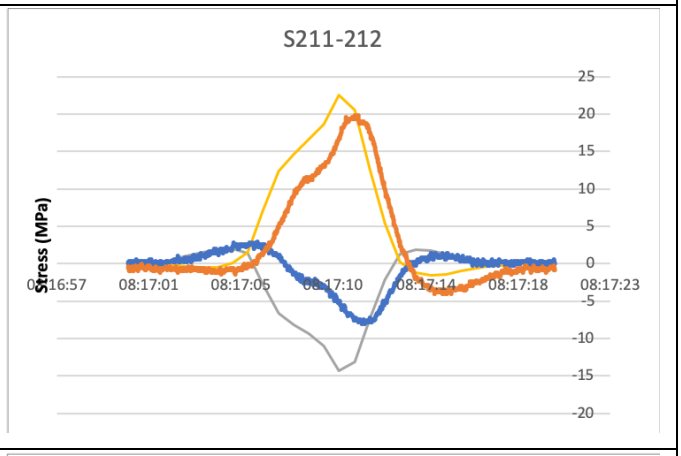
S211-212
Stress (MPa)
25
20
15
10
5
0
-5
-10
-15
-20
08:16:57
08:17:01
08:17:05
08:17:10
08:17:14
08:17:18
08:17:23

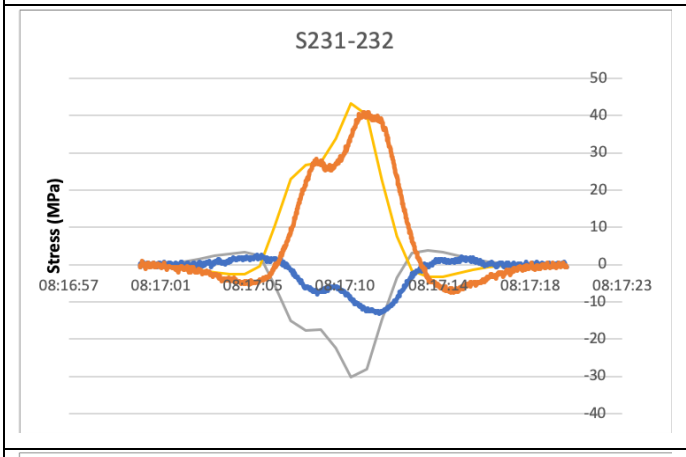
S231-232
Stress (MPa)
50
40
30
20
10
0
-10
-20
-30
-40
08:16:57
08:17:01
08:17:05
08:17:10
08:17:14
08:17:18
08:17:23

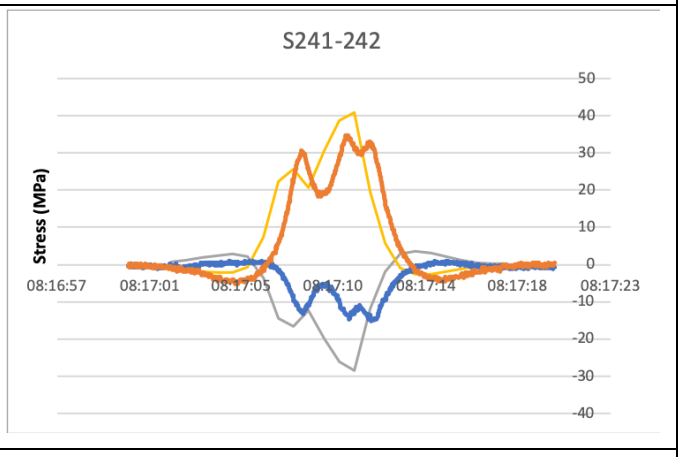
S241-242
Stress (MPa)
50
40
30
20
10
0
-10
-20
-30
-40
08:16:57
08:17:01
08:17:05
08:17:10
08:17:14
08:17:18
08:17:23

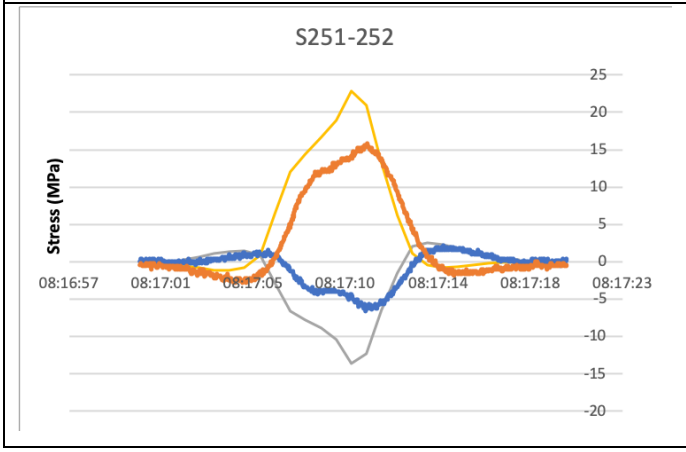
S251-252
Stress (MPa)
25
20
15
10
5
0
-5
-10
-15
-20
08:16:57
08:17:01
08:17:05
08:17:10
08:17:14
08:17:18
08:17:23

Appendix 2.3. Model Calibration of the Strengthened Bridge: in the Lane.

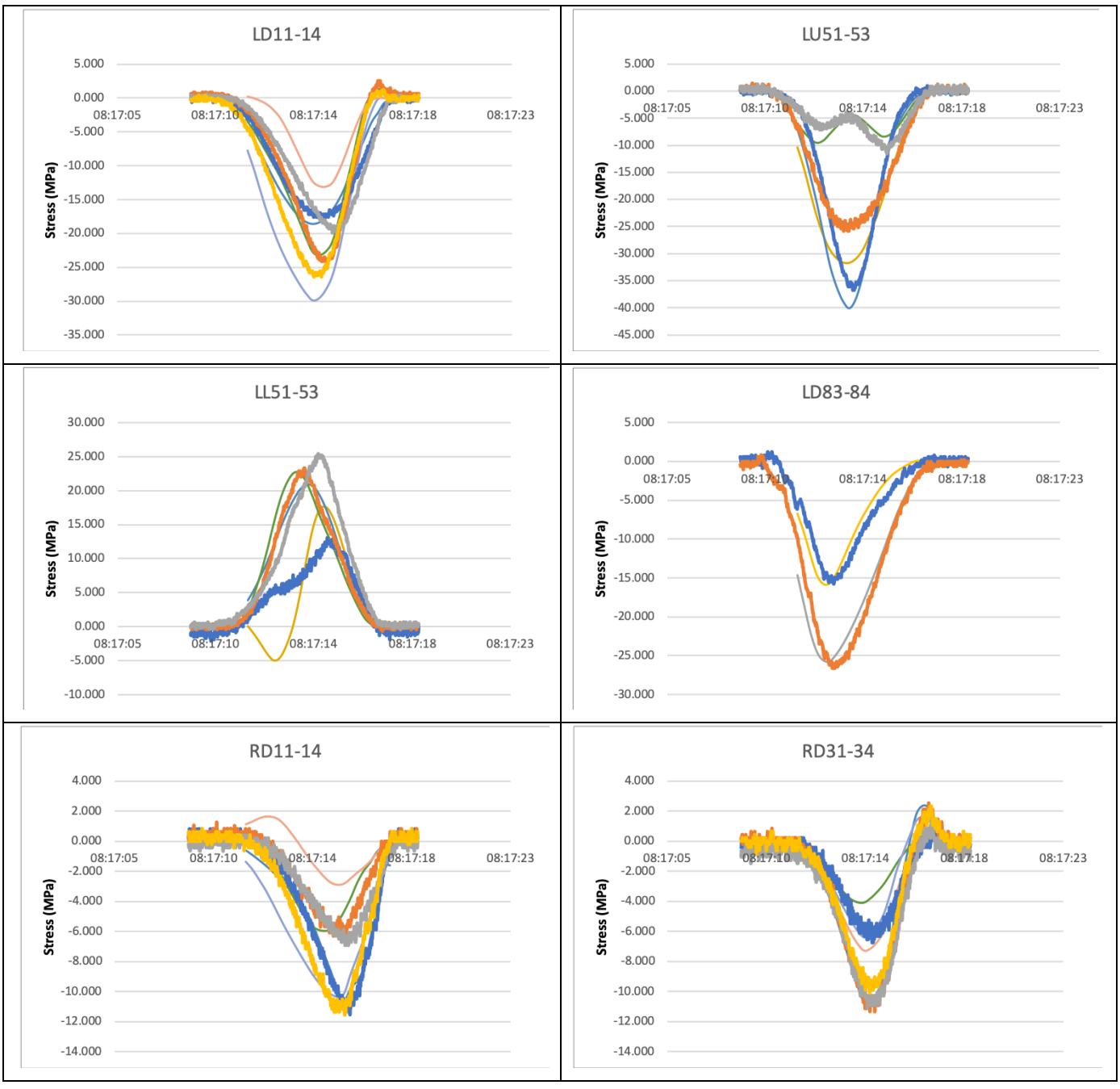

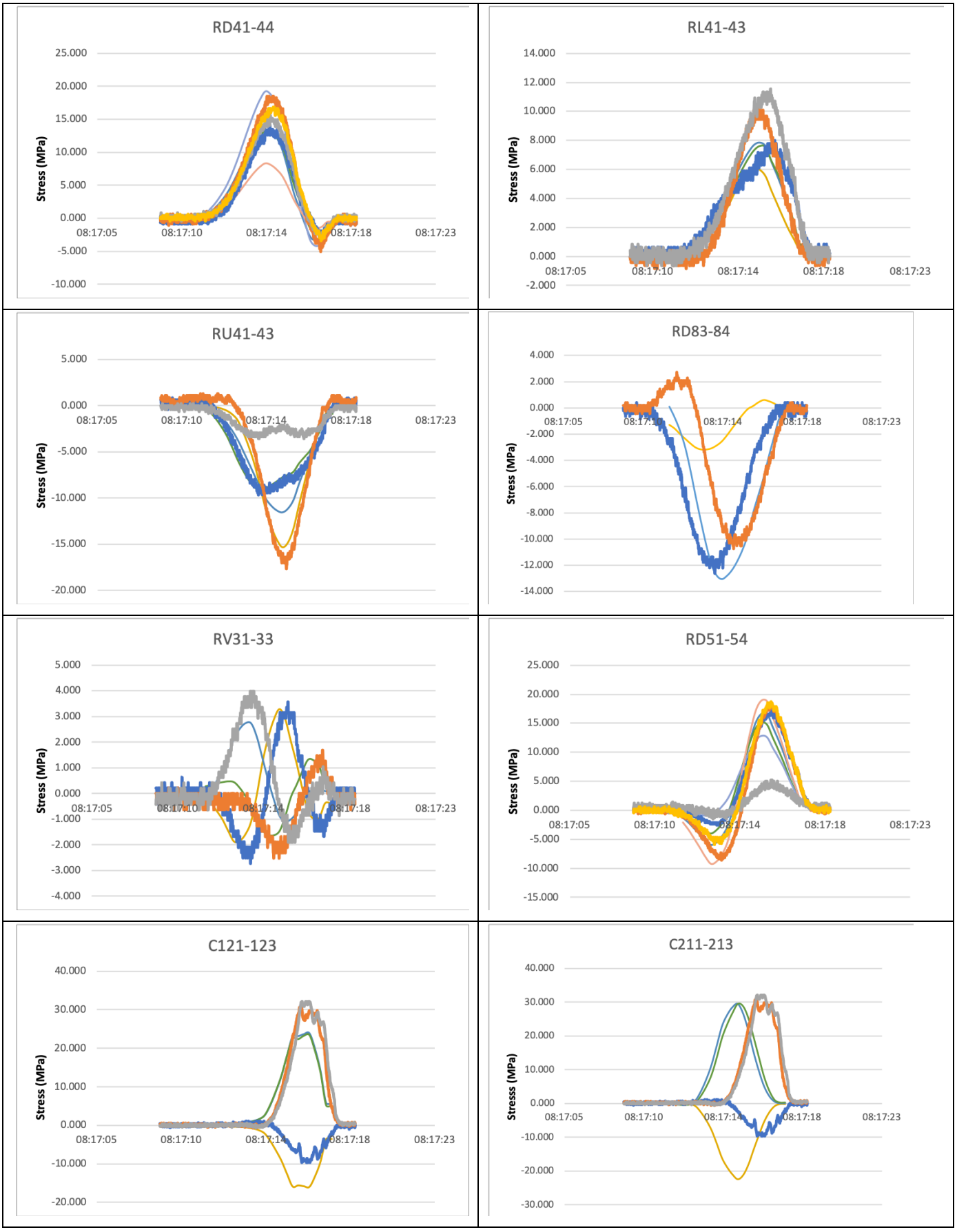
RD41-44
Stress (MPa)
25.000
20.000
15.000
10.000
5.000
0.000
-5.000
-10.000
08:17:05
08:17:10
08:17:14
08:17:18
08:17:23
RL41-43
Stress (MPa)
14.000
12.000
10.000
8.000
6.000
4.000
2.000
0.000
-2.000
08:17:05
08:17:10
08:17:14
08:17:18
08:17:23
RU41-43
Stress (MPa)
5.000
0.000
-5.000
-10.000
-15.000
-20.000
08:17:05
08:17:10
08:17:14
08:17:18
08:17:23
RD83-84
Stress (MPa)
4.000
2.000
0.000
-2.000
-4.000
-6.000
-8.000
-10.000
-12.000
-14.000
08:17:05
08:17:14
08:17:18
08:17:23
RV31-33
Stress (MPa)
5.000
4.000
3.000
2.000
1.000
0.000
-1.000
-2.000
-3.000
-4.000
08:17:05
08:17:18
08:17:23
RD51-54
Stress (MPa)
25.000
20.000
15.000
10.000
5.000
0.000
-5.000
-10.000
-15.000
08:17:05
08:17:10
08:17:14
08:17:18
08:17:23
C121-123
Stress (MPa)
40.000
30.000
20.000
10.000
0.000
-10.000
-20.000
08:17:05
08:17:10
08:17:14
08:17:18
08:17:23
C211-213
Stresss (MPa)
40.000
30.000
20.000
10.000
0.000
-10.000
-20.000
-30.000
08:17:05
08:17:10
08:17:14
08:17:18
08:17:23

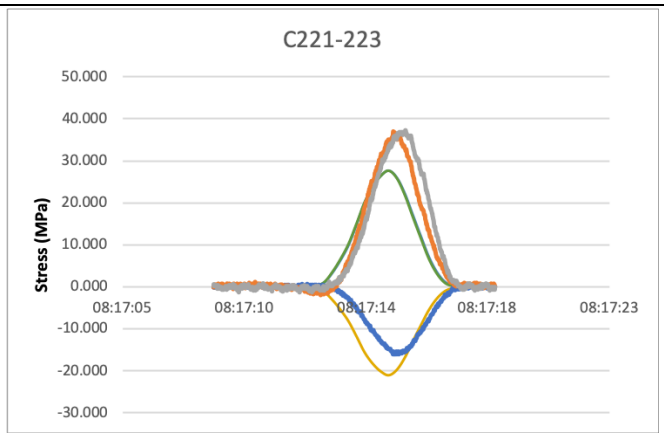
C221-223
Stress (MPa)
50.000
40.000
30.000
20.000
10.000
0.000
-10.000
-20.000
-30.000
08:17:05
08:17:10
08:17:14
08:17:18
08:17:23

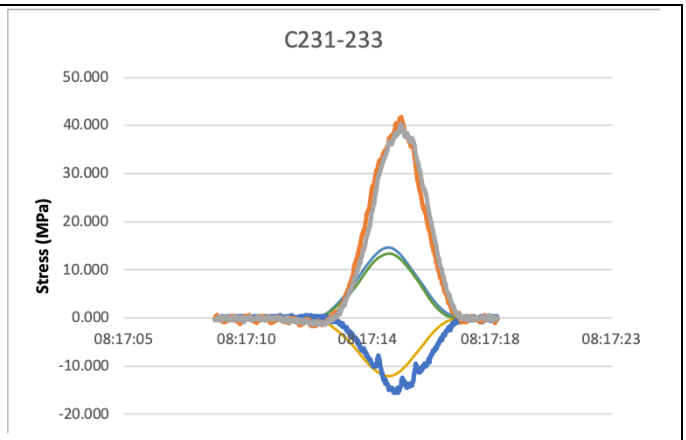
C231-233
Stress (MPa)
50.000
40.000
30.000
20.000
10.000
0.000
-10.000
-20.000
08:17:05
08:17:10
08:17:14
08:17:18
08:17:23

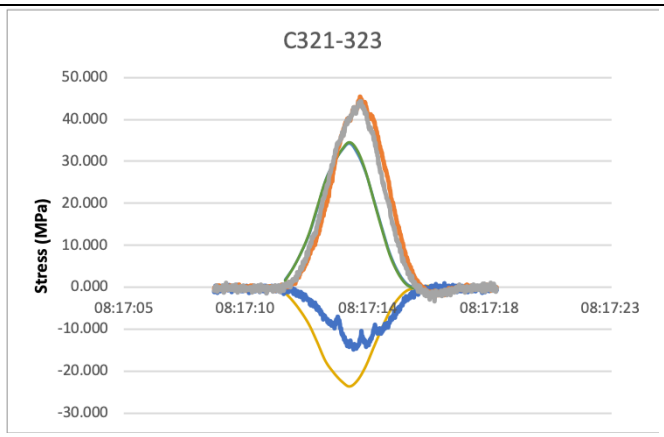
C321-323
Stress (MPa)
50.000
40.000
30.000
20.000
10.000
0.000
-10.000
-20.000
-30.000
08:17:05
08:17:10
08:17:14
08:17:18
08:17:23

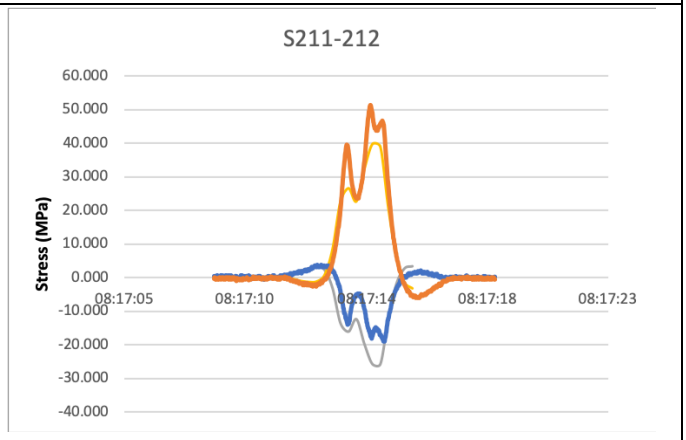
S211-212
Stress (MPa)
60.000
50.000
40.000
30.000
20.000
10.000
0.000
-10.000
-20.000
-30.000
-40.000
08:17:05
08:17:10
08:17:14
08:17:18
08:17:23

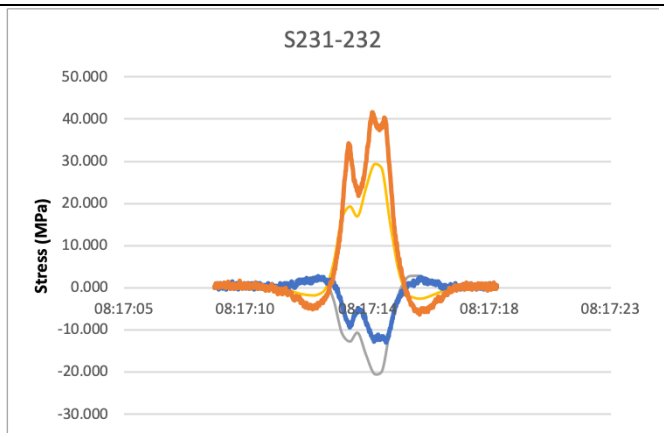
S231-232
Stress (MPa)
50.000
40.000
30.000
20.000
10.000
0.000
-10.000
-20.000
-30.000
08:17:05
08:17:10
08:17:14
08:17:18
08:17:23

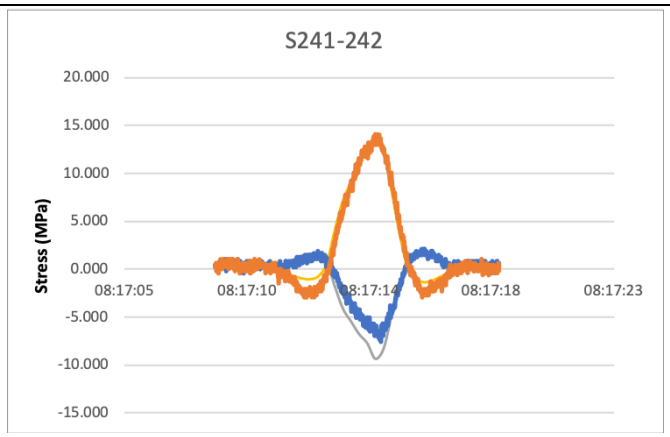
S241-242
Stress (MPa)
20.000
15.000
10.000
5.000
0.000
-5.000
-10.000
-15.000
08:17:05
08:17:10
08:17:14
08:17:18
08:17:23

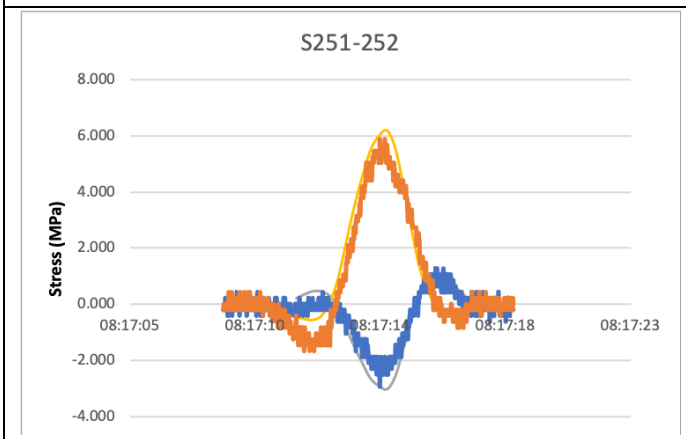
S251-252
Stress (MPa)
8.000
6.000
4.000
2.000
0.000
-2.000
-4.000
08:17:05
08:17:10
08:17:14
08:17:18
08:17:23

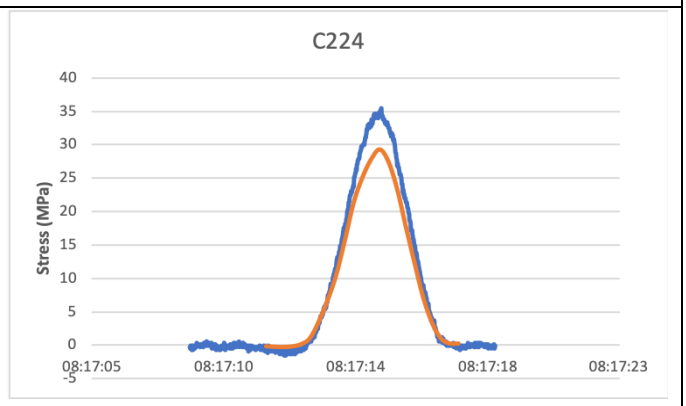
C224
Stress (MPa)
40
35
30
25
20
15
10
5
0
-5
08:17:05
08:17:10
08:17:14
08:17:18
08:17:23

Appendix 2.4. Model Calibration of the Strengthened Bridge: On the Axis.

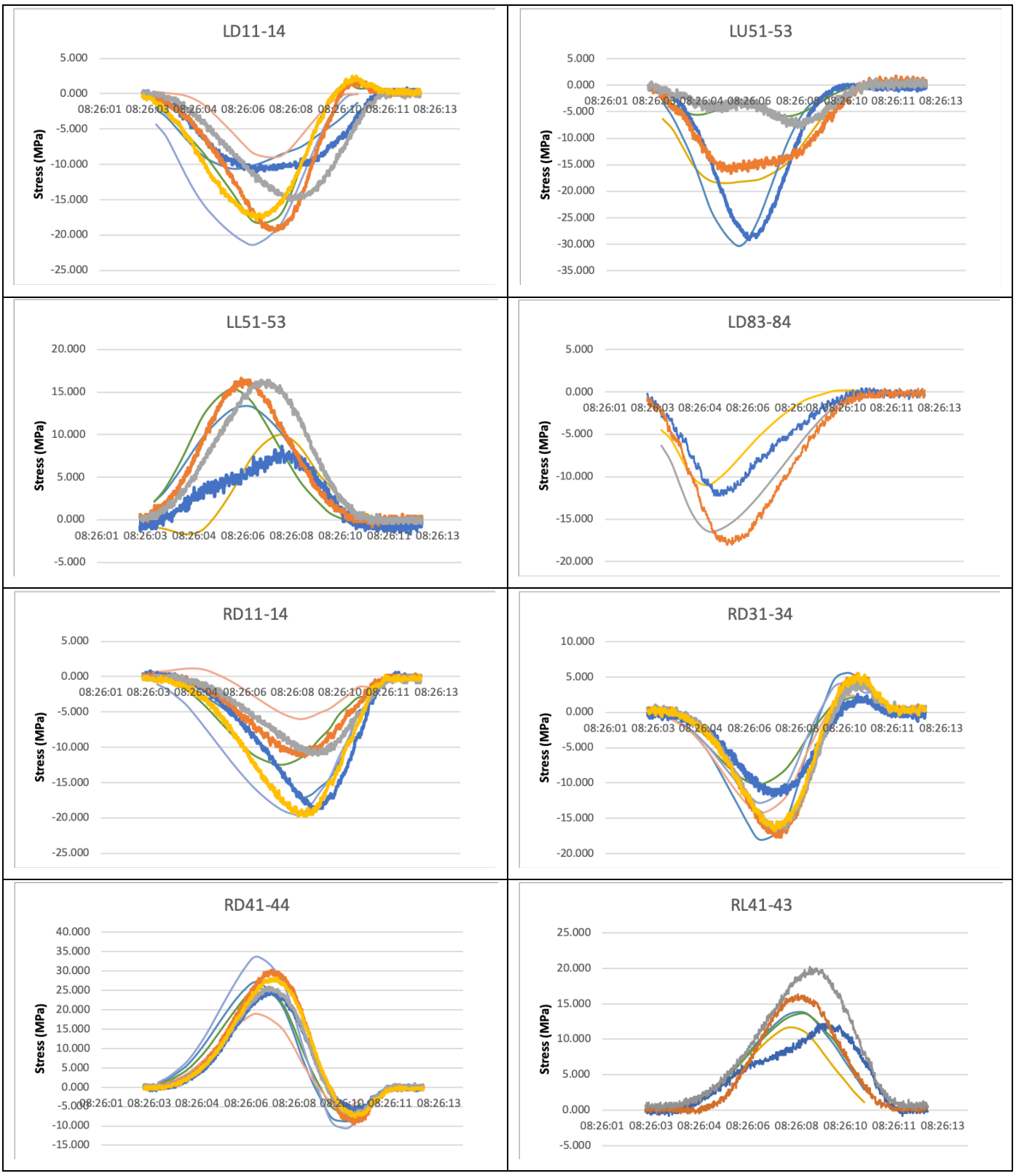

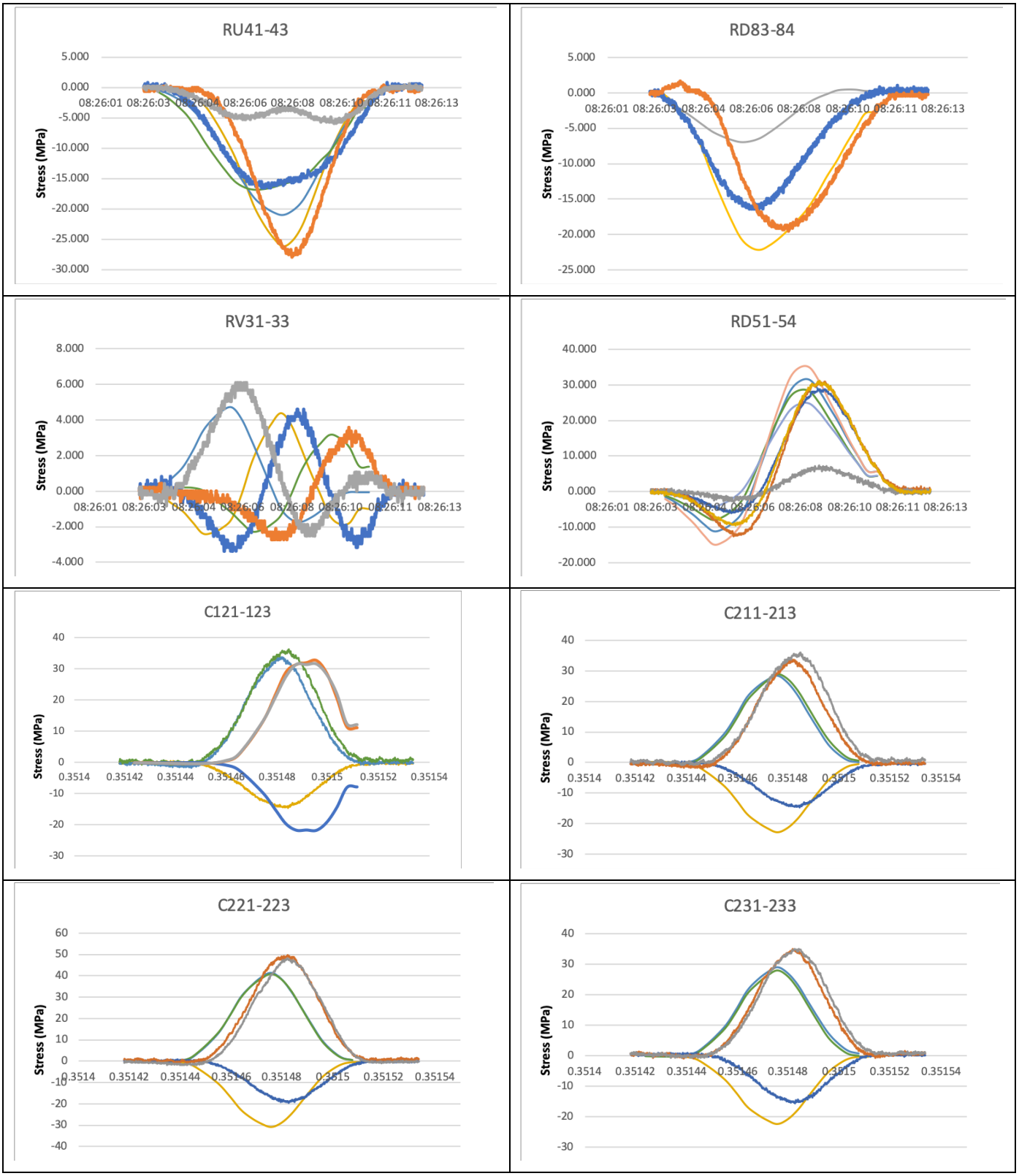
RU41-43
Stress (MPa)
RD83-84
Stress (MPa)
RV31-33
Stress (MPa)
RD51-54
Stress (MPa)
C121-123
Stress (MPa)
C211-213
Stress (MPa)
C221-223
Stress (MPa)
C231-233
Stress (MPa)

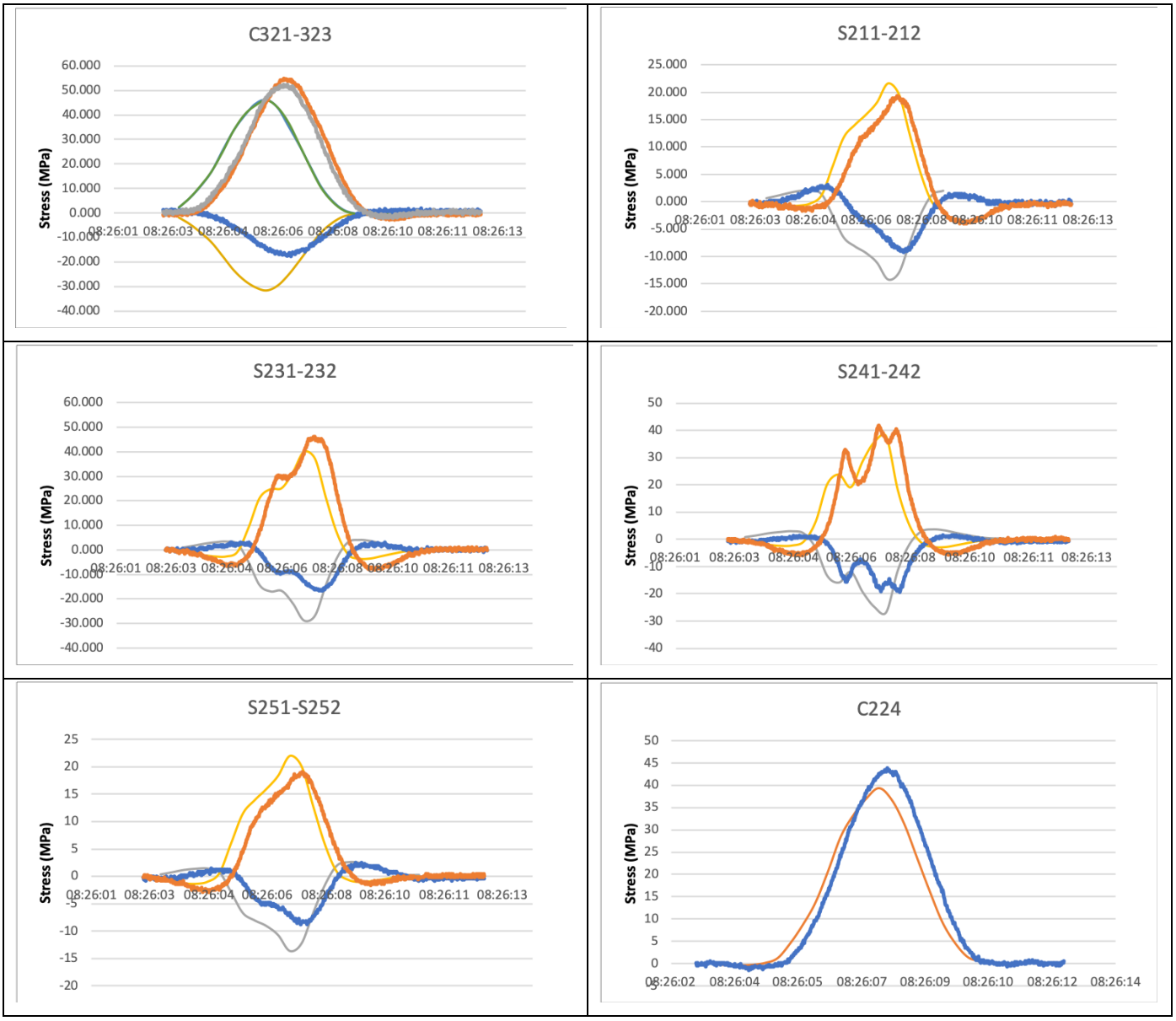
C321-323
Stress (MPa)
60.000
50.000
40.000
30.000
20.000
10.000
0.000
-10.000
-20.000
-30.000
-40.000
08:26:01 08:26:03 08:26:04 08:26:06 08:26:08 08:26:10 08:26:11 08:26:13
S211-212
Stress (MPa)
25.000
20.000
15.000
10.000
5.000
0.000
-5.000
-10.000
-15.000
-20.000
08:26:01 08:26:03 08:26:04 08:26:06 08:26:08 08:26:10 08:26:11 08:26:13
S231-232
Stress (MPa)
60.000
50.000
40.000
30.000
20.000
10.000
0.000
-10.000
-20.000
-30.000
-40.000
08:26:01 08:26:03 08:26:04 08:26:06 08:26:08 08:26:10 08:26:11 08:26:13
S241-242
Stress (MPa)
50
40
30
20
10
0
-10
-20
-30
-40
08:26:01 08:26:03 08:26:04 08:26:06 08:26:08 08:26:10 08:26:11 08:26:13
S251-S252
Stress (MPa)
25
20
15
10
5
0
-5
-10
-15
-20
08:26:01 08:26:03 08:26:04 08:26:06 08:26:08 08:26:10 08:26:11 08:26:13
C224
Stress (MPa)
50
45
40
35
30
25
20
15
10
5
0
-5
08:26:02 08:26:04 08:26:05 08:26:07 08:26:09 08:26:10 08:26:12 08:26:14